Experimental and Computational Studies on a Pulverised Fuel Stove

C.S.Bhaskar Dixit

December 30, 2003

Acknowledgements

It is with a deep sense of gratitude I acknowledge the guidence and support I have received from my research supervisors *Prof.* P. J. Paul and *Prof.* H. S. Mukunda. They have been supportive at all stages of my research and have helped me face all kinds of problems encountered during the course of research. I have always felt cared for.

I have greatly benifited from the tenure I have spent in this seat of learning. The facilities available (and access to them) at CGPL for experimental as well as computational work are exceptional.

I am grateful to *Prof.* B. N. Raghunandan, Chairman, Department of Aerospace, for his concern and words of encouragement.

The encouragement received from *Prof.* Y. Vrushabhendrappa, Principal, Bapuji Institute of Engineering and Technology, Davanagere and my colleagues at BIET is gratefully acknowledged.

I am indebted to Dr. N. K. S. Rajan and Dr. S. Dasappa who have always been helpful with useful suggestions during experimental work.

I have had the pleasure of association with Dr. Nikhil Patel, Dr. P. A. Ramakrishna, Sudarshan Kumar Vatsyayan, Jaydeep Basani, Abhishek, Lazer, Venkatesh. N, Mathew George, Biju Kumar, Saha, and Ravindra with whom I have had many fruitful discussions, academic and otherwise. I thank them for the enlivening moments I have spent with them.

I wish to acknowledge the support received by G. Sridhar, H. V. Sridhar and D. N. Subbukrishna during research. Our luncheon meeting discussions will always be cherished.

I have received help in many ways from Gayathri, Sheshagiri, Wali, Sankarlingam, Chowthri, C. Sridhar, Lakshmi, Swathi, Nisha, Anusuya, Nagaraj Upadhyaya and Vishwanath which is acknowledged gratefully.

Support from V. S. Hegde, Srikanth Padubidri, Sridhar pawar, Prashanth Katti, Padma, Reena, Sachin Deshpande, Ananda, Binoy, Deepak and Avinash was valuable during experimental work.

Help received from Mrs. Prema of MRC, Mrs. Manjula of Physics department, Mr. Jarali of SSCU, Mr.Siva of Chemical Engg. Dept. for Thermo-

gravimetry and Digital Scanning Calorimetry results is gratefully acknowledged.

Help received from ever dependable Ramesh Acharya during the course of experimental work is gratefully acknowledged.

Assistence from T. C. Sridhar, Thirupathaiah, Mallaiah, Anil, Venu, Shankar, Anantha, Channakeshava, Muniraju, Paulraj, Jayatheertha, Goravaiah and Narasamma was very valuable during experimentation.

The forebearence and support I have received from my wife Uma has gone a long way in completing this work. I also thank my parents-in-law for there support during the course of research.

C. S. Bhaskar Dixit

Contents

Abstract

This thesis is concerned with scientific studies on a pulverized fuel stove that can utilize pulverized agro-residues or leaf droppings in a manner that one gets very high conversion efficiencies with little emissions.

The objective of thesis originates from the recognition that (a) nearly half the population of the world depends on biofuels for domestic cooking needs, (b) the cooking practices as well as the nature of the food cooked varies widely depending on the geographic and cultural environment, (c) to meet this requirements one would need a variety of designs that would utilize biofuels (d) the fuel wood drawn from forest and plantations resources, solid bio-stock from agro-residues like corn cobs, cotton stalk, other bio material with ill defined shapes and sizes as the bio-fuels are used in rural environment in the order of perceived importance, (e) most solutions available in the literature and adapted in the field are meant for fuel wood class of biomass or sawdust and, (f) other bio residues would not meet the requirement because they would burn up fast due to their high surface area and fine size. This thesis aims at providing a scientific basis of the design of a stove that could meet the objectives of high efficiency and minimal emissions at near constant power. It is also intended that the design should not demand a device that needs electricity, so that a large number of developing country households deprived of electricity can still benefit from the design.

The starting point for the design is the sawdust-based system that has been found all over the world - a cylindrical stove with a central porthole being lit from the bottom. Such a stove in its normal mode of functioning will have a flame in port and consequently the combustion process that can be described as fair; the deficiency of such a stove is the somewhat enhanced sooting tendency. This particular configuration on which scientific work was done in this laboratory earlier is intended to be examined further in depth in the present research towards (a) determining the influence of density of packing, size of the pulverized material and moisture content on the functionality of the stove, features not considered in earlier work (b) understanding the combustion behavior in the port through detailed measurements of com-

position and temperature profiles in the port as well as temperature profile in the solid block, simultaneous with measurement of weight loss with time, implying the power of the stove and on occasions, simultaneous with a water boiling experiment.

The most important departure from all the earlier work in this laboratory and the rest of the world is the attempt to obtain stable premixed combustion behavior of the combustible gases from the port of the fuel block (known as the gasification mode). This effort, partly aided by serendipity led to a remarkable result that was subsequently justified through experimental and computational studies. The central part of the design of the stove that leads to the gasification mode of functioning is the use of air supply geometry at the bottom different from normal ones consisting of a circular port equivalent in diameter to the vertical port. The geometry at the bottom is arranged in the form of a thin slot with an area such that the air inducted is for gasification (about 30 % stoichiometric air flow). Experimental studies revealed that shortly after ignition the oxygen level in the port came down dramatically to less than 8% and with the surface temperatures of vertical fuel port not exceeding 950 K, creating conditions that would not sustain a gas phase flame in the port. The heterogeneous reaction between oxygen and the carbon at the surface provided the necessary exothermicity for sustained operation. The heat at the surface would be conducted inside and the volatiles that would be generated at temperatures exceeding 600 K would pass through the hot packed bed of partly converted material and issue out of the surface as fuel vapor that would be very close in composition to the gases from a gasifier. In order to ensure stable combustion of the gases a metal device is used. This allows air to be drawn in for combustion at two locations - one from the periphery of the stove and another from the annulus region.

Current experiments have been conducted on a stove design that aims at providing about 2.5 kW of input power with burn duration of about an hour to hour and a half. Experiments made on as-received sawdust or pulverized leafy bioresidue have shown gasification mode of functioning for at least thirty minutes. During this period the burn-out of the fuel in the air entry zone at the bottom increases the oxygen fraction in the port that would also be responsible for the increase in surface temperature of the port, both acting together to create the conditions for the flaming combustion in the port. The near constant power of the stove in the later half is about 10% higher than the earlier part.

Parametric studies have shown that the packing density of the pulverized fuel should be moderate - between 40 to 45% of the density from the biomass from which the pulverized fuel is derived. Higher densities would lead to larger ignition delay and when ignition problem is overcome low power level

would result. Packing at even lower densities than indicated would lead to flaming combustion in the port and run-away power levels. Studies on particle size showed that between 0.5 and 1 mm, there appeared no difference in performance of the stove. With respect to moisture content in the pulverized material, up to 15% moisture content (sun dry material can be expected to have 10% moisture) would be conducive to operation in the gasification mode.

In an attempt to explore the possibility of extended gasification duration, studies were conducted in single port configuration having air entry from the bottom with a horizontal baffle to control the flow rate. The baffle also doubled as a fuel holder which assisted in ignition of the fuel block. This configuration has exhibited gasification behavior for about 20 min but there have been problems of extinction needing re-ignition. Also conversion percentage was low at about 50%. To overcome these drawbacks multi-port design was employed. Vertical air entry configuration was chosen. Multi-port arrangement has successfully prevented flame extinguishment with gasification mode operation in the central port sustained for about 20 min. Side ports became active automatically by this time establishing stable combustion at the device exit. Stove with this configuration have achieved conversion percentages in excess of 68%.

Emission measurements using standard hood design have revealed that this stove configuration has a CO emission factor of 12 g/kg fuel which represents a performance superior to conventional biomass stoves which typically show 45 g/kg. NO_x emission factors were determined to be about 1 g/kg fuel which falls in the range of reported data for NO_x. The emission performance is significant considering this configuration can burn those classes of biomass like pulverized leafy fallings and crop residues which are known to be far more emission intensive.

Studies with different pulverized leafy fuels have indicated these fuels have lower volatile release rates and therefore exhibit lower power level operation for a given port configuration compared to sawdust fuel.

An analysis has been carried out on the condensed phase thermal profile with moving pyrolisis front. This unsteady thermal analysis that accounts for moving pyrolisis front has provided the predictions for the rate of movement of the pyrolisis front. The comparison of the temperature profiles and the pyrolisis front movement rates with measured data is excellent.

The single port configuration was computationally analyzed with an aim to understand the aero-thermo-chemical behavior of the stove operation in combustion and gasification modes. The g-phase of tangential entry stove was subjected to a 3 dimensional analysis using a commercial CFD code CFX TASCflow with combustion modeled using single step overall reaction.

It was possible to obtain combustion and gasification modes of stove operation computationally also by varying the fuel release pattern. A fuel release pattern biased towards the bottom of the port as seen in the experiments, when used for the calculations, resulted in gasification mode operation while uniform fuel release pattern induced combustion mode operation. Comparison of g-phase temperature profiles in combustion mode seems satisfactory. The comparison of g-phase temperature profiles in the gasification mode appears intriguing. An explanation for the behavior is sought in faster hydrogen combustion compared to carbon monoxide some thing not accounted for in the calculations with single step chemistry.

Chapter 1 contains an introduction with literature survey justifying the need for development of clean combustion devices without the aid of electrical artifices especially for fuels derived from fine agricultural residues and tree droppings. The emission levels from various biomass stoves and the impact of these emissions on global warming are brought out in the literature survey. An overview of the proposed research work is also provided.

Various tools and techniques used during the course of experimental work are described in Chapter 2.

The combustion and gasification modes of operation of a single port tube stove are described in Chapter 3. Studies conducted to establish the causes of flash back, an event which brought about the mode switch, are presented. The experimental results presented include predicted and measured pyrolisis front propagation rates, efficiencies and emissions from the single port stove. Necessity for a multi-port stove is also brought out.

Studies conducted on multi-port stoves with an objective to determine the stove configuration which would ensure no-loss-of-flame and high fuel utilization criteria are described in Chapter 4. Measured emission factors of CO and NO_x from the stove are also presented.

Studies conducted to extend the utility of tube stove to other fine fuels generated from pulverizing leafy biomass are presented in Chapter 5. Pulverized leafy biomass has exhibited lower power levels compared to sawdust in similar geometries. It has been possible to explain this behavior using volatilization rate data obtained from TGA (Thermo Gravimetric Analysis) of various pulverised fuels.

Chapter 6 describes the study on modeling the g-phase of tangential inlet single port tube stove to examine the gasification and combustion modes of operation of the tube stove.

Concluding remarks and scope for future work are presented in Chapter 7.

List of Figures

List of Tables

Nomenclature

$\bar{k}$	Average conductivity of porous bed, W/m K
ΔH	Heat of reaction for pyrolisis of wood, J/kg
$\dot{m}$	Mass loss rate per unit height of the bed, kg/m.s
$\dot{r}$	Pyrolisis front propagation rate, m/s
ϵ	Porosity, see equation (3.18)
η	Efficiency
μ	Dynamic viscosity, Pa.s
ν	Kinamatic viscosity, m^2/s
ρ_p	Loading density of the pulverised fuel, kg/m^3
Gr	Grashoff number
PIC	Products of Incomplete Combustion
Pr	Prandtl number
B	Blocking effect, see equation (3.20)
c_p	Specific heat of hot char, J/kg K
c_{pw}	Specific heat of green biomass
d	Port Diameter, mm
f	Fraction volatilized
g	Acceleration due to gravity m/s^2
h	Heat transfer coefficient, W/m^2K

H_c	Heat of combustion, MJ/kg, see equation (6.2)
h_c	Enthalpy of char, J/kg
h_v	Enthalpy of volatiles, J/kg
h_w	Enthalpy of wood, J/kg
h_{fi}	Heat of formation of i^{th} species, MJ/kmol
h_{si}	Sensible enthalpy of i^{th} species, MJ/kmol
k_c	Conductivity of hot char, W/m K
k_w	Conductivity of wood, W/m K
m_i	Initial biomass weight, kg
r	Radius, mm
r^*	Radius of the pyrolisis front, m
T^*	Temperature of the pyrolisis front, K
T_g	Gas temperature, K
t_g	Time of gasification, minutes
T_s	Port surface temperature, K
t_{FB}	Time of flash back
Nu	Nusselt number
AR	Aspect Ratio, the ratio port height h to port diameter d

Chapter 1

Introduction and Literature Survey

1.1 Introduction

Conversion of solid fuels to energy — heat in the present case — is known to be more difficult compared to that from liquid or gaseous fuels. This is because solid fuels appear in a variety of shapes and sizes and may have considerable moisture in them all of which are true with bio-fuels considered for study in this thesis.

In the case of gaseous and liquid fuels, the fuel flow rate can be controlled as desired and hence the processes related to mixing the fuel and oxidant, central to the combustion process, can be handled with greater precision compared to those for solid fuels. The varying shapes and sizes of solid fuels imply varying degree of volatile generation and hence significant excursions in the local air-to-fuel ratio. Values close to stoichiometry lead to high flame temperatures and very small fractions of products of incomplete combustion. Lean combustion will result in low flame temperatures, unfavorable to obtaining high efficiency, but favorable to reducing the emissions. Rich combustion is unfavorable to efficiency and emissions. Because of these considerations, the issue of designing solid fuel combustion systems is still open.

The issue is open for other considerations as well. Biomass is used as a cooking fuel in (a) remote small communities due to sheer necessity since the state cannot provide other fuels of choice at locally affordable prices as in cities, (b) villages in developing nations have no access to fuels such as LPG, but have to depend on field collected biomass residues and (c) urban poor located in slums who need to depend on collection of garden wastes, dry kitchen wastes and avenue tree droppings in addition to purchasing low

grade fire wood. The estimated size of people that depends on these sources amounts to half the world population.

The requirements of clean and efficient combustion are more easily handled if air can be supplied to the combustion system at the desired rate at identified locations. These can be accomplished if a blower can be used. This needs electricity. But most communities that need to use biomass for heat do not have electricity. Hence combustion devices need to be built without the aid of electric artifices.

Studies of *Natarajan* (1993) in India and the reports on wood energy in their information bulletins (Wood energy news, several volumes in the period 1992 – 1998, *Anon* (1996, 1997) for example) show that fire wood is considered a fuel of choice amongst the variety of biomass available; other agricultural residues are used if fire wood is unavailable. The problems of using other agro-residues are that the material is small in size and burns up fast. This will imply very fluctuating power levels, fast burn up and therefore much greater periodicity in feeding and more attention. This technical problem of using fine agricultural residues and tree droppings including leafy biomass as candidates for domestic fuel has not been addressed at all; it is not that devices that use fine biomass material for domestic applications do not exist. But they are used only for sawdust (fine shavings of wood). They are not contemplated for use with any other biomass and the design itself has been researched upon to a small extent. Both scientific examination of the device and exploration of it for other fine biomass remain to be undertaken.

Amongst devices that have been explored in the literature somewhat extensively are wood stoves in a variety of forms and this literature includes science of the combustion process to some extent, efficiency related issues, and more extensively, problems related to emissions from stoves to those involved in cooking and others around. The literature relevant to the work of this thesis is reviewed here.

1.2 Literature Survey

Emmons and Atreya (1982) have discussed the essentials of the combustion process calling it a science of fire. After a suitable ignition process, the biomass loses volatiles around 250 to 300°C (called the pyrolisis process) and the pyrolisis gases burn in the gas phase with the oxygen in the surrounding atmosphere and the flame provides the heat feed back to maintain the steady combustion process. The char that remains behind — typically 20 to 25% — will get oxidized by the oxygen diffusing from the surrounding atmosphere into carbon monoxide and this burns very close to the surface leading to

bluish flame. They address the whole range of issues that affect the operation of a stove and the efficiency of operation. The data on the heats of combustion of the biomass, the volatiles and char indicate that the volatiles, constituting about 75% biomass, have 80% of the calorific value of biomass. The 25% char has a calorific value 1.5 times the calorific value of biomass.

Krishna Prasad and colleagues at Eindhoven University in the Netherlands have done substantive work on the science of stove functioning and stove design. Most of the work is related to the stoves using fire wood as the fuel. Many of the studies are summarized in *Prasad et al.* (1985). The paper examines the fundamentals of combustion of wood, the processes that occur in open fires and closed stoves, performance estimation procedures, indoor air quality as related to emissions from stoves, heat balance and stove economics. Amongst the several useful results, the one on water boiling efficiency dependence on the height of the pan from the fuel bed is important. Efficiency increases with reduction in the height of the pan bottom from the fuel bed indicating that extra flame height that might contribute to better conversion of soot would actually reduce the efficiency. The functioning of fire wood based stoves calls for periodic loading of biomass and in the case of small domestic stoves this process leads to typical consumption rate as shown in Fig. 1.1 in which it is clear that the volatiles are generated with large peaks. It is not obvious that air that is inducted by the flame for combustion will match the demand by the fuel generation process. This leads to a continuous change of fuel-to-air ratio at which the combustion proceeds—some times rich and other times lean.

When it is rich, sooting is unavoidable and when it is very lean, the flame may be incapable of being sustained and the stove will begin to smoke. While the hazards of sooting are limited to the bottom of the vessel turning black with sooty deposit (largely), the hazards due to smoking are far more serious. Several intermediate compounds of pyrolisis are known to be irritating to the eyes (the aldehydes, in particular) and some other compounds are carcinogenic (*Smith*, 1994; *Bhattacharya et al.*, 2002a,b).

Another compound that is formed due to incomplete combustion is carbon monoxide (CO), a poisonous gas even at low concentrations. This is formed within the flame since the diffusive combustion process separates the oxidizer rich zone from the fuel rich zone and if there is inadequate residence time, part of the CO will remain unoxidized and it will circulate around the stove region since its density at ambient temperature is comparable to that of air. A good way of eliminating it would be to provide for premixed mode of operation, some thing impossible to achieve with classical fire wood stoves. Hence one should attempt to create a design that will positively prevent the smoking tendency as well as the generation of carbon monoxide. Sooting

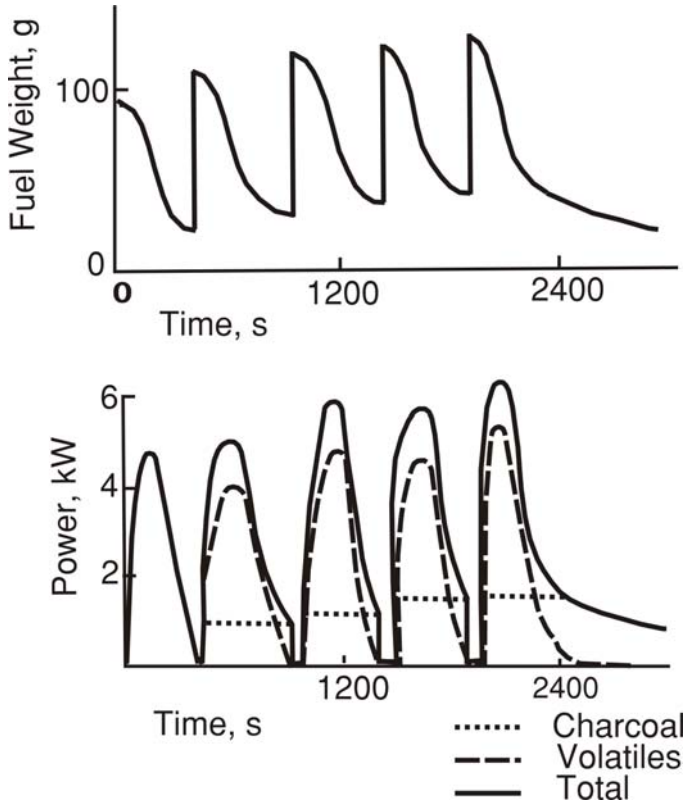

Figure 1.1: Fuel consumption rate in a conventional stove from *Prasad et al.* (1985)

tendency is undesirable, but could be tolerated to a limited extent. The paper deals with many other aspects of stoves like efficiency measurements, heat balance and indoor air quality.

Studies of *Ballard-Trameer and Jawurek* (1996) show the linkage between higher CO emissions and intermittent fuel feeding. Figure 1.2 shows burn rate and emission measurements from a typical one pot metal stove with periodic fuel supply. Notice that peak burn rate, is roughly four times the mean burn rate. Increased CO emissions are in phase with increased burn rates caused by intermittent fuel feed.

Baldwin (1986) in his book on biomass stoves addresses the fundamentals of combustion and heat transfer as well as stove design, construction and testing procedures. This work is a useful introduction to those wishing to understand or design wood burning stoves. Emission aspects have not been addressed in this book.

Bhattacharya et al. (2002a) describe twenty four different variety of wood and charcoal burning stoves from several south East Asian countries and

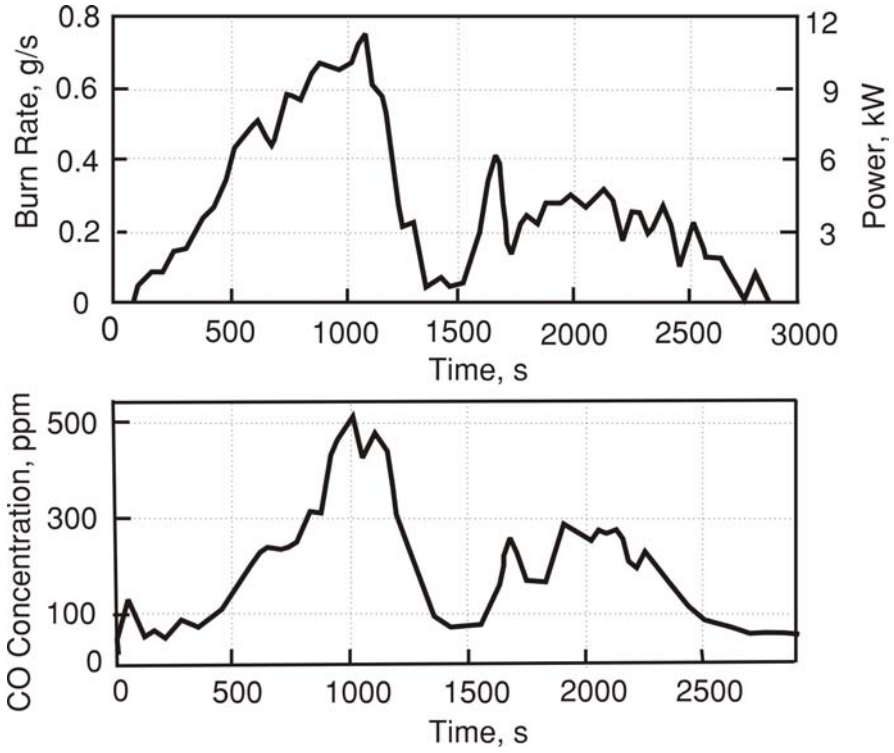

Figure 1.2: Emission pattern from a conventional stove from *Ballard-Trameer and Jawurek* (1996)

have measured emissions from these stoves. See Figs. 1.3 and 1.4 for the photographs of a few of the stoves discussed in the above paper. Most stove designs are based on fired clay construction with a grate at the bottom or at a height a little above the bottom zone, a combustion zone above the grate and three projections for placing a vessel. The emission measurements are made in a standard hood design. The water boiling efficiencies vary between 10 to 25 %, with many designs showing efficiencies less than 15 % and one stove—Harsha cook-stove—showing efficiency of 25.2 %. The emissions of various other GH gases are presented in Table. 1.1 taken from their paper.

CO emissions reported from various authors are compared in Fig. 1.5 as a function efficiency of stove. Emissions in the range of 25 to 170 g/kg fuel are reported for stove efficiencies ranging from 10–25%. Generally, CO emissions increase with increase in stove efficiencies. This is due to fact that higher stove efficiencies are obtained when the stove functions near stoichiometry or slightly fuel rich condition. Due to lack of O_2 or improper mixing, CO gets formed. Fuel lean combustion will bring down CO but cause larger energy

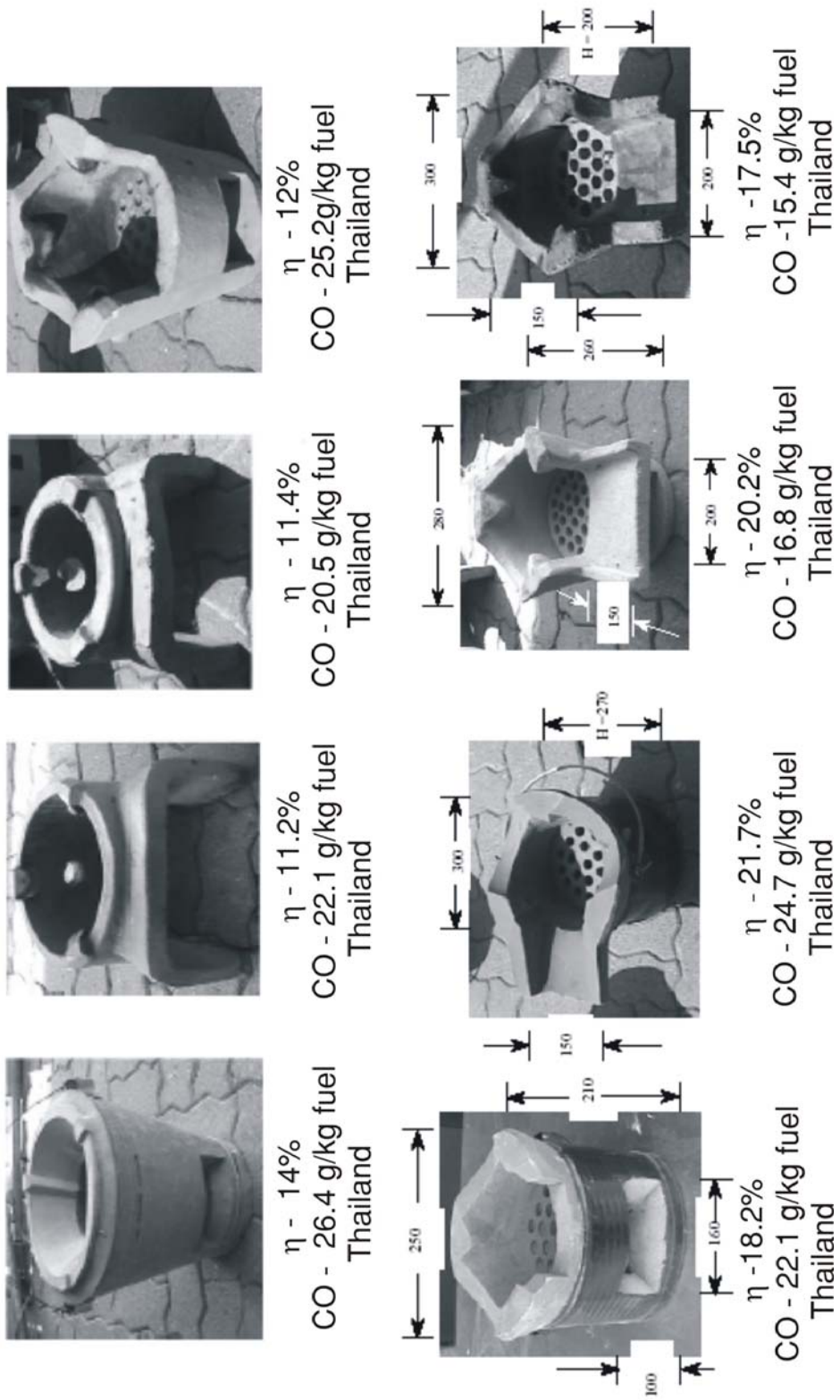

Figure 1.3: Photographs of a few stoves discussed in *Bhattacharya et al.* (2002a)(continued...)

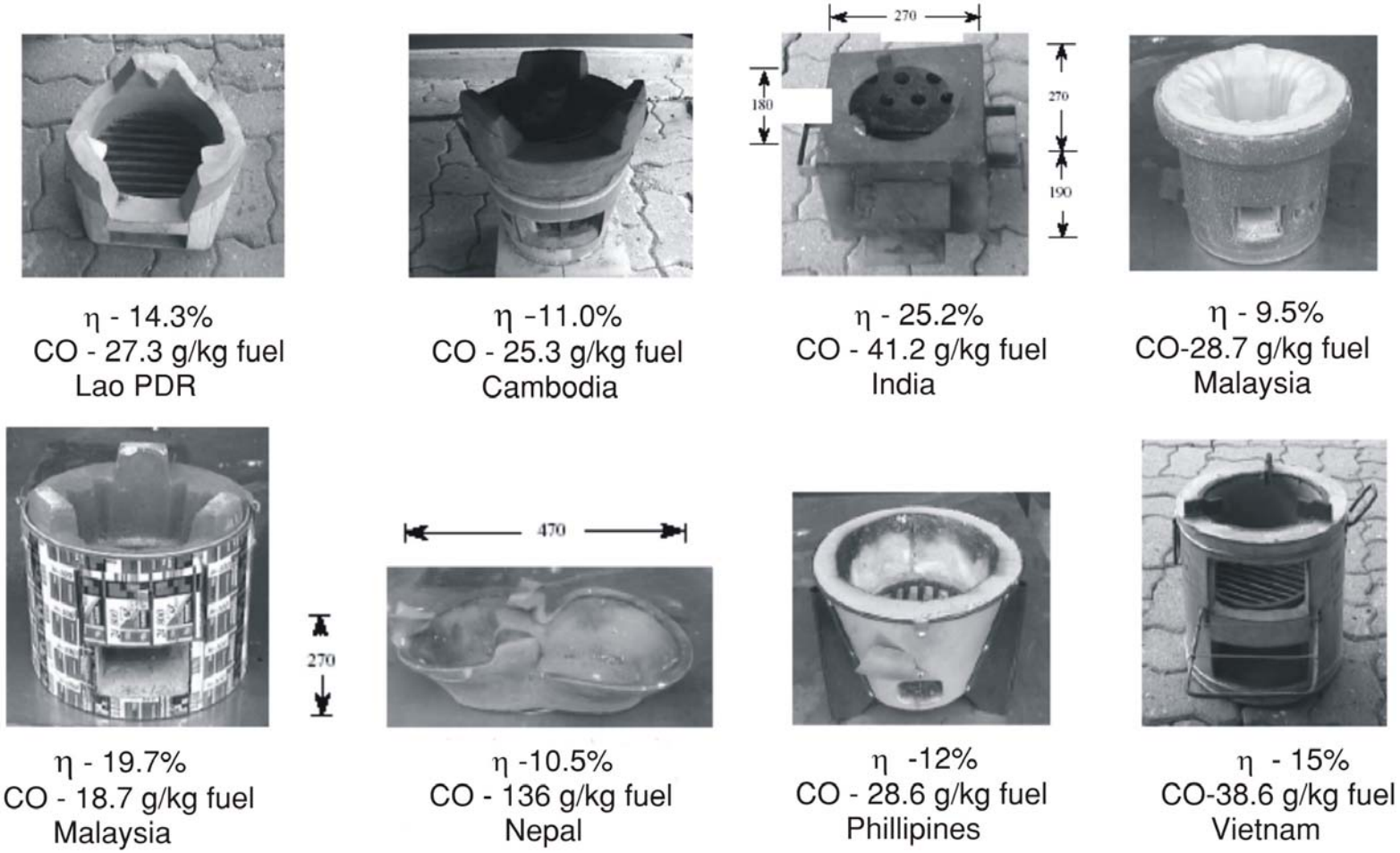

Figure 1.4: (continued...)Photographs of a few stoves discussed in *Bhattacharya et al.* (2002a)

Table 1.1: Emission factors of selected wood-fired cookstoves from *Bhattacharya et al.* (2002a)

Name of cookstoves	Emission factors(g kg^{-1} fuel used)				
	CO	CO_2	CH_4	TNMOC	NO_x
Cambodian traditional	25.3	1580	2.7	22.4	0.01
Lao traditional	27.3	1579	8.4	16.3	0.1
Vietnamese traditional	38.6	1608	3.9	3.3	0.07
Nepalese one-pot ceramic	136.0	1344	26.8	20.4	0.1
Thai-bucket cookstove	26.4	1596	10.0	8.9	0.12
Roi-et clay	22.1	1626	4.2	2.8	0.1
Roi-et cement	20.5	1625	5.0	3.4	0.12
RTFD improved wood/char	19.1	1603	10.8	6.5	0.11
Rungsit stove	25.2	1584	11.0	10.2	0.1
Chinese traditional	24.4	1570	5.4	8.4	0.1
Malaysian traditional	28.7	1562	8.1	6.2	0.16
QB Phil. charcoal/wood	45.1	1568	9.7	9.5	0.2
Phil. charcoal/wood	28.6	1603	8.9	7.5	0.17
Nepal one-pot metal	136.0	1344	26.8	20.4	0.07
Nepalese two-pot ceramic	113.0	1408	29.5	7.8	0.05
Nepalese two-pot metallic	45.6	1530	18.9	14.2	0.07
Lao improved cookstoves	51.9	1565	6.0	10.0	0.19
Viet. improved cookstove	47.1	1577	5.3	7.6	0.15
Indian 'Harsha' cookstove	41.2	1597	12.3	7.7	0.2
S.pen, narn char/wood clay	16.8	1613	10.0	5.3	0.2
S.pen, nam char wood cement	15.4	1612	10.5	5.5	0.15
Bang Sue stove	22.1	1585	12.4	9.5	0.11
Bang Sue modified	24.7	1581	14.0	7.9	0.13
Malaysian improved	18.7	1603	13.7	9.3	0.11

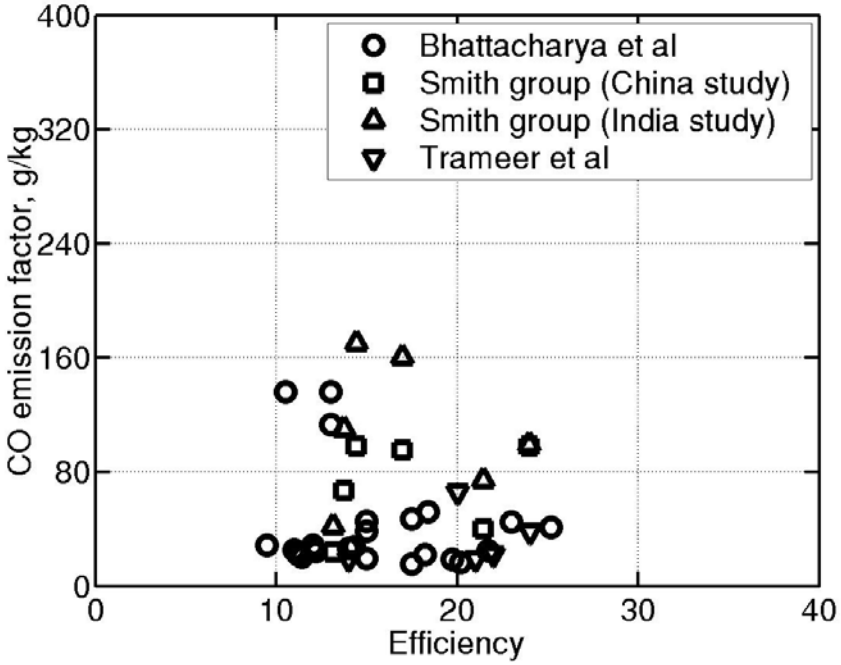

Figure 1.5: Comparison of CO emission (in g/kg fuel) results for biomass stoves as a function of stove efficiency from *Bhattacharya et al.* (2002a); *Zhang et al.* (2000); *Smith et al.* (1998); *Ballard-Trameer and Jawurek* (1996). High emission (above 75g/kg fuel) in 10-17% range is due to poor combustion strategy. If this data is discounted, an increasing trend in emission is observed.

losses from the stove through flue gases leading to lower efficiencies. Product gas temperatures are also lowered bringing down heat transfer efficiency. From *Bhattacharya et al.* (2002a), representative values of emissions of CO are about 45 g/kg fuel, NO_x of 0.2 g/kg, CO_2 of 1.7 kg/kg fuel. Stoichiometric requirements for combustion require 1.9 kg CO_2 per kg fuel (Every 23 kg of biomass has 12 kg carbon generating 44 kg CO_2; therefore one would expect $44/23 = 1.9$ kg CO_2 per kg fuel). It appears that measured CO_2 per kg fuel is based on biomass with 10% moisture content (according to proximate analysis presented in the paper) though this is not explicitly stated in the paper. The values when charcoal alone is used as the fuel also show 2.5 kg CO_2 per kg fuel. Based on the elemental analysis of char presented in *Bhattacharya et al.* (2002a) the charcoal should yield 3.1 kg CO_2 per kg char. Charcoal with 5% moisture (from proximate analysis) should still yield 2.9 kg CO_2 per kg char. This implies 14% char is considered as carbon residue which appears to be a large number.

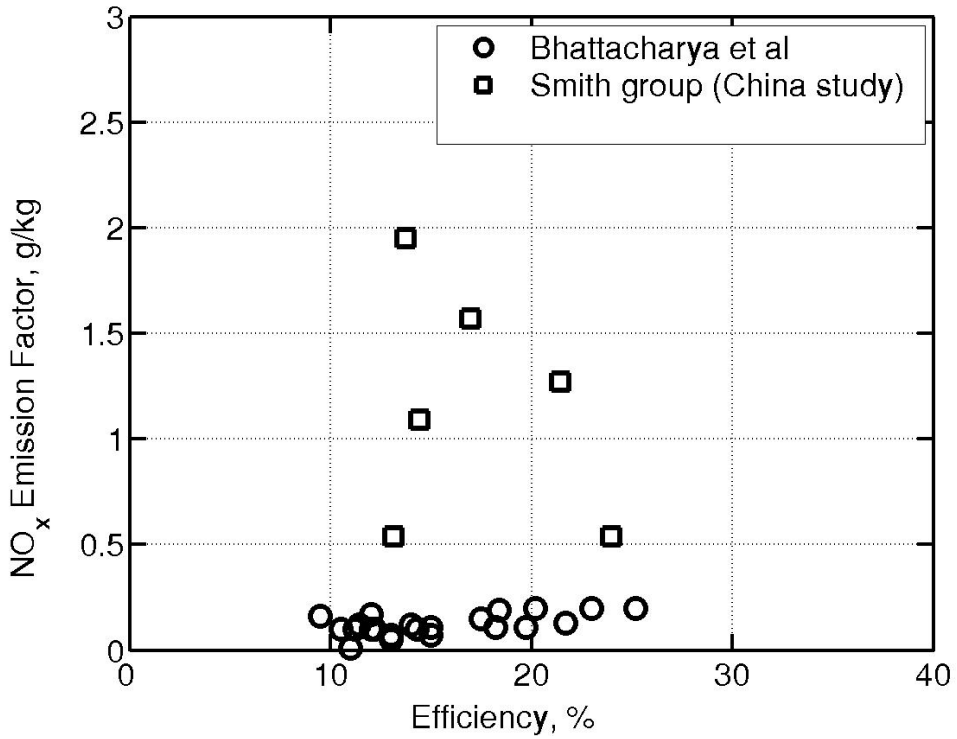

Figure 1.6: Comparison of NO_x emission results (in g/kg fuel) for biomass stoves as a function of stove efficiency from *Bhattacharya et al.* (2002a); *Zhang et al.* (2000)

Tests conducted by (Smith et.al,1999) indicate '...every g of char (0.81 g carbon in char) generated through primary wood combustion would be converted during secondary char burning to: 0.66 g C_{CO_2}, 0.12 g C, $_{CO}$, 0.0059 g C_{CH_4}, 0.0068 g C_{TNMHC} and 0.002 g C_{TSP} and 0.0099 g carbon in remaining char and ash as unburnt residue ...'. The emission of air borne PIC (Products of Incomplete Combustion) may be higher than the reported values if calculation is based on a lower amount of carbon residue left over in ash. A few NO_x emission results are available in stove literature. These are compared in Fig. 1.6. Of the two measurements reported, results from *Bhattacharya et al.* (2002a) have indicated low values of NO_x of about 0.2 g/kg fuel while results from *Zhang et al.* (2000) have shown scattered values between 0.2 to 2 g/kg fuel. The reported values of NO_x are very low compared to NO_x emissions from other stationary combustion sources. This is probably due to lower temperatures encountered in the stove operation and also shorter residence times in the hot zone.

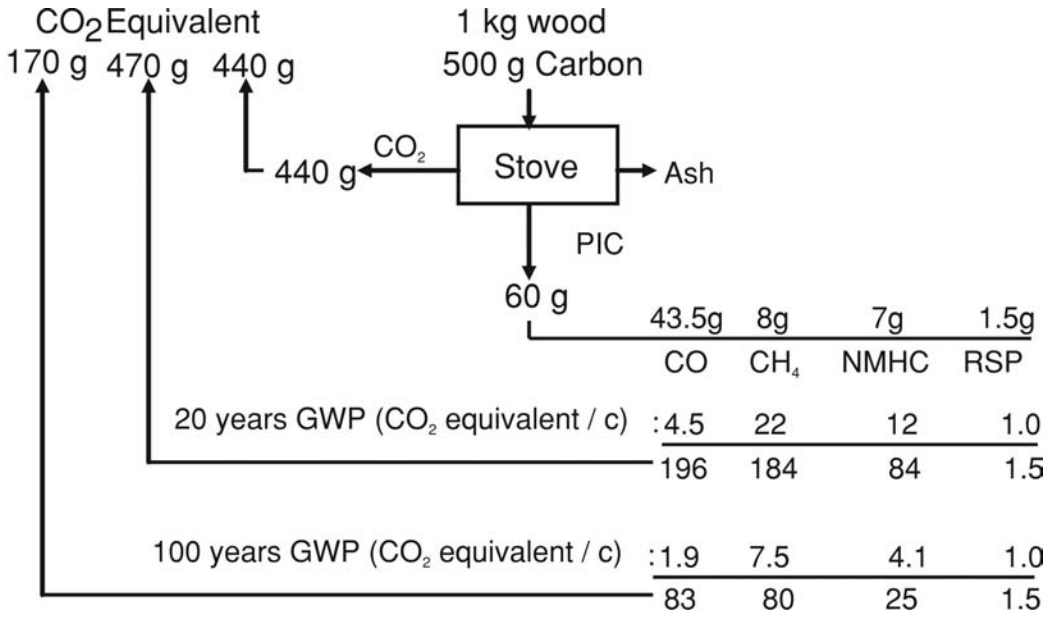

Figure 1.7: Global Warming Potential (GWP) of various Products of Incomplete Combustion (PIC)(*Smith*, 1994)

Bhattacharya et al. (2002b) studied the effect of pot size on efficiency and concluded that pot size did not affect efficiency of stoves tested. This is so because the choice of stove power for the chosen heating task is proper. Usage of very large stove (more heat will go to heat up the stove itself) or vessel (heat loss from vessel is nearly equal to heat input) would cause heating time per unit mass of water to rise resulting in decreased efficiency. A similar study conducted by *Mukunda et al.* (1988) has brought out this fact.

Smith (1994) has been involved in assessment of stoves, their efficiency and indoor pollution issues over a period of time and has contributed significantly to these subjects. One of the important conclusions of his study is that unless biofuels are used at higher combustion efficiency, there is no guarantee that a zero carbon balance is assured. This strong conclusion is not simply due to excessive use of fuel affecting sustainability. It is more related to the nature of emissions. Based on the measurements of stoves discussed earlier by *Bhattacharya et al.* (2002a,b) the emissions of CO, CH_4 and NMHC (non-methane hydrocarbons, the products of incomplete combustion) are about 4.5%, 2.2%, 1.2% respectively. *Smith* (1994) has accounted for the Global Warming Potential (GWP, for short) of these gases, as shown in Fig. 1.7 and has drawn the conclusion that the products of incomplete combustion

may contribute the same magnitude of emissions as CO_2. By invoking the rate of decay of these compounds in the atmosphere, the above conclusion is more accurately stated that the non-CO_2 gases have a global warming potential 20 to 110% as large as CO_2 emitted during their generation (*Smith*, 1994). This can be seen from Fig. 1.7. Each kg of biomass contains about 500 g carbon out of which 440 g goes to CO_2 while 60 g goes to Products of Incomplete Combustion like CO, CH_4, Non-Methane HydroCarbons and Respirable Solid Particulates. For a 20 year life span of the product gases, it is seen that total GWP of carbon in PIC is 470 g which is greater than GWP of CO_2 generated during generation of those PIC's. This is due to the fact that different gases have different interactions with other gases, life times and heat trapping abilities summarised by Hayes and Smith (1993). This is the argument that he has used to emphasize that cookstoves must be designed so that the non-CO_2 emissions from incomplete combustion be limited. In other words one must aim at very high combustion efficiency. Otherwise, he has argued that an efficiently burning fossil fuel stove has lesser GWP than a poorly burning biofuel stove! This particular view point does not find adequate appreciation amongst stove designers.

Thus, there is a greater motivation to understand and design efficient biofuel stoves both in terms of combustion and heat transfer.

Mukunda et al. (1988) noted that all the earlier work on wood burning cook stoves including those of Krishna Prasad and group had achieved efficiencies no more than 42% even in well designed laboratory version stoves. It has been known from the work in several laboratories that the efficiency of kerosene stoves, as well as gas stoves, is about 65 to 70 %. They investigated the reasons for this feature and also evolved designs that could produce high efficiency. The principal findings of their work are as follows.

1. The efficiency of the cook stove is directly related to the peak flame temperature. Kerosene and gas stoves produce flame temperatures of 1700 K and biomass stoves of good design produce flame temperatures of 1200 K and poorer design about 1000 K; also in biomass stoves the flames will be unsteady and local temperatures can fluctuate between the peak and a lower temperature (typically, the variation could be between 700 to 1200 K). Since the heat absorbing surface is limited (the bottom portion and a part of the vertical surface of a cylindrical vessel), the differences in the flame temperatures have a direct effect. If we take the ratio of temperature differences as $(1700 - 300)/(1200 - 300) \sim 1.6$, then this explains the differences in efficiencies to the first order correctly.

2. The peak efficiency of a wood burning stove occurs at a slightly fuel rich

condition close to stoichiometry. This implies a sooting flame. Thus a very efficient stove is not emission friendly. Thus if one wants to optimize on emissions some sacrifice in efficiency should be accepted.

3. Provision of a metal plate (with a relatively small vertical space for the flow of gases) over which the cooking vessel is placed leads to an enhancement of thermal efficiency (by about 6%). They have also provided a design of single pan metal stove that ensures limiting the peak power level by limiting the size of the fuel feed port. The basis of this approach was that users want high rate of cooking and expect that this is achieved by enhanced feed rate. This stove design is more suitable to thin agro-residues like cotton stock, mulberry stock and prepared fuel wood stock. Field study has shown that this has yet to achieve user friendliness even though it promises efficiency of 35 to 37%.

All the stoves discussed and worked upon by others have essentially the problems of a periodicity of consumption rates leading to poor emission performance. The next important advance that has taken place is due to the work of *Reed et al.* (2000). In the statement of the problem they indicate "...over 2 billion people cook badly on inefficient wood stoves that waste wood, cause health problems and .... Electricity, gas or liquid fuels are preferred for cooking – when they can be obtained .... In the last few decades, many improved wood stoves have been developed .... but they are more difficult to manufacture, often more heat goes into the stove than the food, and they do not offer good control of cooking rate.... Because of the problems of wood cooking, people often cook on charcoal. However, charcoal manufacture is very wasteful of energy and very polluting, so the problems of wood stove are externalized but not solved".

This statement of problem has valid points, but some difficult to appreciate. While the reason for the choice of charcoal instead of wood is clearly the absence of smoke and health hazards, it does not appear related to the control of burn rate. The acceptability of a stove by any community is strongly related to cooking habits and some times culture when it concerns the use of traditional fuels namely, biomass. When the fuel is changed to kerosene or gas, the control and cleanliness of cooking are so much improved that people change their habits to new ways of accepting the technology with little problem. The technology of biomass based stoves should aim at providing a bag of solutions by including as many points of acceptability as possible.

The work of *Reed et al.* (2000) and *Reed and Larson* (1996) has resulted in two stove designs. Both the designs have a fundamental combustion behavior that is very elegant. The idea is to use biomass in the form of chips/flakes of small size and load it into a cylindrical combustor. Air is provided at a

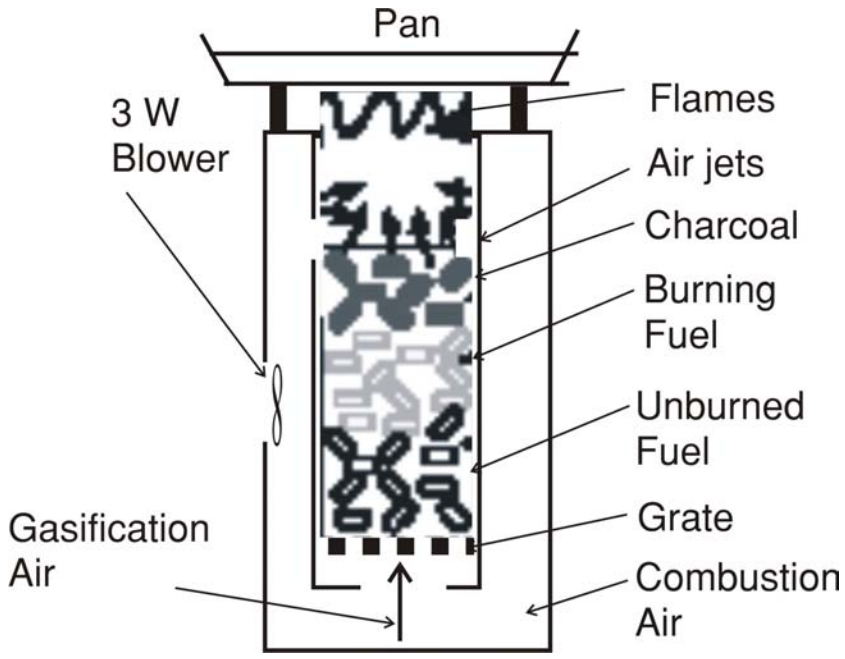

Figure 1.8: Gasifier stove with external power in the form of a 3 W blower from *Reed et al.* (2000)

positive pressure from the bottom. This air flow takes place through the bed to the top. The top is then lit with sprinkled alcohol or kerosene. The use of alcohol ensures smoke free start-up. The system now works as a reverse downdraft gasification system. The flame propagates towards the bottom. As it moves through the bed, the biomass loses volatiles and becomes char and the gases that come from the bottom pass through the char bed and get converted to producer gas. The gas comes out of the top of the bed at temperatures of 700°C to 800°C and is ready to burn. Air is introduced into the top region from the sides and this leads to combustion of the gas. Since definite amounts of air are introduced at the bottom and the top region, combustion can be expected to be completed in a short region. These result in a compact clean combustion system. This design uses a small blower of 3 W capacity to provide air for gasification as well as combustion and both the flows can be managed to control the power output and completeness of combustion for a 3 kW output as shown in Fig. 1.8. The ratio of power delivered by the stove in kW to the electrical power needed is about 1000 and this encourages one to design and deploy a small blower to improve the quality of combustion. Such small blowers are expensive and assume the availability of electricity. It would be necessary that the chips are relatively

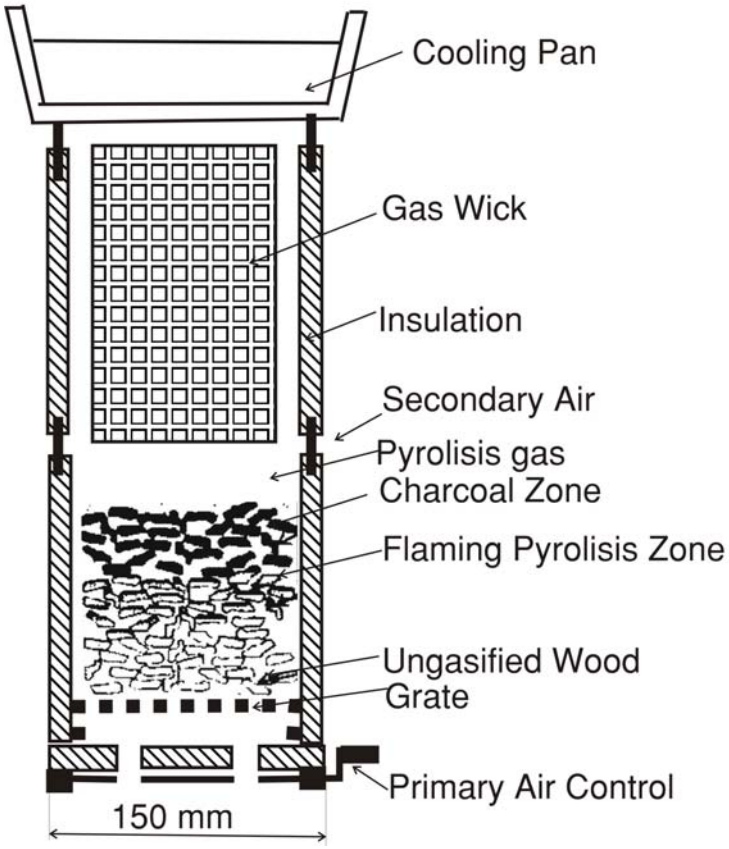

Figure 1.9: Gasifier stove without need for external power from *Reed et al.* (2000)

small in size to prevent short-circuiting of the flows. Thus one would need a prepared fuel and electricity for the operation. While the first aspect can be managed, to ensure the availability of power for the operation becomes a serious issue in rural environment of nearly all developing countries. One can then conceive of stored energy strategies. These lead to many complications that may not be workable in rural conditions. The design would also be expensive to build since the small power blower itself is expensive. Perhaps, when built in large numbers, cost would come down; but there seems no serious motivation towards this since the availability of electricity is uncertain in these situations.

The second design recognizes this and does not demand electricity. While the fuel loading strategy is the same as above, the combustion region is arranged to be around the vessel and this is achieved by having the cylindrical chamber around the vessel. Fig. 1.9 shows the details.

In this design, it would be necessary to use the vessel of the right kind for

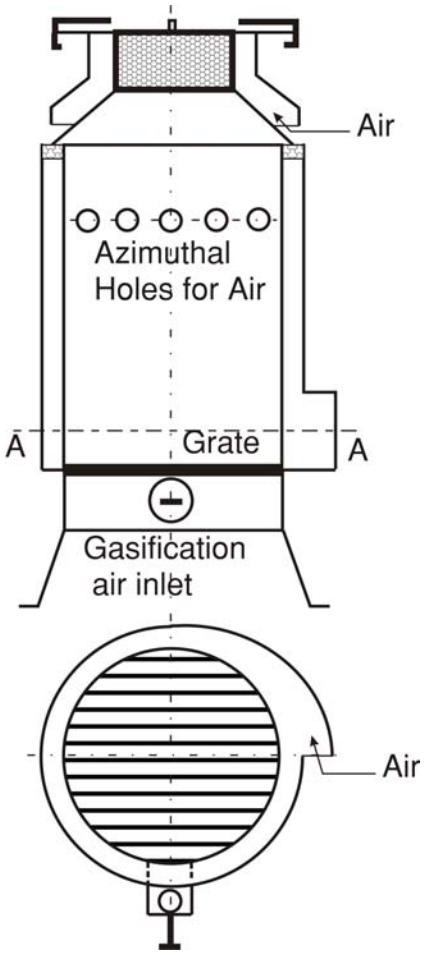

Figure 1.10: Gasifier stove without need for external power developed at CGPL, IISc

cooking. Also, the use of the stove will be limited to specific cooking items - cooking vegetables, rice and lentils. Frying over a pan becomes a problem that cannot be solved with this design.

Work was done at CGPL, IISc to overcome some of the deficiencies. Fig. 1.10 shows the design of the stove. A thin metal walled stove with an annular region for taking the air and delivering to the top region by free convection along with a bottom region from which air can be drawn through the bed by free convection constitute the essential features of the stove. The primary issue about the stove is that the matching of the flow rates to get stoichiometric mix of combustible gas and air for complete combustion takes place over a period of time smaller than the total operational period. This constitutes a loss of emission performance of the stove even though efficiency

by water boiling tests vary between 27 to 33%.

Most work done on stoves are those enabling the use of woody biofuel. This is due to perception over thousands of years in rural and other environments passed on from generation to generation that it is appropriate to use firewood for domestic use. Till about fifty years ago, the population was low all over the world, and nature provided for solid biofuels in plenty. The last fifty years has seen dramatic increase in population, large differences in economic levels between different strata of population and consequent indiscriminate use of natural biofuels. These have been caused by those living on the fringes of the forests as well as those having access to the powers to use forest biomass in the industrial sector or for urban needs with almost no thought for the consequences. This has become alarming that courts of law are passing judgments to protect the forest wealth. The poor and the needy are left with lower grade fuels arising from agricultural operations. These fuels like leaf droppings from trees, cotton stock, coconut pith, sugarcane tops and leaves as well as trash and a whole host of fine biomass is rarely employed as a cooking fuel since the technology simply does not exist. This is the reason for declaring them as low grade fuels even though they are in no sense inferior in terms of calorific values compared to wood. Combustion of these fuels in stoves always results in higher emissions as confirmed by measurements of *Zhang et al.* (2000). They have determined emission factors of over 54 fuel stove combinations of India and China. A summary of their results is shown in Table. 1.2. It can be seen that average emissions from crop residues are about 50% higher than woody biomass. Various biofuels like wood and crop residues are not significantly different in their structure and energy content. Loose biomass burns faster emitting more PIC's. Pulverization would convert these multiple fuels into common physical form (with a possibility of controlled combustion) and it needs to be used in sawdust-like stoves.

In the case of sawdust generated in timber processing units, a stove design has been prevalent over several decades in many countries. This stove is called the tube stove. Its scientific exploration was made only recently by *Mukunda et al.* (1993). The authors set out to examine the classical tube stove shown in Fig. 1.11 to ensure (a) smooth ignition, (b) good combustion with little soot or smoke, (c) as high an efficiency as possible, (d) a power level of 2 to 3 kW, and (e) the possibility of using different vessels and shapes. One of the points that was not paid attention to at this stage was the relative diameters of the port (vertical central region as in Fig. 1.11) and the horizontal segment that draws in the air. The bottom horizontal segment had the same dimension as the vertical portion. In this configuration it was found that having exposed segment of fuel, shorter than the

Table 1.2: Mean, minimum and maximum emission factors of each fuel type (gram of compound per kg of fuel)(*Zhang et al.*, 2000)

Fuel Type		CO_2	CO	CH_4	C_{TNMHC} [a]	TSP	NO_x	SO_2
Wood	Min	987	19.7	0.4	0.03	1.17	0.12	nd [b]
(Instant)	Mean	1450	58.7	2.7	2.27	3.05	1.16	0.01
	Max	1620	111.0	74.0	9.68	5.87	2.77	0.06
Wood	Min	1410	24.1	53.7	0.29	1.51	0.12	nd
(Ultimate)	Mean	1520	69.2	5.1	4.34	3.82	1.19	0.01
	Max	1630	123.0	19.9	17.70	8.73	2.78	0.06
Crop Residues	Min	834	23.6	0.04	0.05	1.12	3.93	nd
	Mean	1130	86.3	4.56	4.35	8.05	0.7	0.22
	Max	1370	223.0	15.90	19.70	29.0	2.21	2.64
Coal	Min	1070	11.0	nd	nd	0.03	0.08	nd
	Mean	2280	71.3	2.9	0.66	1.3	0.91	2.7
	Max	2910	210.0	16.9	6.9	10.0	3.86	20.5
Kerosene	Min	3120	2.4	nd	0.09	0.05	0.22	nd
	Mean	3130	7.4	0.03	0.39	0.13	1.1	0.03
	Max	3130	10.9	0.06	0.92	0.28	1.69	0.06
Gases	Min	1850	nd	nd	nd	nd	0.07	nd
	Mean	2980	3.7	0.14	1.6	0.26	1.76	0.33
	Max	3440	31.2	1.62	8.8	1.62	4.51	2.54

[a] Gram of carbon in TNMHC.

[b] nd: not detected or background level greater than flue gas concentration.

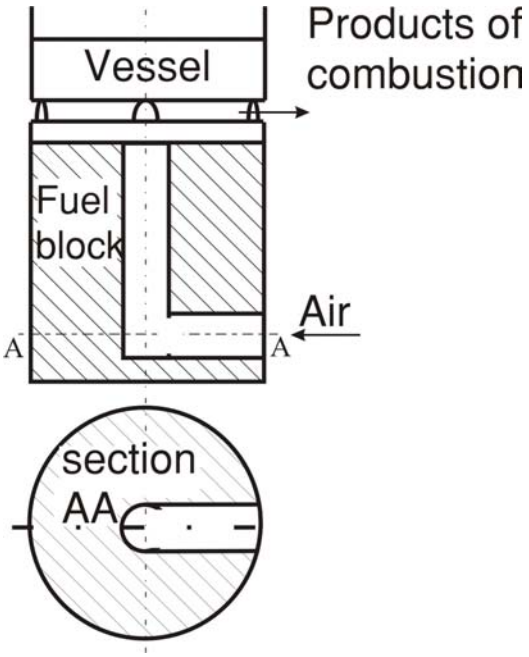

Figure 1.11: Tube stove for sawdust

fuel web thickness for volatilization helped causing smooth ignition. If this segment was larger, lower portion of the stove generated large amounts of heat resulting in large amount of volatilization. Almost from the beginning, the power level became so large that the stove functioned in a highly fuel rich state and unburnt products escaped into surroundings. This obviously caused smoking of the stove. They have conducted experiments over a range of parameters like the height-to-port diameter ratio, outer-to-port diameter ratio and determined the power level dependence on the port diameter as well as the above mentioned ratios, and also determined from the rate of propagation of the pyrolisis front, the web required to meet the demand of a specific burn time. From these data, correlations have been generated for designing a stove for a given power level and a burn time. They have brought up the use of multiple ports but not adequately addressed the performance behavior.

Kapur et al. (1984) have discussed a tube-in-basket burner for rice husk. The design proposed is specific to rice husk and is not applicable for pulverized fuel in general.

Ravi et al. (2002) have used computational tools to study the combustion behavior of tube stoves. While the actual details of the calculation are unavailable in the paper, the results show that the peak temperature does not

exceed 1100 K. In fact most of the tube is filled with gas at 500 to 700 K. This cannot happen in a vigorously combusting system unless unrealistically low reaction rate parameters have been set. This conclusion appears consistent with the wide profile of carbon monoxide and oxygen over the same zone. They seem to have abandoned the infinite reaction rate hypothesis because of unrealistically high temperatures. In a finite reaction rate process with only a forward reaction step, use of a proper specific heat would have allowed the realistic peak temperature to be achieved. And in a diffusive combustion process that the stove experiences, the infinite reaction rate assumption would have provided a model for consumption rate to be predicted, if needed.

1.3 What is Planned for the Present Work?

A review of the literature suggests that fine agro-residues need consideration. These cannot be used in a classical wood stove because the burn rate is very large and hence, each feed would be consumed fast and undesirable emissions would indeed be an issue following the results of Prasad and colleagues discussed earlier (Fig. 1.1). This leaves an alternate namely a tube stove. Tube stove has been known for use with sawdust. It has not been explored for other fine agro-residues that are in powder form or close to it so that the material can be pulverized and used in the stove. There are other stove designs like basket stove for rice husk (Kapur et al 1984); but these are so specific that they cannot be recommended for a mix of fuels. In any case rice husk is an industrial agro-residue and cannot be considered available for domestic use in a larger picture of changing scenario of bio-fuel use in which rice husk is contemplated for power generation using fluidized bed combustion based boiler-turbine systems. Also the earlier studies including those conducted at this laboratory have not addressed the issue of clean combustion adequately. The work by *Mukunda et al.* (1993) which is the only work in this area discusses the quality of flame as 'bluish' or sooty and the central scientific basis for this behavior has not been examined. Thus the aim of this work is to (a) extend the study of the standard tube stove to examine if the basis of functioning can be traced to gasification and subsequent combustion, (b) make necessary measurements of the thermal field and compositional field, both in the gas phase (g-phase) and the condensed phase (c-phase) and relate them to the operational behavior of the stove, (c) examine if the operation of the stove in the gasification mode can be extended to the complete duration of the operation and in requiring to do this, examine several conceptual variants of the stove design, (d) support several of the above conclusions, particularly the gasification and combustion modes

of functioning by a reactive flow computation of the stove, and (e) evolve a few configurations that may be practical to meet the objectives of a multi-fuel agro-residue based pulverized fuel stove meeting as many objectives of a good design as possible.

The approach taken in this work is to first examine a number of configurations that were evolved in a step-by-step manner towards the goal of obtaining clean combustion; when it could not be adequately obtained, to characterize the extent and maximize it. In doing this search, it was uncovered that the stove would extinguish and needed re-ignition. This was thought as an important issue and the reasons for local extinguishment, more importantly, the conditions leading to extinction were to be uncovered. After these conditions discovered, the methods to overcome them are addressed. When these were resolved, the principal question of how much energy could be gotten out of a given stove was addressed. Initial experiments showed that extraction of energy at power levels lower than 25% of peak power level seemed unattractive to users. Hence, a criterion was defined as to how much energy could be extracted at power levels beyond 35% of the peak power. This also meant enquiring as to what power level the stove would function up to a certain period of time. This period of time was chosen as an hour because this period was noted from field level studies on cooking practices in villages. Thus both power level of the stove for an hour and the fraction of mass consumed in this duration without re-ignition were taken as the criteria for the choice of the parameters for the stove design.

The operating power level of stove is an important design parameter which has been addressed at length in *Mukunda et al.* (1988). They have stated stoves capable of transferring 0.6–2 kW to the pot are most suitable for kitchen applications. This was derived from an analysis of earlier work and the authors' own experience with stoves. Stoves transferring 0.6–1 kW to the pot which implies an input power of 2–3 kW is considered for study in the present work.

Chapter 2

Tools and Techniques

This chapter describes various tools used during the study of pulverized fuel stove. Various materials used as fuels are listed and described. Typical experimental procedure employed during the course of experimental study is given followed by a brief outline of different measurement techniques used during experimental study.

Figure 2.1 shows a representative single port stove configuration used during experimentation. The typical configuration of pulverized fuel stove consisted of a vertical central port with horizontal air inlet(s) at bottom. The stove was prepared by packing sawdust / pulverized fuel into a cylindrical metallic container. The fuel block thus prepared had a central port and horizontal air inlet(s) at the bottom for providing gasification air entry.

The density of packing has a major influence on the combustion process and power delivered. Normal packing gives a density of 225 kg/m^3. Hard packing gives 300 kg/m^3 (both with sawdust of intrinsic density of 560 kg/m^3).

Experiments were conducted in this stove for various port diameters (d) and heights (h). A parameter aspect ratio, which is the ratio of port height above air inlet to port diameter, was used to characterise the port geometry.

Various measurements made on this and other configurations of pulverized fuel stoves included weight loss vs time to know the power level of stove, c-phase temperature distribution, c-phase pyrolysis front propagation rate, g-phase temperature and distribution, g-phase composition, efficiency and emission measurements.

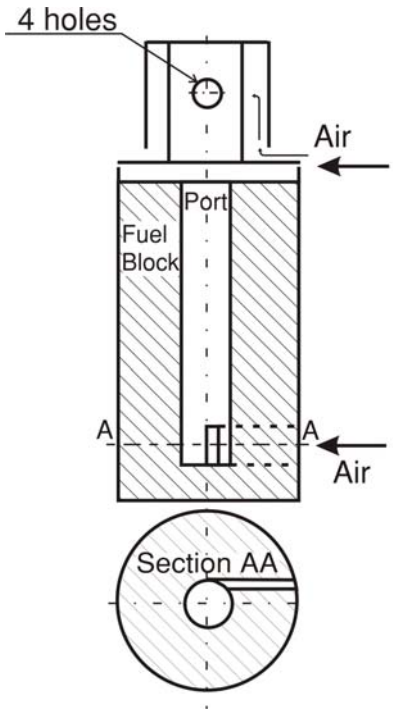

Figure 2.1: A schematic diagram of single port pulverised fuel stove

2.1 Materials

Tube GAS stove (TuGAS stove, for short) was tested for different types of powdery biomass. The fuels used were sawdust and pulverized fuel. Experiments were conducted using sun-dry sawdust (10% moisture) sourced from local saw mill. Sawdust and pulverized fuel used are characterized by properties like particle density, moisture content and particle size distribution. Sawdust can have wide ranging particle densities (400 kg/m^3 to 1100 kg/m^3) depending upon the source from which it is obtained. Pulverized fuel is prepared from various leafy biomass separately collected from tree fallings. The leafy biomass was pulverized using hammer mill of capacity 30 kg/hour. A mesh size of 3 mm was used giving an average particle size of 1 mm. Pulverized fuel thus generated can be loaded into stove to obtain performance similar to sawdust stove. Pulverized leafy biomass on which tests were conducted include (*Anon*):

Leucaena leucocephala (Soobabul): Extensively planted worldwide and covering up to 5 million ha at present. In India it is thought to be a weed with tremendous natural regeneration. This plant is cultivated as a fod-

der species and for green manure. This is also cultivated as an energy plantation. Native of tropical America and now cultivated throughout tropics (Pan-tropical) The bio fuel obtained in the form of pods was pulverised and used in the present study.

Dendrocalamus strictus (Bamboo): The lower parts of the culms are sometimes solid. Drought tolerant. The most common and most useful bamboo in India. Combustion characteristics of the leaves of this tree was studied.

Acacia auriculiformis (Firingi jali): This plant is cultivated extensively in the social forestry program and native of tropical Australia. Planted widely in the Old World for pulp and fuelwood, particularly in India and Southeast Asia. Leaf droppings of this tree was used in the pulverised fuel stove.

Figures 2.2 (a)–(c) show photographs of these leafy biomass in their natural form.

2.2 Experimental Tools

The experimental studies on the stove consisted of measurement of mass loss rate, temperature, oxygen and composition. The pyrolysis front location in c-phase was also determined.

The tools used for these studies were

- Weighing balance
- Thermocouples
- Oxygen monitoring equipment
- Gas analysers
- Data acquisition system and computer

The following subsections describe these tools.

2.2.1 Weighing balance

A strain gauge based weighing machine with digital display and RS-232 output which could communicate mass data to personal computer were used for measurement of instantaneous mass of fuel during stove operation. The

(a) Lucaena Leucocephala

(b) Acacia Auriculiformis

(c) Dendrocalamus Strictus

Figure 2.2: Photographs of leafy biomass in their natural form.

Figure 2.3: A photograph of the weighing machine.

interface details are given in Appendix A.3. The instrument had 15 kg range and 0.5 g least count. The steel weighing platform was of size 200 mm × 250 mm. In order to shield the balance from heat transmission, 20 mm thick refractory brick was placed between the weighing platform and the stove in the photograph of Fig. 2.3.

ASCII Data was transmitted to the computer through RS-232 interface. Four combinations of data output from balance were possible: gross and tare, net and tare, gross and net, and count. Of these, gross and net were selected for all the experiments. Data transmission modes available were 'continuous send' and 'send after weight is stable'. Data transmission was set to continuous send mode. The serial set up used was 9600 baud, 8 data bits, 1 stop bit and no parity.

Earlier, exploratory experiments were conducted using 15 kg range, 2 g least count weighing balance with only a digital display without interfacing capabilities. During this phase of experimentation mass data was recorded manually at known times. Both the balances used were calibrated against

standard mass to verify the accuracy of mass records obtained. Data from various measurements were acquired and stored in digital form. Noise in data was removed using averaging technique.

2.2.2 Thermocouples

Temperature measurements were made in c-phase as well as g-phase of the stove. Depending upon the requirement, thermocouple probes were designed and used. The c-phase temperature measurement was made using K type mineral wool insulated thin thermocouples (100 μm diameter), R type 50 μm bare wires with different mounting techniques were used for c-phase and g-phase measurements and R-type 100 μm bare wires with suitable mounting techniques for g-phase measurements. K type shielded thermocouple was used for g-phase measurements during exploratory phase of experimentation.

All the thermocouple junctions were formed using oxy-LPG flame as heat source. Bead sizes were gauged using travelling microscope. Junction sizes of 50 μm R type wires were about 120 μm while 100 μm wires had junction sizes about 250 μm. Radiation correction based on bead size was applied suitably. The procedure employed for radiation correction is set out in Appendix A.2 The calibration of mV output in terms of temperature for various types (K and R) of thermocouples was available in the data acquisition system itself. Temperature of boiling water was measured to check the correctness of calibration.

2.2.3 Oxygen monitor

Oxygen measurement is made using chemical cell based oxygen monitoring equipment. A photograph of monitoring equipment used is shown in Fig. 2.4 (a). The monitor is capable of sensing volumetric composition of oxygen based on partial pressure of oxygen in the sample gas to which cell membrane is exposed. The cell output is about 11 mV in ambient air and it falls linearly to zero in nitrogen atmosphere. The Figaro make (Japanese) cell (KE-25) has a response time of 14$\pm$2 s in which 90% of applied concentration level is recorded. A faster response (95% response in less than 10 s) 'citicell' (from UK) make cell was also used during experiments.

The sample gas from the combustion region was drawn through a probe and a calcium chloride filter as shown in Fig. 2.5 (a). The typical system volume downstream of sample probe inlet including cooling and cleaning space was about 50 ml. It was found that typical sample gas flow rates of about 5 l/hour through the sensing volume was enough for monitoring oxygen. This

(a) O_2 monitor Unit

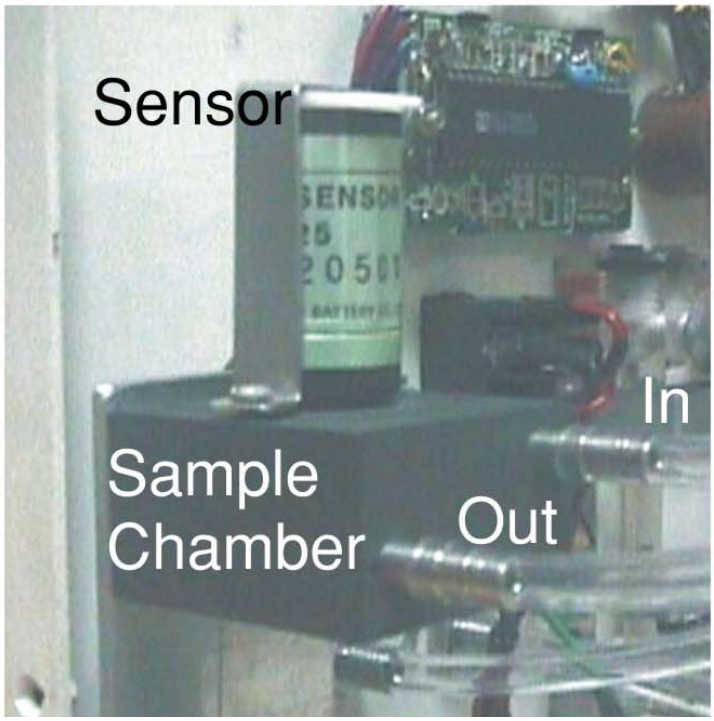

(b) Sensor Mounted on chamber

Figure 2.4: Oxygen monitoring equipment

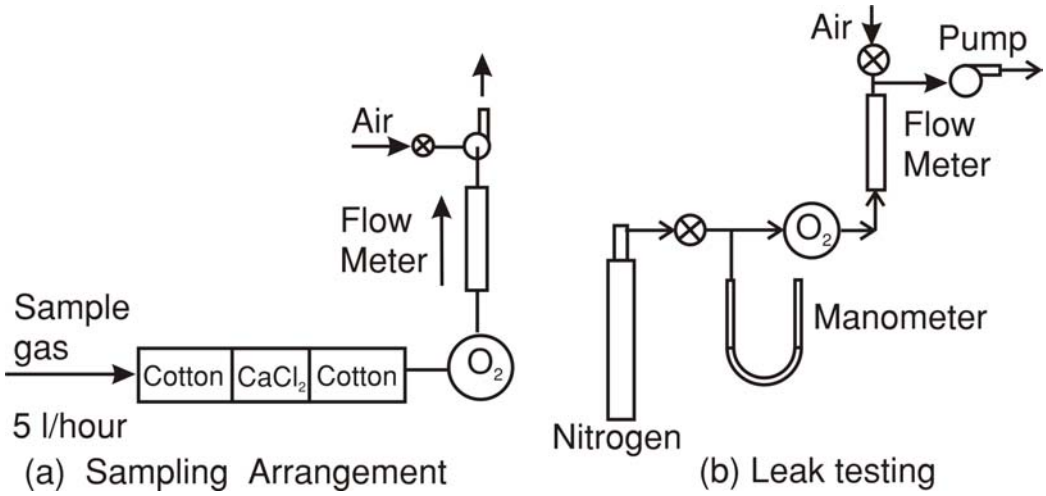

Figure 2.5: Sample gas conditioning and sensor mount leak testing.

means the sensor will see the sample 36 s after it enters probe inlet. This delay was accounted for while analyzing simultaneous measurements.

Depending on the location of diaphragm pump relative to monitor, sample gas could be drawn or pushed through oxygen monitor. The sample gas was drawn through the monitor to minimize the volume between sample gas inlet and the sensor and also to reduce the number of system elements that could potentially cause leakage. This also allowed bypass control of pump as just sufficient fraction of available suction could be applied at the monitor outlet. This necessitated the sensor mounting on the sampling volume chamber to be leak proof. This leak testing was done using an arrangement shown in Fig. 2.5 (b). Bottled nitrogen was allowed to enter monitor at the specified flow rate at a positive pressure. Then pump suction was applied such that pressure in the sensor chamber became negetive. If the monitor was leak tight, it would read zero for nitrogen flow in either case.

Oxygen sensor output was conditioned in the monitoring equipment to provide a linearized output of 0–1 V. The oxygen monitor output was calibrated in ambient air and nitrogen to fix ambient and zero oxygen concentrations. The oxygen monitor output was acquired through personal daq equipment using dasylab software. The monitor output was converted to oxygen volume percentage by using suitable multiplier.

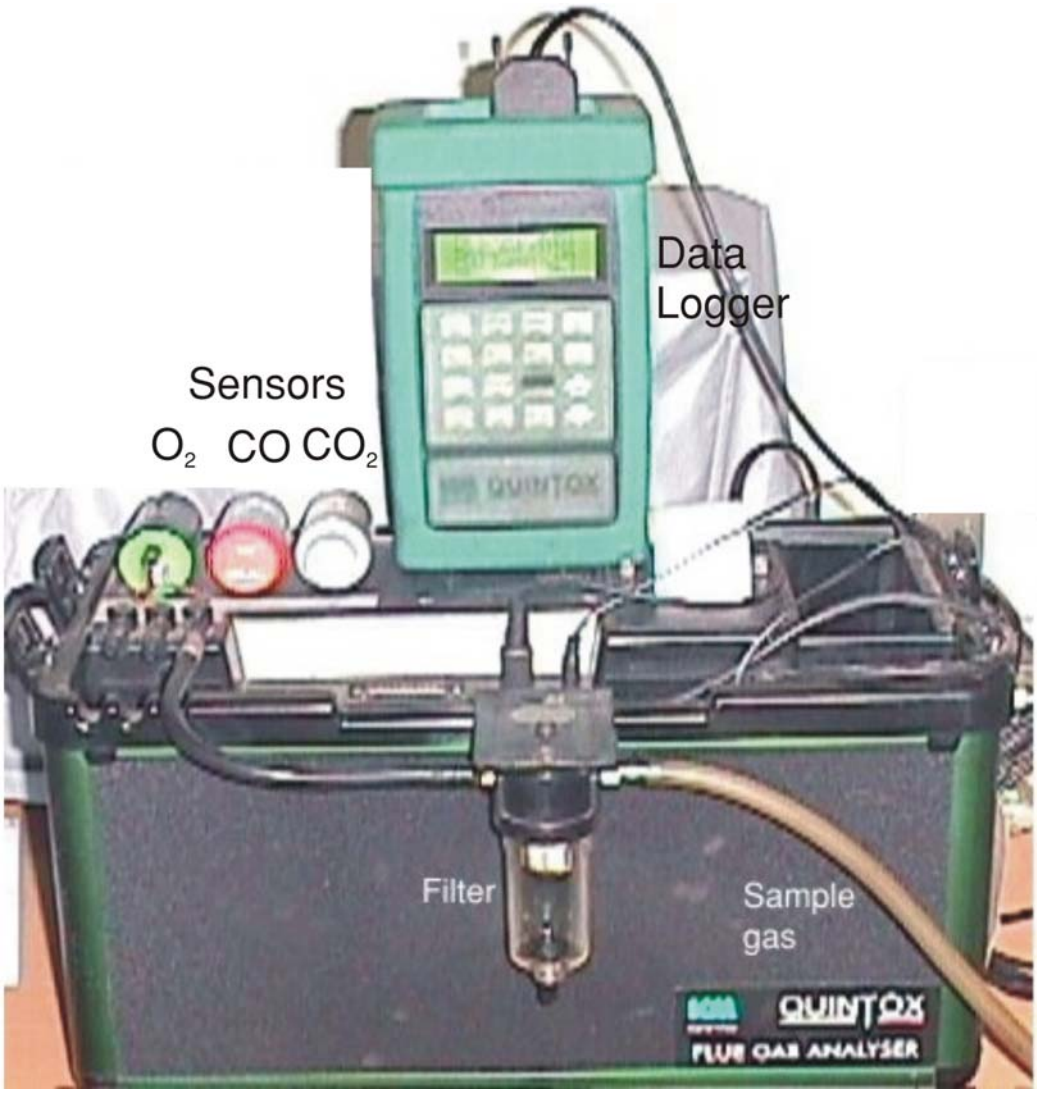

Figure 2.6: Quintox analyzer used for composition measurement.

2.2.4 Composition Analyzers

Composition measurement was made using two different analyzers. They are the UK make Quintox analyzer shown in Fig. 2.6 and German make Maihak gas analyser shown in Fig. 2.7. Quintox analyser had a built-in pump of a nominal flow rate 2 l/min. The sensors used were NDIR (Non Dispersive Infra Red) type except for oxygen which was a chemical cell. Analyzer also had a built in paper filter. Composition measurement during exploratory studies was made using Quintox analyser shown in Fig. 2.6 (a). The gases

Figure 2.7: Maihak analyzer used for composition measurement.

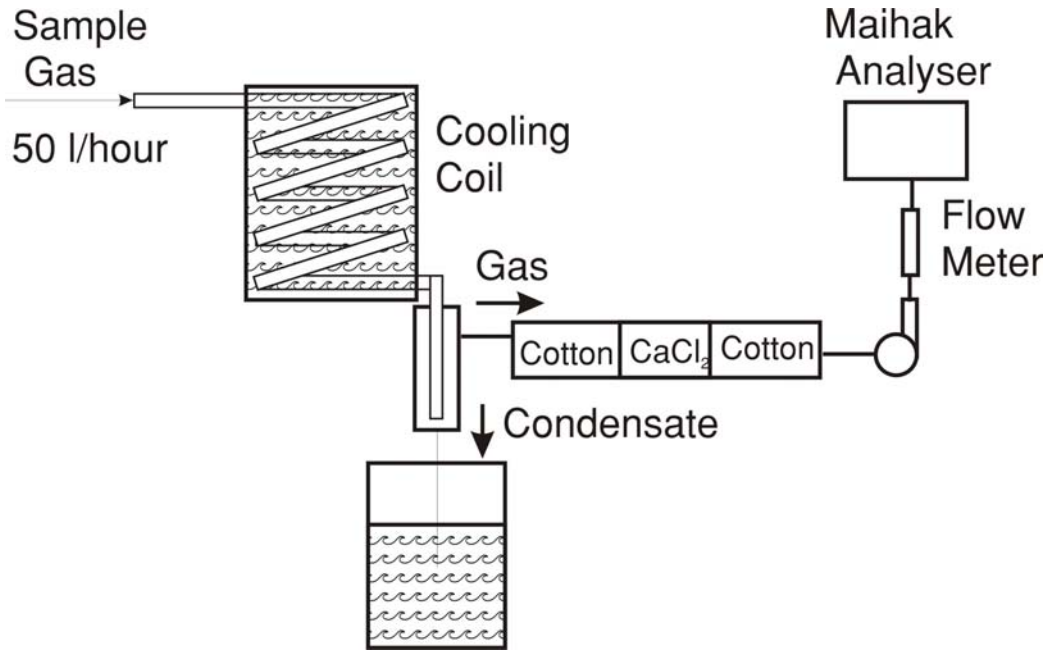

Figure 2.8: Sample gas conditioning circuit.

analysed are CO, CO_2 and O_2. Specifications for CO are range 0–10%, accuracy ±5% of reading from 0.1–10%, resolution 0.01%. Specifications for CO_2 are range 0–'Fuel value', accuracy ±0.3%, resolution 0.1%. Specifications for Oxygen are range 0–25%, accuracy −0.1 to +0.2% and resolution 0.1%. The calibration of instrument was checked by measuring composition of calibration gas whose true composition was known apriori. Equipment had a print out facility through which composition data could be recorded.

Maihak Analyser had the necessary CO range for gasification measurements. G-phase composition was analysed for CO, CO_2, CH_4, O_2 and H_2. The sensors are based on Non Dispersive Infra Red (NDIR) technique except for O_2 which is paramagnetic and H_2 which is thermal conductivity type. Measurement range for vol % of various gases are CO 0–25%, CO_2 0–25%, CH_4 0–10%, O_2 0–25% and H_2 0–20%.

The instrument was supplied with conditioned sample gas at a minimum required flow rate of 50 l/hour. A separate pump was used for this purpose. Hot gas was first cooled by passing it through a copper coil. Moisture condensed was drained to a water trap. The sample gas was further conditioned by passing the gas through cotton filter with a layer of calcium chloride for moisture removal. Figure 2.8 shows the typical arrangement employed for sample gas conditioning. Instrument is calibrated using calibration gas of

Figure 2.9: Personal daq USB based data acquisition system.

known composition (by Gas Chromatography) obtained from Bhoruka gases limited before measurements are made to ascertain accuracy of measurement.

The instrument is capable of PC interface through RS-232 port. The interface details are given in Appendix A.3. The serial set up used was: 9600 baud, 8 data bits, 1 stop bit and no parity. Analyser was capable of collecting data at various time intervals minimum being 1 second.

2.2.5 Data acquisition system and computer

The US make Iotech Personal Daq data acquisition system was used to acquire data from thermocouples as well as oxygen monitoring equipment in most of the experimental measurements made. Figure 2.9 shows a photograph of this unit. The analog signal outputs were acquired into PC through this data acquisition hardware. This system digitized analog data and communicated it to computer through USB port. The system was supplied with 12 V DC, 1000 mA power externally. The system has a scanning speed of 80 Hz. The instrument is capable of acquiring data from a maximum of 20 differential inputs which could be from thermocouples, voltages or both, when used along with channel extension unit.

The highest acquisition rate possible in personal daq equipment is 80 Hz.

This corresponds to a sampling duration of 12.5 ms when acquiring data from a single channel. Sampling duration for each channel represents the integration time for that channel.

The sampling duration has a direct bearing on sampling rate. If data is being acquired by several channels, the acquisition rate is automatically adjusted to the maximum possible value based on sample duration and number of channels, with a message to that effect. The sampling duration of each channel is an input acquisition parameter which could be selected from a set of values given in a pull down menu, ranging from 12.5 ms to 640 ms.

R type thermocouples used for data acquisition were from 50 μm and 100μm diameter wires with junction sizes between 120 μm and 250 μm diameter. The time constant variation was about 10 to 40 ms for these thermocouples (Calculation is given in appendix A.1). A sampling duration of 110 ms was set for data acquisition during experiments.

Data acquisition system had provision for selecting the type of thermocouple (K, R etc.,) and it provided for automatic ambient temperature compensation for the type of thermocouple selected. Setting was made specifying the type of thermocouple so that suitable calibration and ambient temperature compensation could be applied while acquiring data from personal daq unit.

A few experiments were also made using a high speed PCI slot Data acquisition system, DAC 2000 which has scanning rates of 200 kHz. This unit had a separate thermocouple interfaces DBK-19 card for thermocouples and DBK-13 card for voltages. These experiments were made at high acquisition rates using filters to remove noise to confirm certain observations made from personal dac based measurements.

A 700 MHz, 512 MB RAM windows 2000 Operating System Personal Computer which was a part of Local Area Network was used for data acquisition. This gave good portability for data. Dasylab software was used to acquire, display, store and manage data. This software facilitated simultaneous acquisition from RS-232 port as well as USB port (personal daq) of the computer.

2.2.6 Hood for emission measurement

Experiments were conducted to determine emission factors of pollutants, Carbon monoxide and oxides of nitrogen. For measurement of these quantities standard hood design was used. The hood was constructed according to the specifications prescribed in CIS 1315 z (Part 1) 1991, Annex–2 of Bureau of Indian Standards. A dimensioned sketch of hood used along with experimental arrangement is shown in Fig.2.10. The hood method of de-

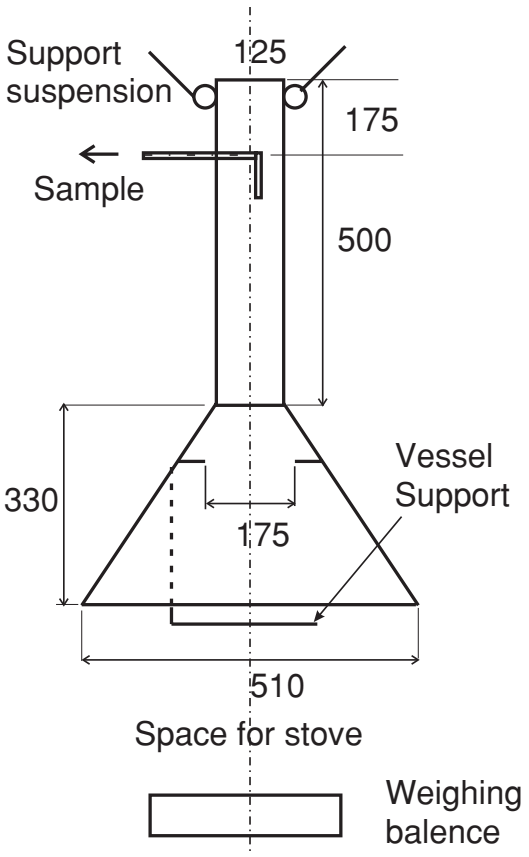

Figure 2.10: Hood employed for emission measurements

termination of pollutants is widely accepted technique (*Bhattacharya et al.*, 2002b; *Smith et al.*, 1998; *Ballard-Trameer and Jawurek*, 1996). The method will give accurate results provided it is made sure all the products generated during stove operation pass through the hood and hood does not interfere with stove operation (*Ballard-Trameer and Jawurek*, 1996). During experiments volumetric concentrations of CO, O_2 and NO_x were measured. The method employed for calculation of emission factors of these pollutants from biomass of known composition is given in Appendix B.

2.3 Experimental Procedure

Figure 2.11 shows the schematic diagram of a typical fuel block tried during the course of experimentation. The procedure followed to construct this fuel block is set out below. The typical configuration of pulverized fuel stove

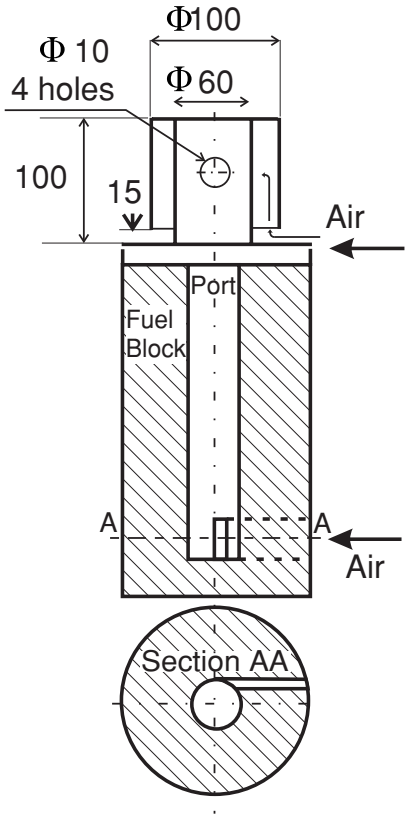

Figure 2.11: A typical fuel block structure with combustion device in position.

consisted of a vertical central port with horizontal air inlet/s at bottom. The stove was prepared by packing sawdust / pulverized fuel into a cylindrical metallic container. The fuel block thus prepared had a central port and horizontal air inlet/s at the bottom for providing gasification air entry. To prepare such a fuel block the typical procedure adopted would be as below.

Required amount of Sawdust / pulverized fuel was weighed and set apart. Required amount of fuel depends upon fuel block volume and the desired density of operation. The single inlet stove had a 30 mm size side window at a location about 25 mm from the bottom. Powdery biomass was filled up to the bottom level of side window and was rammed thoroughly to form a pulverized biomass bed. A Poly Vinyl Chloride (PVC) tube of required diameter (40 mm, say) with a slit in bottom as shown in Fig. 2.12 (a) to serve as a locator for horizontal limb is centrally placed properly aligned with side window. A annular locator inserted at the top helped to achieve this. A 30 mm high thin wooden piece/s was inserted from side into the locator groove provided in the vertical tube as shown in Fig. 2.12 (b). Powdery biomass

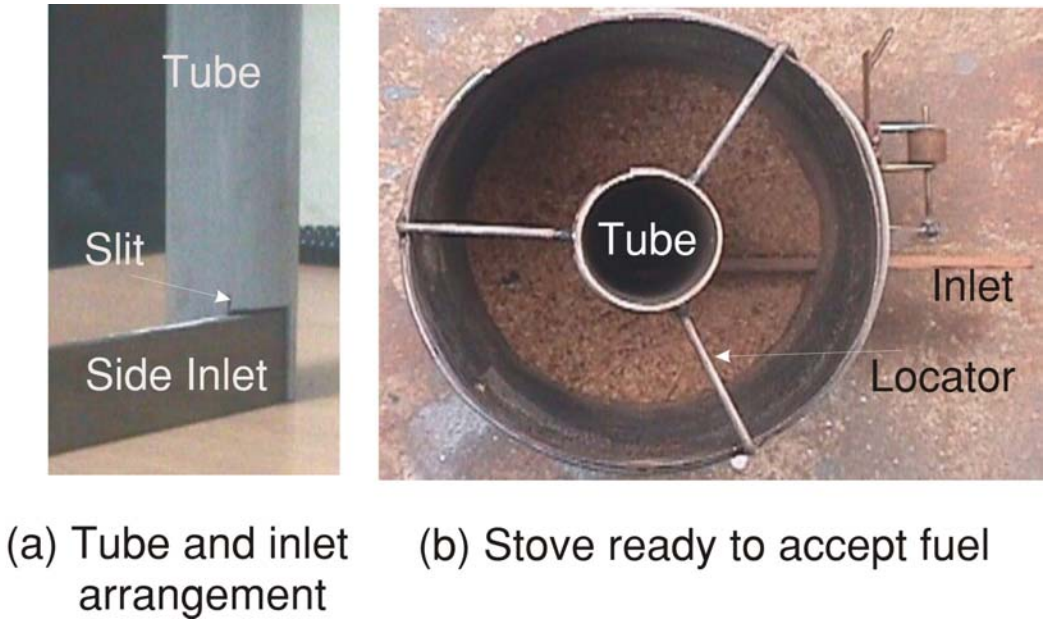

Figure 2.12: Sketch showing tools for fuel block preparation.

was properly packed around the side inlet. Fuel was then poured into the container and rammed in position with the help of a 25 mm diameter wooden stick. Then all the remaining sawdust was poured into container and rammed such that fuel block top surface was 5 mm below the container rim. The tube used to cast the fuel block was pulled out in a gradual fashion just before ignition of fuel block. The wooden piece used to form horizontal inlet/s was also pulled out.

The port and inlet were inspected using a light source for possible blockages due to sawdust collapse. Preparation of the fuel block required care as horizontal inlet dimensions were small and if air inlets became blocked due to loose sawdust in the port bottom, functioning of stove was seriously impaired. The air inlets were cleaned using thin stick without disturbing compacted fuel. A few drops of kerosene were sprinkled around the rim of port as well as port bottom to aid ignition. Ignition of fuel block required a sequential procedure where fuel block was ignited at the top, first to create necessary draft for establishment air flow into the fuel block. Then air inlet/s at the bottom were ignited one by one. After this, the top cover or combustion device was placed over the fuel block with proper centering.

Any deviation from this procedure was limited to fuel block preparation and was generally due to requirements dictated by measurements made. These variations are brought out in the next section.

2.4 Measurement Techniques

In this section various measurement techniques employed during the course of investigations are presented. The measurement techniques employed for pyrolysis front location, c-phase and g-phase temperature, composition of oxygen and in some cases other components are discussed separately. In c-phase, the quantities measured were temperature and location of pyrolysis front at various times. In g-phase, temperature, volumetric composition of oxygen and composition measurements were made. The techniques employed to make these measurements are described in the following subsections.

2.4.1 Pyrolisis front location

The position of pyrolisis front at various times in a combusting stove is indicative of fuel consumption pattern in the stove. This was determined using a novel technique consisting of introducing thin paper sheets into the fuel block radially. A typical example of positioning the paper sheet at locations 120 degrees apart is shown in Fig. 2.13. Paper sheets of suitable size were positioned in the stove at the required position and then, sawdust was poured for compacting, thus embedding the paper sheets into the fuel block. Care was taken to see that sawdust was properly compacted on either side of paper. The edge of paper was stiffened using thin plywood strips to facilitate removal of paper sheet. Fuel block was ignited and allowed to function for a known duration after which, air was isolated from fuel block using ceramic wool blanket. This ensured that combustion was arrested. Paper sheet/s were retrieved by pulling them out, holding the plywood sheet reinforcement. This technique provided a method to examine the fuel consumption pattern in the c-phase.

2.4.2 C-phase temperature

C-phase temperature measurements were made with the aim of determining radial and vertical temperature distributions in the fuel block. Two different measurement techniques were employed. Mineral wool insulated 100 μm diameter thermocouples were used to determine radial temperature distribution. The technique employed to locate thermocouples at the desired position in the c-phase consisted of pasting thermocouples using tree gum on to a piece of paper of same dimensions as one half of the cross section of fuel block. A schematic with thermocouples in position is shown in Fig 2.14 (a). The paper had an edge stiffened with a thin strip of plywood as explained in 2.4.1. Thermocouples were located on this paper sheet with junctions located

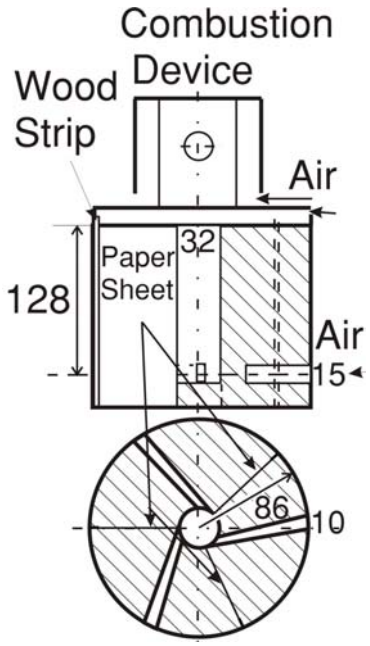

Figure 2.13: Sketch showing location of paper sheets in fuel block.

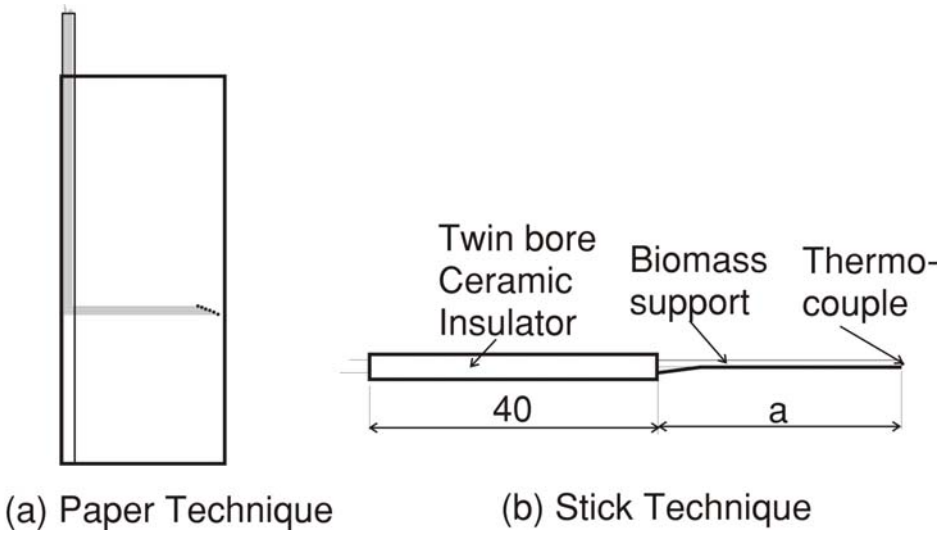

Figure 2.14: Techniques employed for preparing sensors for c-phase temperature measurements.

at the desired position and in this position they were glued to paper sheet. Coordinates of junctions were measured and the paper sheet was integrated into the fuel block such that measuring junctions of the thermocouples are at the desired positions. Stove was packed as explained in the previous section. Sufficient care was taken to see that sawdust was properly packed on either side of paper sheet. Then cold junctions were taken out from the top edge of the fuel block and were connected to data acquisition system. The stove was allowed to function for the required duration after which paper sheet was extracted to obtain simultaneous record of pyrolysis front location and corresponding temperature.

A second technique that was employed consisted of mounting R type 50 μm wires on to a coconut leaf rib as shown in Fig 2.14 (b). Biomass was employed for mounting thermocouple as it would blend with biomass of fuel block and pyrolyse along with it offering minimum intrusion to the processes that took place in c-phase. Bare wire thermocouples were mounted on thin coconut leaf ribs such that junction would sit on one end and junction was pasted to the biomass stick using a cyano - acrylate based adhesive. The other end of stick was inserted into a hole of twin bore alumina based ceramic insulator, about 50 mm long, through which thermocouple wires were passed. This arrangement could be inserted to the required depth into prepared fuel block through 3 mm diameter holes made in the stove wall. Cold junction was at least 45 mm away from stove wall. A 40 mm long 3 mm inner diameter mild steel tube welded to stove body served as a support which would maintain the position of junction in the c-phase. The probes are wound with teflon tape to prevent bare wires from touching the metallic body of stove. The central theme of all techniques involved usage of biomass for supporting thermocouples. This strategy is found to give reliable results.

2.4.3 G-phase temperature

G-phase measurements were made using 50 μm and 100 μm diameter R type thermocouples. During the exploratory phase of experimentation g-phase temperature measurement was made by introducing a K type shielded thermocouple embedded in 1 mm diameter inconel tube into g-phase through c-phase in radial directions at known length intervals. A minimum of 20 data points were recorded at each location and temperature at that location was determined as average of all these values. During later experimentation, three different mounting techniques were employed for measurement of g-phase temperatures. These techniques are described as follows.

50 μm diameter R type thermocouples were used in the first technique where measurements were made in aspect ratio 4 stove. It was thought pru-

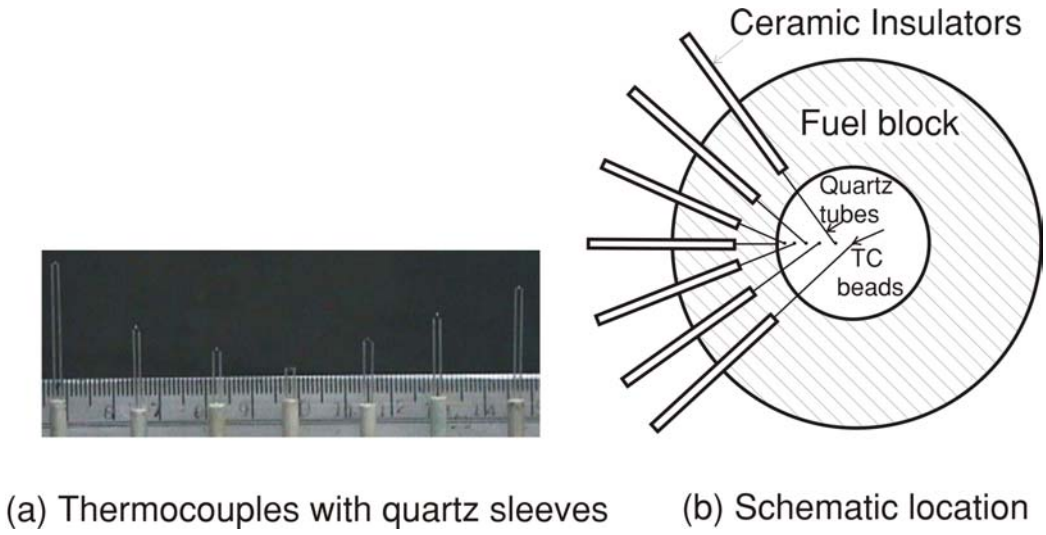

Figure 2.15: Location of thermocouples for g-phase temperature measurement.

dent to use R type thermocouples as g-phase temperatures were likely to exceed the measuring limit (1200°C) of K-type thermocouples when stove was functioning with flame in port. Fig. 2.15 (a) shows photograph of a set of thermocouples. Thermocouples were put into g-phase as shown in Fig. 2.15 (b). Maximum projection into g-phase was 20 mm since radial distribution was all that was looked at. Thermo-couple probes were prepared with quartz sleeves of different lengths so that hot junctions could be put at desired positions in the radial direction with shortest possible overhang. Thermocouples were positioned at a location about a port diameter (40 mm) below fuel port exit. Construction of fuel block turned out to be tricky. Fuel block was first compacted up to the level where thermocouples were required to be positioned using a flexible cardboard sheet wound tube. Central PVC tube which served as core was removed leaving the card board sheet in position. Thermocouples were inserted into g-phase region in a staggered arrangement shown in Fig. 2.15 (b). Fuel block over this level was constructed by hand. The paper sheet strengthened the port surface and prevented it from collapsing. It turned out that central flexible card board sheet remained in position altering flow patterns in the port.

The next experiment was conducted using the same set of thermocouples. In this run the fuel block was prepared without internal paper support. Stove was carefully packed with central core up to the level where the thermocouples were required to be positioned and then the central tube was removed. The thermocouples were inserted into the fuel block. Then, using moist saw-

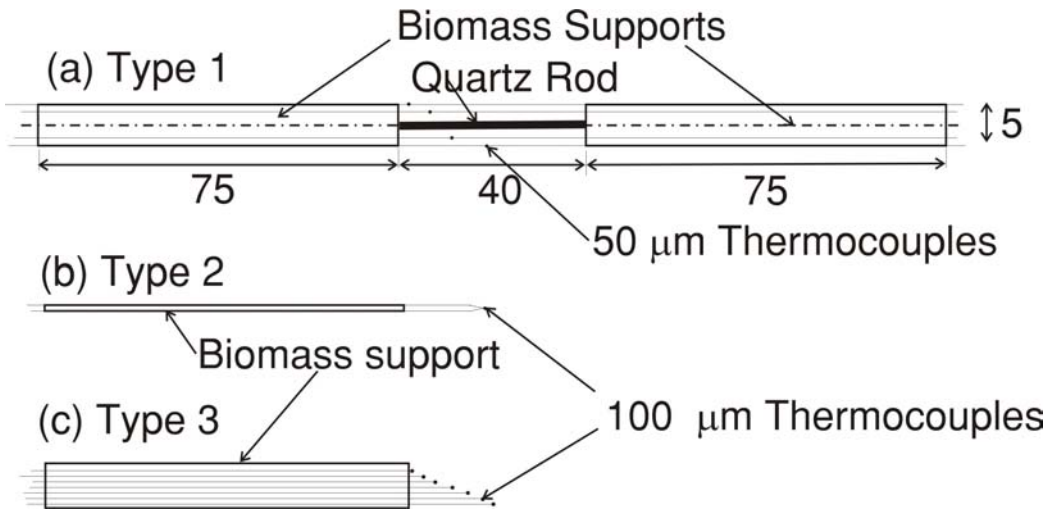

Figure 2.16: Types of thermocouple sensors for g-phase measurement

dust mixed with a little amount of tree gum, the port structure above the thermocouple level was completed. Moisture and gum in sawdust gave necessary strength to bind sawdust particles together during construction of port above the level of thermocouples. Four experiments were conducted using this technique. Separate sensors were built for each run as quartz sleeves were good for one run only.

The second technique consisted of mounting thermocouples on to a wooden cylinder (A piece of pencil) 5 mm in diameter with a central quartz tube 2 mm in diameter as shown in Fig. 2.16 (a). The central quartz tube, 40 mm long, was heated in the g-phase while wooden ended traverse the c-phase. Thermocouple beads were at known distances from wooden ends of quartz tube distributed on the circumference of the cylinder. Thermocouples were stretched across and pasted using cyano - acrylate adhesive. This assembly was inserted into the packed stove radially in a careful manner. This technique avoids manually constructing fuel port over and above thermo-couple level. Measurements were made at a level 120 mm above air inlet.

In the third technique 100 μm thermocouples were used. Probes were prepared by mounting them on coconut leaf ribs as explained in subsection 2.4.2, the difference being the hot junctions were protruding out by different lengths. A schematic diagram of probe is shown in Fig. 2.16 (b). These probes were pushed into fuel block radially to the desired positions at different vertical locations.

In another arrangement six thermocouples were pasted on to a thin plywood strip 8 mm wide as shown in Fig. 2.16 (c) such that measuring junctions

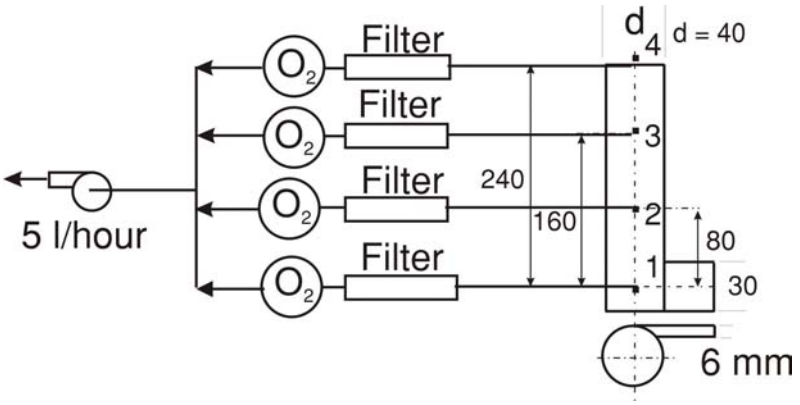

Figure 2.17: Arrangement for simultaneous oxygen and temperature measurement

would protrude by different lengths into g-phase and the whole assembly was radially pushed into fuel block through a thin slit in the wall of the stove. Usage of thicker wires proved less tedious but involved higher conduction losses.

2.4.4 Oxygen measurement

Oxygen measurements were made along with g-phase temperature measurements. Simultaneous temperature and oxygen measurements at four axial locations in the port of the stove were also made. It was decided to maintain a low flow rate of about 5 l/hour for oxygen measurement. This made cooling system of Fig. 2.8 inessential. Moisture trap was also done away with since cotton and calcium chloride filters were sufficient to take care of moisture collected at the flow rates maintained. Figure 2.17 shows a typical arrangement employed for acquiring multi point oxygen data. In this arrangement oxygen probes consisting of 3 mm OD and 2.5 mm ID with coaxial K type thermocouples used for simultaneous measurement of temperature and oxygen fraction at four locations along the axis of stove. In this experiment the sample gases from four monitoring locations were drawn through filter and sensor separately with common suction applied to a manifold as shown in Fig. 2.17.

2.4.5 Composition measurement

This experiment was conducted with an aim of measuring g-phase composition simultaneous with c-phase temperatures around the same location. Power level of the stove during the operation was monitored using a mass

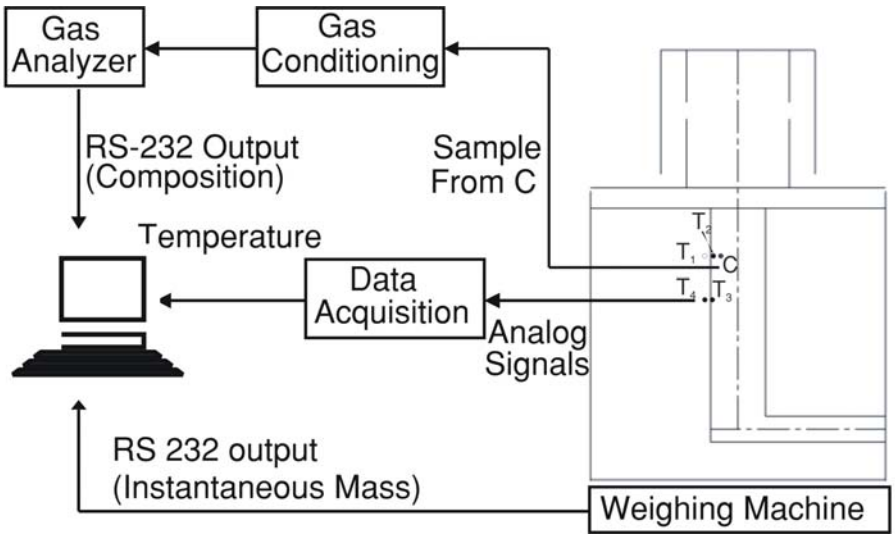

Figure 2.18: Experimental arrangement for c-phase temperature and g-phase composition measurement. Results are presented in Fig. 3.8

balance of least count 0.5 g. A typical experimental arrangement for composition measurement is shown in Fig. 2.18. Location of thermocouple probes and composition probe are also shown in figure.

2.5 Summary

Various tools used during the course of experimental study are introduced with a brief description of their utility. The different fuel materials on which experiments were conducted are also enumerated. Experimental procedures and measurement techniques employed during the course of experimentation are set out.

Chapter 3

Single Port Studies

This chapter is concerned with single port studies on a pulverized fuel stove of power level between 2 to 3 kW (amounting to 0.45 to 0.7 kg/hr of sawdust with slightly higher rates for fuels with higher ash content) with the burn duration of about an hour.

The criteria for selection of port diameter and aspect ratio (AR) for the required power level and burn duration are also set out in *Mukunda et al.* (1988). Corelations are presented in the paper relating outer diameter of fuel block, port diameter, burn duration and power level for stoves with AR = 5.5. For the required burn duration and power level, fuel web thickness and port diameter can be determined. Based on these criteria, it was deduced that pulverized fuel stove with a port diameter of about 40 mm and AR in the range of 4–6 would meet the power demand noted above. A fuel web thickness of 55 to 65 mm would account for the burn duration.

3.1 Combustion and Gasification in Tube Stove

Consider the working of the classical model tube stove of shown in Fig. 3.1. The fuel block is prepared by compacting pulverized biomass with a central port and an air inlet at the bottom as shown in the sketch. The fuel port, wetted with small amount of liquid fuel like kerosene, is ignited at the top, first and bottom air inlet region next. Hot product gases thus generated traverse the port supplying heat to port wall causing pyrolisis of the biomass resulting in volatile release. The volatiles released enter the port where they receive air from air inlet and burn in the port in diffusion mode. The resulting flame at the port exit, shown pictorially in Fig. 3.2 is fuel rich in nature. This is due to incomplete mixing in the port. Also, arrangement for fuel vapour to receive additional air at exit is not provided. This mode of stove operation

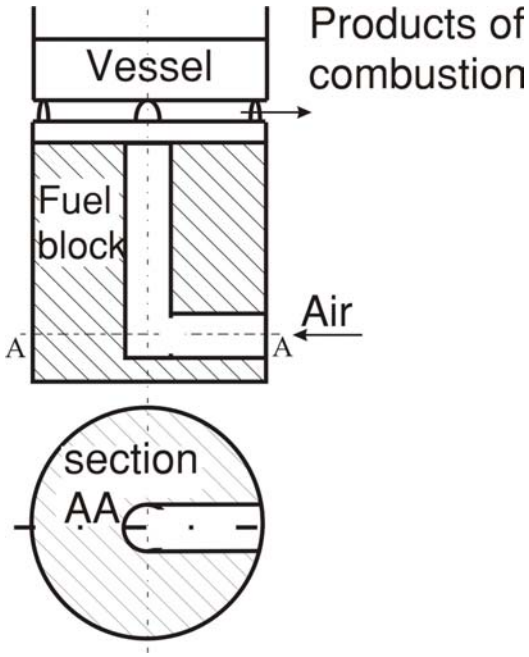

Figure 3.1: Schematic of a classical tube stove

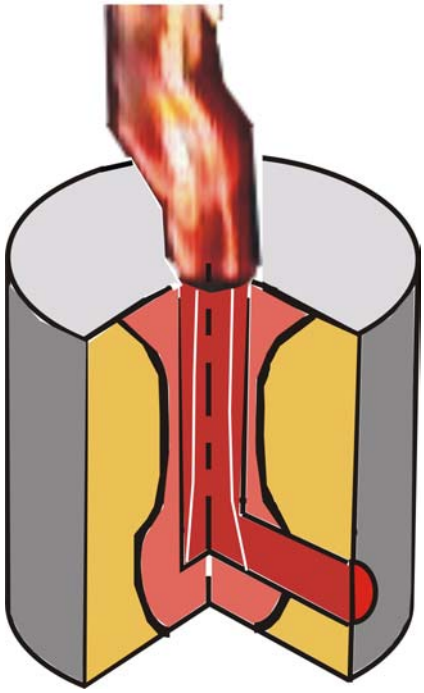

Figure 3.2: Combustion mode operation

is referred to as *combustion mode*. The heat transferred from the flame to the surface of the fuel block causes pyrolisis of the fuel block. With time, the pyrolisis front moves into the fuel block, with the front location roughly similar to that shown in the Fig. 3.2.

If one were to reduce the size of the air inlet, the amount of air inducted into the port is reduced. Under the conditions of reduced availability of air in the port, the volatiles released through the walls of the port do not burn immediately with air, but only mix with it since the mixture will be very rich. The mixture then moves up till the outlet is reached. It will burn in a partially premixed mode over the fuel block and the flaming process is strictly limited to the top region. During this mode there is no flame in the stove port. It is this process in which the fuel block with its arrangement of a central port that is physically red hot on its inner surface, but with no gaseous flame in the port generating a combustible gaseous fuel-air mixture for it to burn up at the outlet is called the *gasification mode*. Like in the case of combustion mode, the condensed phase processes include the formation of a pyrolisis front and its movement inside the solid block. In addition, it must be noted that the gases that issue from the wall are passing through the hot

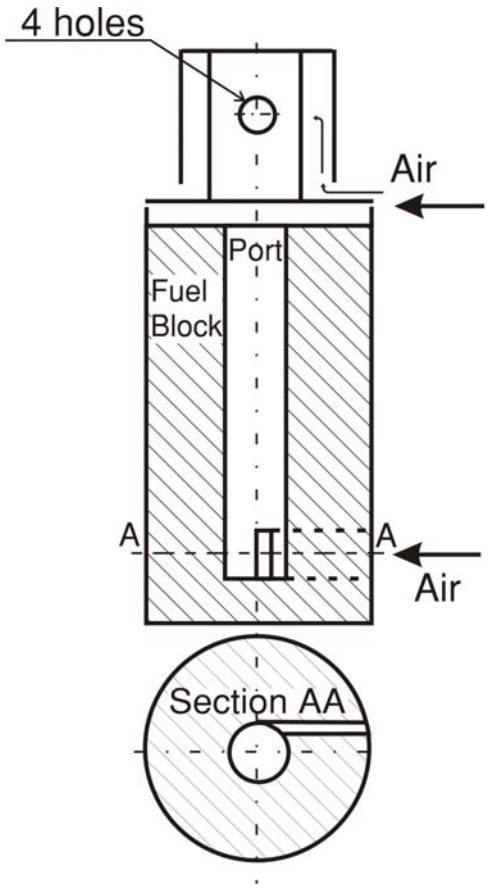

Figure 3.3: Schematic of a tube gasifier stove

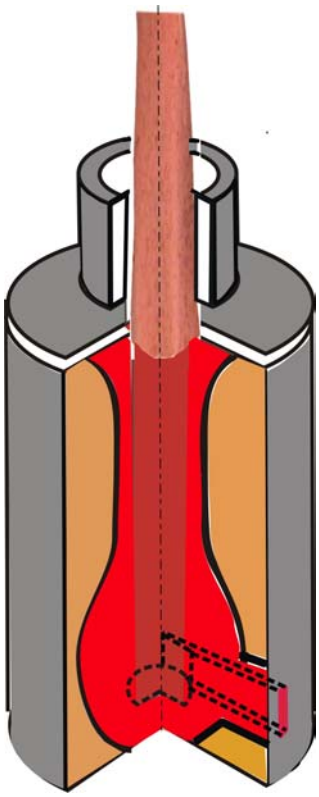

Figure 3.4: gasification mode operation

radial char bed inwards and hence the process of reaction of the gases from pyrolisis with the red hot char lead to products that are similar to a normal gasification process (*Mukunda et al.*, 1994) - CO, H_2 and CH_4 apart from more complex compounds of C-H-O.

The premixed gas out of the port of the fuel block needs additional air for combustion. This process, when stabilized with the addition of a combustion device of the kind shown in the Fig. 3.3, leads to a flame of exemplary quality can be obtained at the port exit. A pictorial view of a stove operating in gasification mode is shown in Fig. 3.4.

The device is placed on the stove such that a gap of $\sim$ 2–3 mm exists between stove and the device through which air is drawn into combustion zone. In addition, preheated secondary air enters the combustion zone through holes present in the inner wall of the device. This two stage addition of air ensures better quality combustion. The device with dimensions shown in the

Table 3.1: Combustion mode operation in single air inlet stove(Inlet dia = Port dia).

Ex	Date	d^a	AR	ρ	m_i	0-30 mins		0-60 mins		t_g	Data
No	'01/'02	mm		$\frac{kg}{m^3}$	kg	% Mass	Power kW	% Mass	Power kW	min	
1	18/11	40	9.0	260	2.40	18.6	3.6	33.8	3.3	.	T 3.6 (a)
2	19/11	40	9.0	260	2.40	21.0	4.0	50.3	3.9	.	C 3.6 (b)

[a] d = Port Diameter, AR = Aspect Ratio, ρ= Average fuel block density, m_i = Initial biomass weight, % mass = % mass converted, t_g= Time of gasification, minutes and data acquired (T = Temperature, C = Composition). Numbers in the data column indicate figure reference numbers where the acquired data is presented.

sketch has performed very well for power levels in the range up to 3 kW.

During the operation of the stove, fuel port surface temperature increases gradually. The degree of premixedness of gases coming out of the fuel port also increases. Roughly after about half the burn time, a threshold value is reached, and the mixture in the immediate lower strata gets ignited which further increases the gas temperatures of the mixture below and these events further cascade themselves into a fast downward propagation causing the flame to get established within the port. These events leading to a fast flame travel back vertically downwards into the fuel port, are condensed into the word 'flash back'. Once this happens, fuel released into the port receives oxygen from the gasification inlet and burns in the port itself in the diffusion mode leading to combustion mode of operation.

3.2 Combustion Mode Operation

To understand the processes that might occur in the gasification mode, it was necessary to establish the behavior of the stove in the combustion mode. Hence, it was thought appropriate to measure the gas phase temperature and composition profiles at certain heights and examine the thermochemical behavior. The dimensions of the stove that was used for these experiments are presented in Fig. 3.5. This stove had a port dia. of 40 mm and side inlet dia. of 40 mm. Measurements of temperature and composition were made inside the port at a height of 230 mm (h/d of 5.8). Experiment numbers 1 and 2 of Table 3.1 give the details of the fuel block used for these measurements. The diametral temperature profile is presented in Fig. 3.6 (a) and diametral composition profile is presented in Fig. 3.6 (b). The temperature profile was asymmetrical indicating a need for distributed air inlet area. The

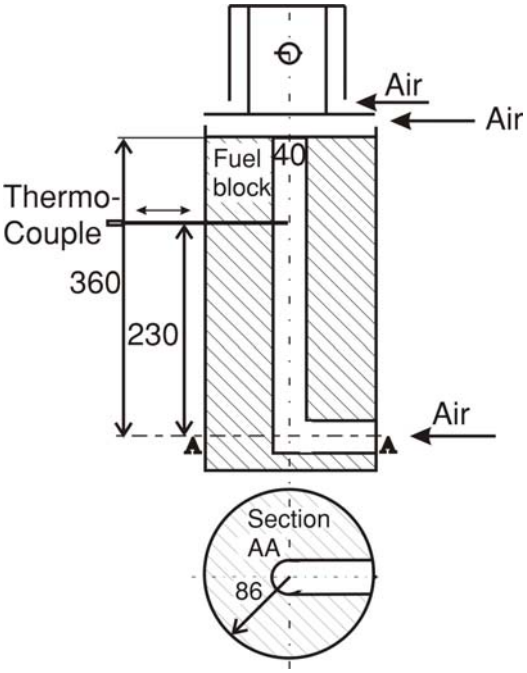

Figure 3.5: Schematic of stove used for determination of g-phase temperature and composition.

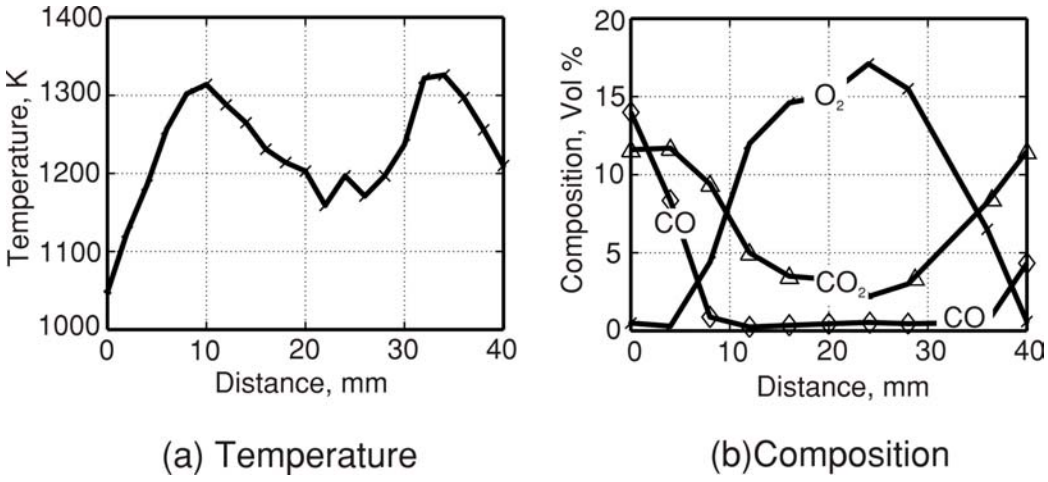

Figure 3.6: Determination of g-phase temperature and composition across the diameter.

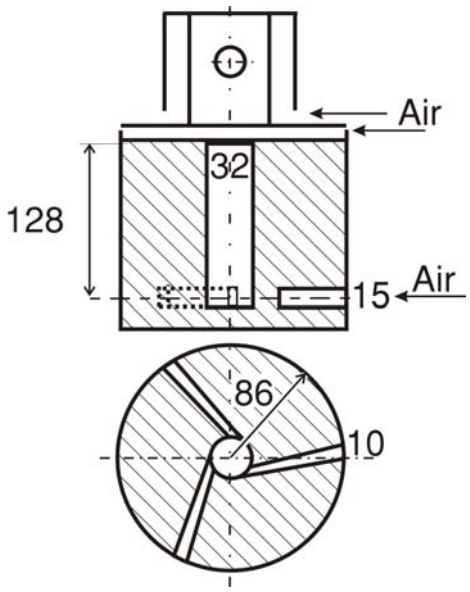

Figure 3.7: Tube stove with three inlets

composition measurements very clearly show large amount of oxygen near core ($\sim$ 14 %). This shows that it would be possible to reduce the size of the inlet to reduce the oxygen fraction in the port.

3.3 Design for Gasification Mode

The tube stove takes in air at ambient temperature with density higher than hot gases leaving the port by at least a factor of 3 (For hot gas temperatures of about 1000 K). To maintain similar velocities between inlet and exit, the inlet area can be a third of port area. On this basis, a port of 35 mm diameter will require about 300 mm^2 inlet area. To ensure uniform fuel consumption from the bottom region, the air inlet area was distributed among three locations 120 degrees apart as shown in Fig. 3.7. Three tapered inlets of cross section 15 mm $\times$ 6 mm at the port end were used to meet area requirements. The inlets were located such that they are tangential to the fuel port. This was done for two reasons (a) tangentially located inlet would deliver air into the port at a location nearer to fuel port surface promoting better diffusive mixing (b) the swirl flow path would provide a little more residence time. Provision of three inlets increased the fuel surface area in the horizontal limb by 25% compared to single horizontal inlet of diameter equal to port. Fuel block details are indicated in experiment no.9 of Table 3.2.

The fuel block would begin functioning with flame in port. Once ignition procedure got completed and the horizontal limbs became red indicating the initiation of pyrolysis over the entire span of horizontal limbs (in a maximum of 7 to 8 minutes), it was observed that the flame in the port disappeared. Volatiles released during pyrolysis of fuel block burnt at the exit. This phenomenon akin to gasification continued for over 30 minutes, during which the flame quality at the port exit was excellent. Preliminary observations like placing water filled vessel over the stove confirmed the non-sooty nature of the flame. The stove functioned at a constant power level of about 1.6 kW.

The part-premixed part-diffusion flame at the exit of port became progressively intense and shorter in height beyond 30 minutes or so, flame at the exit flashed back into the port. This phenomenon was some times accompanied by a barely audible sound and a mild shower of sparks. The smooth contours of gasification flame broke up into ragged mildly sooty tongues leading to combustion mode operation.

This functioning was sufficiently intriguing to prompt further investigation into the process with an aim to understand the reasons for flash back and try to prolong the gasification duration to the extent possible.

3.4 Determination of Causes of Flash Back

To determine the conditions of the fuel port that led to flash back the following quantities, some of them simultaneously, were continuously monitored in the g-phase of the fuel port in various experiments that are described in this section.

- Fuel port surface temperatures
- Composition
- Radial temperature distribution
- G-phase temperatures and oxygen concentrations at several locations

The flash back event originated from fuel port exit. Therefore, to establish the conditions of fuel port that would cause flame flash back, It was thought necessary to continuously monitor the composition of g-phase in the region below the port exit so that g-phase compositional variations could be captured.

Visual observation of the fuel port during the gasification mode operation of the stove had indicated a gradual upward progress of red hot char zone along the port surface. This increase in surface temperature might contribute

Table 3.2: Specifications and performance of selected three inlet stoves of AR = 4

Sl	Date	d	AR	ρ	m_i	0-30 mins		0-60 mins		t_g	Data[a]
No	'01/'02	mm		$\frac{kg}{m^3}$	kg	% Mass	Power kW	% Mass	Power kW	min	
10	19/12	32	4.0	264	0.93	23.8	1.8	44.0	1.6	30	.
11	20/12	32	4.0	264	0.90	24.2	1.8	.	.	30	3.10(b)
18	29/12	32	4.0	250	0.86	.	1.5	.	.	.	P 3.12
25	24/2	32	4.0	240	0.82	20.7	1.6	44.7	1.6	35	T C 3.8

[a]Numbers in the data column indicate figure reference numbers where the acquired data is presented.

to creation of conditions conducive to flash back. It was surmised that port surface temperature data at locations immediately below fuel port exit would hopefully reveal the reasons for the occurrance.

Therefore fuel port surface temperatures along with composition of gases in the region below fuel port exit were continuously monitored in a stove geometry known to operate in gasification mode for part of the burn time from earlier experience, whose dimensions are shown in the schematic diagram inset to Fig. 3.8. Weight loss data of the stove was also acquired to obtain the power level of operation.

The fuel port had 32 mm dimeter. Three tangential inlets of size 15 mm $\times$ 6 mm were used. Fuel block details and stove performance data for this experiment is indicated in #25 of Table 3.2. During the experiment, temperatures of fuel port surface and of points 5 mm radially outwards from surface into the condensed phase were measured at two locations on port surface vertically separated by 25 mm with the upper measurement level 40 mm below fuel port exit. These measurement locations are identified as 1,2,3 and 4 in the schematic diagram inset to Fig. 3.8. G-phase composition was also measured at a location C which is 5 mm into g-phase, as shown in the sketch, 40 mm below tube exit. The position of temperature and composition probes relative to fuel port wall and fuel port exit plane is presented in Table. 3.6. The weight loss data, shown in Fig. 3.8 (c) indicates that power level of operation of the stove is nearly constant for entire recorded duration of one hour.

Consider the fuel port surface temperature data presented in Fig. 3.8 (a). T_2, surface temperature a diameter below fuel port exit, attained 830 K after initial transients as the stove settled down to gasification mode operation. During this mode, T_2 increased gradually until it reached 990 K recording

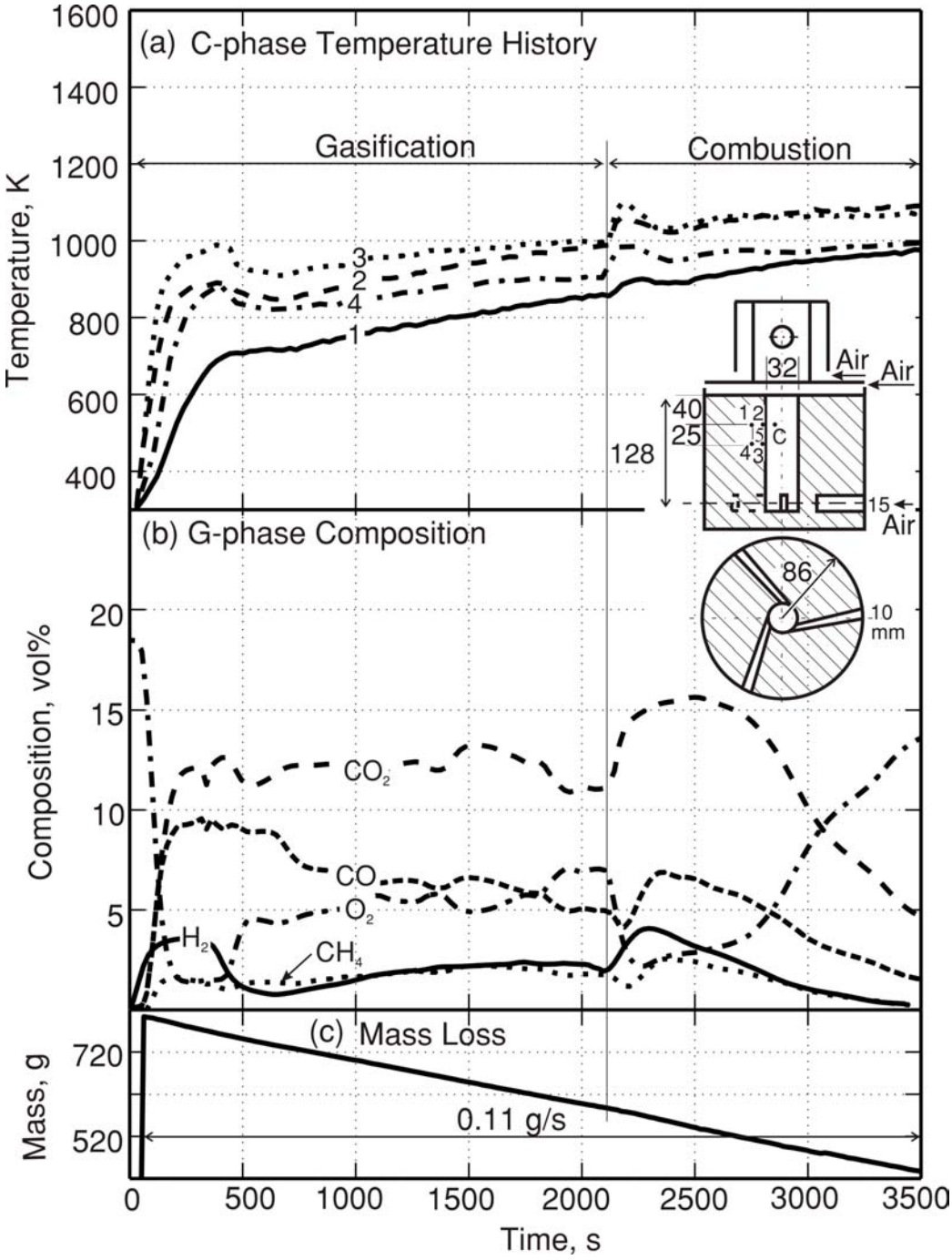

Figure 3.8: C-phase temperature and g-phase composition measurement (Port Diameter = 32 mm Aspect Ratio 4). Figure (a) shows Condensed phase temperature history measured using R type 50 μm diameter thermo-couples at locations 1-4 shown in sectional elevation of the stove. Figure (b) shows simultaneously acquired g-phase composition at location C. Figure (c) indicates mass loss as a function of time during experiment

Table 3.3: Measurement locations for the results presented in Fig. 3.8

Label	Quantity	Description of Position
1	Temperature	C-phase, 5 mm from port wall, 40 mm below exit
2	Temperature	C-phase, On port wall, 40 mm below exit
3	Temperature	C-phase, On port wall, 65 mm below exit
4	Temperature	C-phase, 5 mm from port wall, 65 mm below exit
C	Composition	G-phase, 5 mm from port wall, 40 mm below exit

an increase of 160 K after 35 minutes of operation. At that instant, flame hitherto stabilized at port exit, flashed back into the fuel port. The event was captured by a sharp increase in T_2 by 40 K. It is suspected 990 K might be a threshold port surface temperature in the region below port exit which, once crossed, would permit flame flash back.

T_2 increased at a faster rate then T_3 during gasification mode operation. T_3, 25 mm upstream of T_2, was higher than T_2 by 35 K initially. This difference kept decreasing with T_3 becoming equal to T_2 at flash back. During combustion mode these two temperatures remained equal. It appears during combustion mode operation c-phase surface temperatures may be more uniform spatially in the vertical direction than gasification mode.

C-phase radial temperature differences $T_2 - T_1$ and $T_3 - T_4$ remained constant at 130 K and 100 K respectively indicating constant heat flux into c-phase at a given vertical level in the stove.

From the composition record shown in Fig. 3.8 (b) it is seen that, the beginning of gasification mode of operation, confirmed visually by the absence of flame in the port, was indicated by a small but quick increase in oxygen to 4.5 % as seen in Fig. 3.8 (b) indicating the formation of a fuel rich air fuel mixture at the measured location. During this mode, oxygen gradually increased to about 7% at which flash back occurred leading to a quick drop in oxygen to 2% due to its consumption within the port and associated increase of carbon dioxide. Oxygen increase beyond 2500 s is inferred to be due to reduced air restriction caused by the removal of the ash layer and char oxidation around the inlets that permitted more air into the port.

The equivalence ratio of the mixture is calculated from the measured composition and plotted in Fig. 3.9 assuming no higher hydrocarbons or other fuel components were present. It shows that during gasification mode operation, equivalence ratio of mixture at the measured location fluctuated between 1.4 to 1.8. After 30 min of operation it dropped from 1.4 to 1 in 2 minutes. For the next 3 minutes it stayed at 1 and at the end of 35^{th} minute flash back occurred leading to combustion mode operation confirmed visually

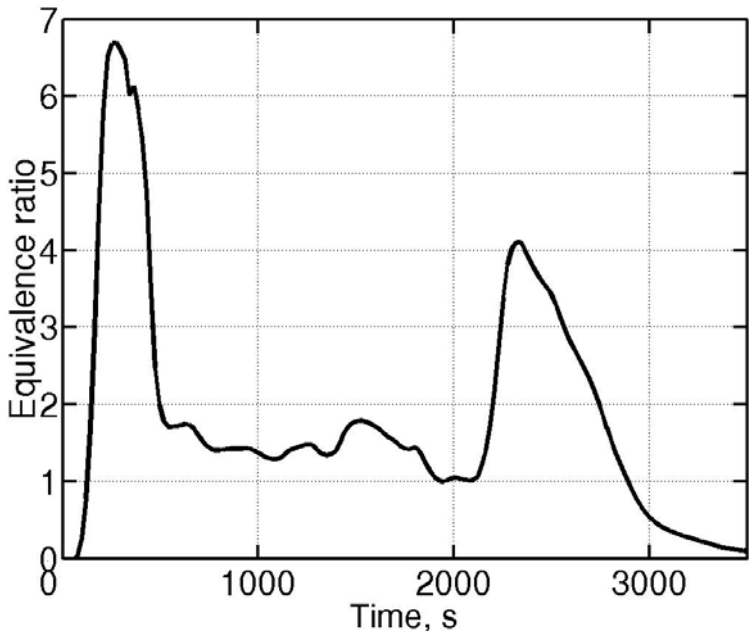

Figure 3.9: G-phase equivalence ratio at a station 40 mm below fuel port exit as a function of burn time

by noting the presence of flame in the port.

Thus, the movement of equivalence ratio towards 1 in the region immediately below the fuel port exit may be one of the causes for flash back. This implies that a fuel release pattern where volatiles are released at larger rates from bottom region may be a feature for gasification mode of operation in the stove.

To confirm whether fuel release was indeed larger in stoves operating in gasification mode, it was necessary to examine the vertical fuel release pattern in the stove during gasification mode.

To achieve the above objective, pyrolysis front positions were determined at three azimuthal positions by inserting paper sheets (see 2.4 for experimental details) into the stove at locations 120 ° apart, as shown in Fig. 3.10 (a).

The experimental summary is indicated in #11 of Table 3.2 of page 52. The stove operated in a gasification mode for the first 30 min after which stove was put off to facilitate removel of paper sheets. Paper sheets extracted from the stove are presented in Fig. 3.10 (b). The char zone on the paper sheet is indicative of the region over which pyrolisis was complete. The border between char zone and unburnt paper represents the pyrolisis front. This is

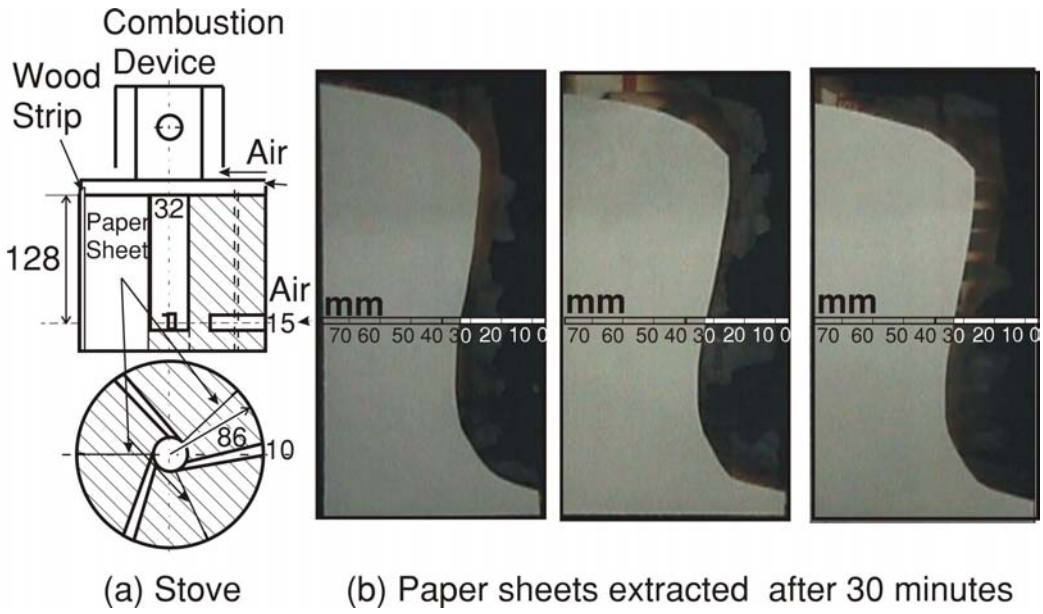

Figure 3.10: Symmetry in propagation of pyrolysis front (Port Diameter = 32 mm, Aspect Ratio 4). The paper sheets were extracted 30 min after initiation of combustion.

found to be about 2–3 mm in width.

The following observations can be made from Fig. 3.10 (b).

- It can be seen that the pyrolisis front moved by same amounts at the corresponding vertical locations in all the three char profiles implying circumferentially uniform volatile release.
- In the bottom region, pyrolysis front had advanced into c-phase by a greater extent compared to upper levels. This indicates that during gasification mode operation, volatile release rates in the bottom region are higher than that in the regions above.
- Profiles shown in Fig. 3.10 (b) indicate that the pyrolisis front had moved through a distance of 30 mm at the end of 30 min at mid height of the stove. This indicates an average pyrolisis front movement rate of 60 mm/hour during first 30 min of stove operation at mid height during the gasification mode operation.
- There was some amount of downward regression of pyrolisis front around the port indicating increased influx of fuel vapours into the port in the region immediately below fuel port exit during gasification mode operation. This influx, which was present during earlier part of stove

operation, may also help to maintain lower air-to-fuel ratio in the region immediately below fuel port exit.

Paper sheets extracted from the stove with different ARs at various times have shown that during gasification mode operation the pyrolisis front movement into the fuel block was always comparatively larger in the bottom region.

Figures. 3.11 (a) show the pictures of pyrolisis fronts extracted from the stoves of AR = 4 stove at various times. From these pictures it is clear that pyrolisis front had progressed to greater depths into the c-phase in the bottom region compared to top region. Figures. 3.11 (b) shows pyrolisis fronts extracted from AR = 6.5 stoves at various times. These pictures also indicate deeper penetration of pyrolisis front into the fuel block in the bottom region. The reasons for experiments on higher AR stoves will be brought out subsequently.

In one of the experiments made for location of pyrolisis front in an aspect ratio 4 stove, paper sheet was inserted into the stove along with nine thermocouples attached to it at known radial locations at mid height of the stove. The pyrolisis front, extracted after 13 min of stove operation, a duration considered sufficient based on temperature indications, is shown in Fig. 3.11 (a).

Locations of thermocouples along with a schematic of the stove used for experiment are shown as inset to Fig. 3.12.

Radial temperature distribution at the instant paper sheet was removed from the stove and corresponding pyrolisis front position are shown in the inset of Fig. 3.12 on the schematic diagram of the stove itself. The thermocouple #5 that was nearest to pyrolisis front indicated a temperature of 588 K at the instant the paper sheet was pulled out. It is therefore inferred that the pyrolisis temperature is about 588 $\pm$ 20 K, the 20 K indicated here being the temperature variation over 2 mm, the pyrolisis zone thickness as seen from the charred paper sheets.

The temporal temperature distribution is presented in Fig. 3.12 (a). Thermocouple #9 was nearest to the fuel port surface. It may be observed that temperature difference between two locations has remained nearly constant after initial transients.

Using the temporal distribution at various locations 1–9 of Fig. 3.12 (a), The radial temperature profiles in c-phase at various times are plotted in Fig. 3.12 (c). The axial coordinate chosen for the plot is a logarithmic scale. The reason for this choice is related to the expectation of the steady temperature distribution in radial coordinate goemetry discussed below.

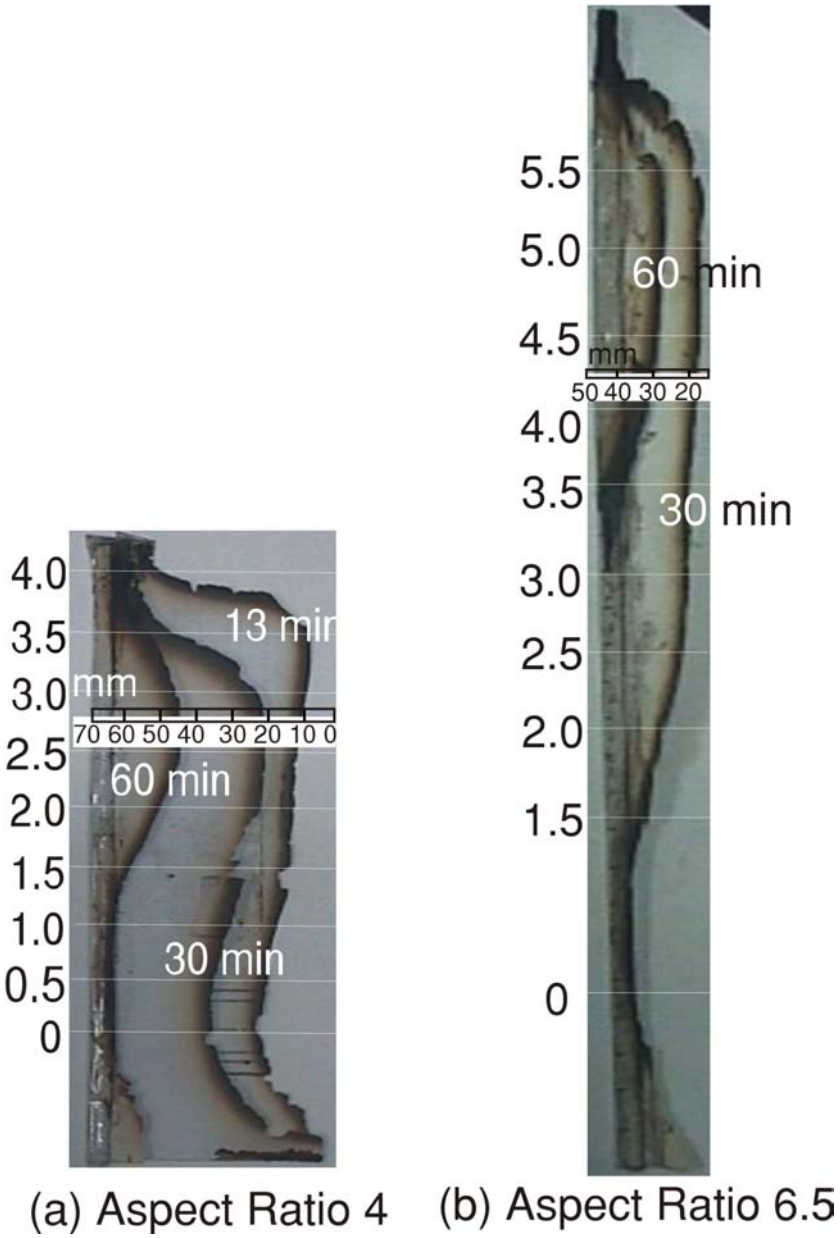

Figure 3.11: Pyrolisis fronts extracted at various times from stoves of AR 4 and AR = 6.5

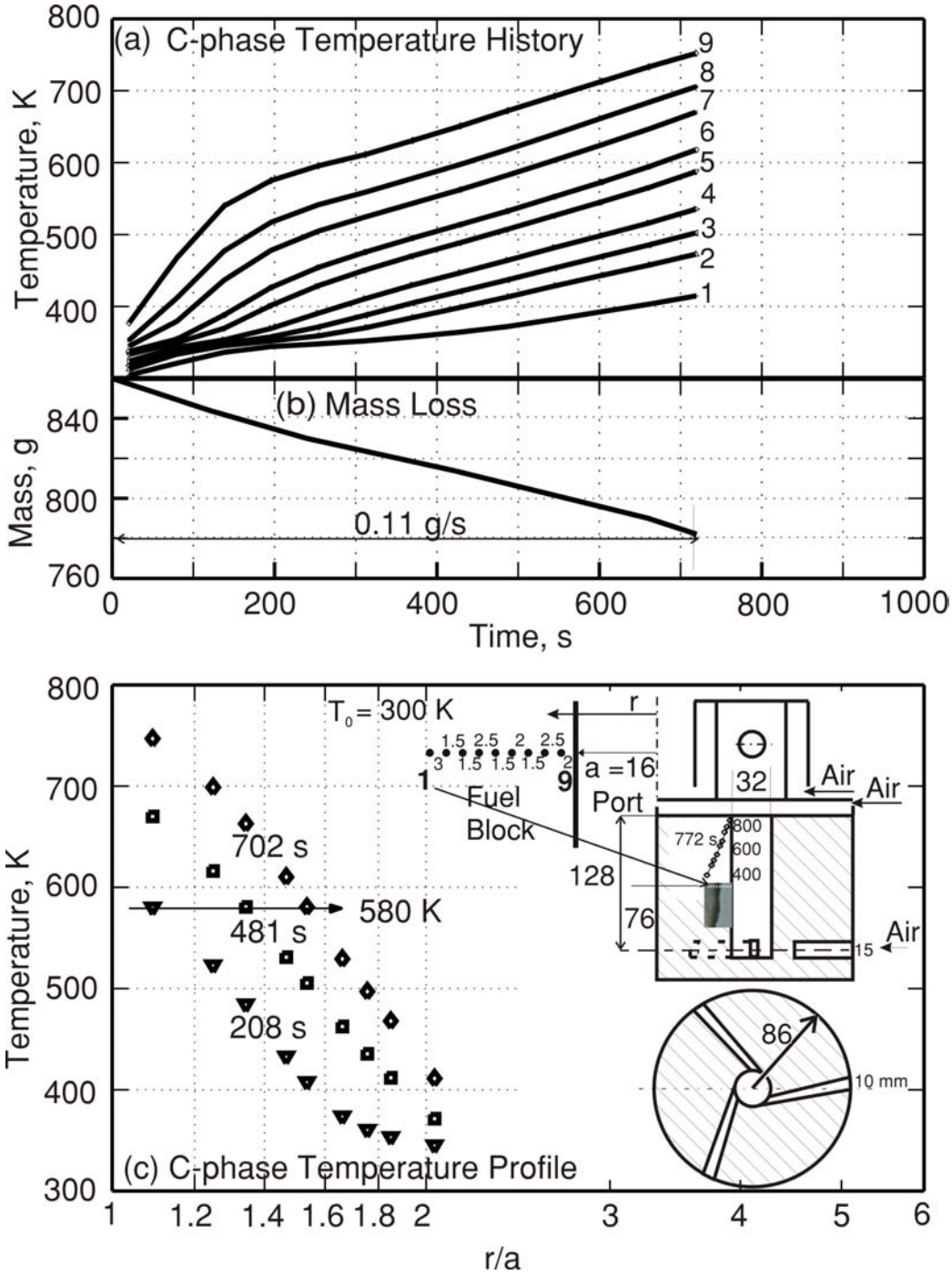

Figure 3.12: C-phase temperature measurement (Port diameter = 32 mm, AR = 4). Figure (a) shows condensed phase temperature history. K type 100 μm diameter thermo-couples are used. Mass loss as a function of time is shown in Fig.(b). Figure (c) shows condensed phase temperature profile at the location shown in schematic diagram.

Steady one dimensional radial heat flow without heat generation in a solid cylinder is governed by heat conduction equation,

$$\frac{1}{r}\frac{d}{dr}\left(r\frac{dT}{dr}\right) = 0 \tag{3.1}$$

For a hollow cylindrical geometry, with inner surface at $r = a$ and outer surface at $r = b$ and surface temperatures maintained T_s and $T_\circ$ respectively, the temperature distribution is given by

$$T(r) = \frac{T_s - T}{T_s - T_\circ} = \frac{\ln(r/a)}{\ln(b/a)} \tag{3.2}$$

Where T is the temperature at any radius r.

Based on the findings from these experiments, made on three inlet configuration stoves, it was surmised that (a) maintaining the g-phase air-to-fuel ratio in the region below fuel port exit low and (b) Larger fuel release from bottom region might help prevent flash back or atleast postpone its occurrance beyond the required operational duration.

One possible way of preventing port exit air-to-fuel ratio go towards stoichiometry to allow flash back could be to reduce the size of air inlet further. In three inlet configuration, further reduction in area was not possible as the individual inlet sizes would become too small leading to difficulties in forming the fuel block. Also three inlet configuration would provide more surface area in the inlet region for given port cross section area paving way for faster fuel consumption in the bottom region. Therefore it was decided to examine the performance of a single restricted tangential inlet stove. It was determined that port of a stove with an inlet size of 30 mm $\times$ 6 mm is about the minimum size that could be ignited with no difficulty. This corresponded to an inlet cross section area which was one seventh the port area.

Figure 3.13 shows a single inlet fuel block geometry which was tested for gasification mode functioning. The fuel port had 40 mm diameter with a single restricted side air inlet of size 30 $\times$ 6 mm. The stove performed such that the gasification mode operation in this stove was again limited to about 30 min of stove operation.

In this geometry, radial temperature profile in the exit region and oxygen concentration in the inlet region were monitored. Location of the probe is shown in the schematic sketch inset to Fig. 3.14. Thermocouple locations are shown in the pictorial view inset to the same figure.

The experimental details are shown in #33 of Table 3.4. The geometry used is shown in the sketch inset to Fig. 3.14. The location of probe near air inlet used to extract samples for oxygen measurement is also shown

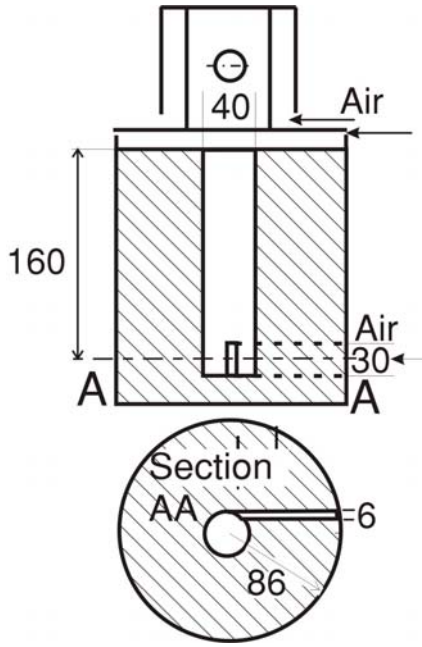

Figure 3.13: Tube stove with single tangential inlet

Table 3.4: Specifications and performance of selected single inlet stoves of AR = 4

Sl	Date	d	AR	ρ	m_i	0-30 mins		0-60 mins		t_g	Data[a]
No	'01/'02	mm		$\frac{kg}{m^3}$	kg	% Mass	Power kW	% Mass	Power kW	min	
33	26/4	40	4.0	240	0.88	26.0	1.9	52.0	1.9	30	T O_2 3.14
34	28/4	40	4.0	240[b]	0.90	14.0	1.1	40.0	1.6	40	T O_2 3.16

[a]Numbers in the data column indicate figure reference numbers where the acquired data is presented.

[b]Higher density bottom region

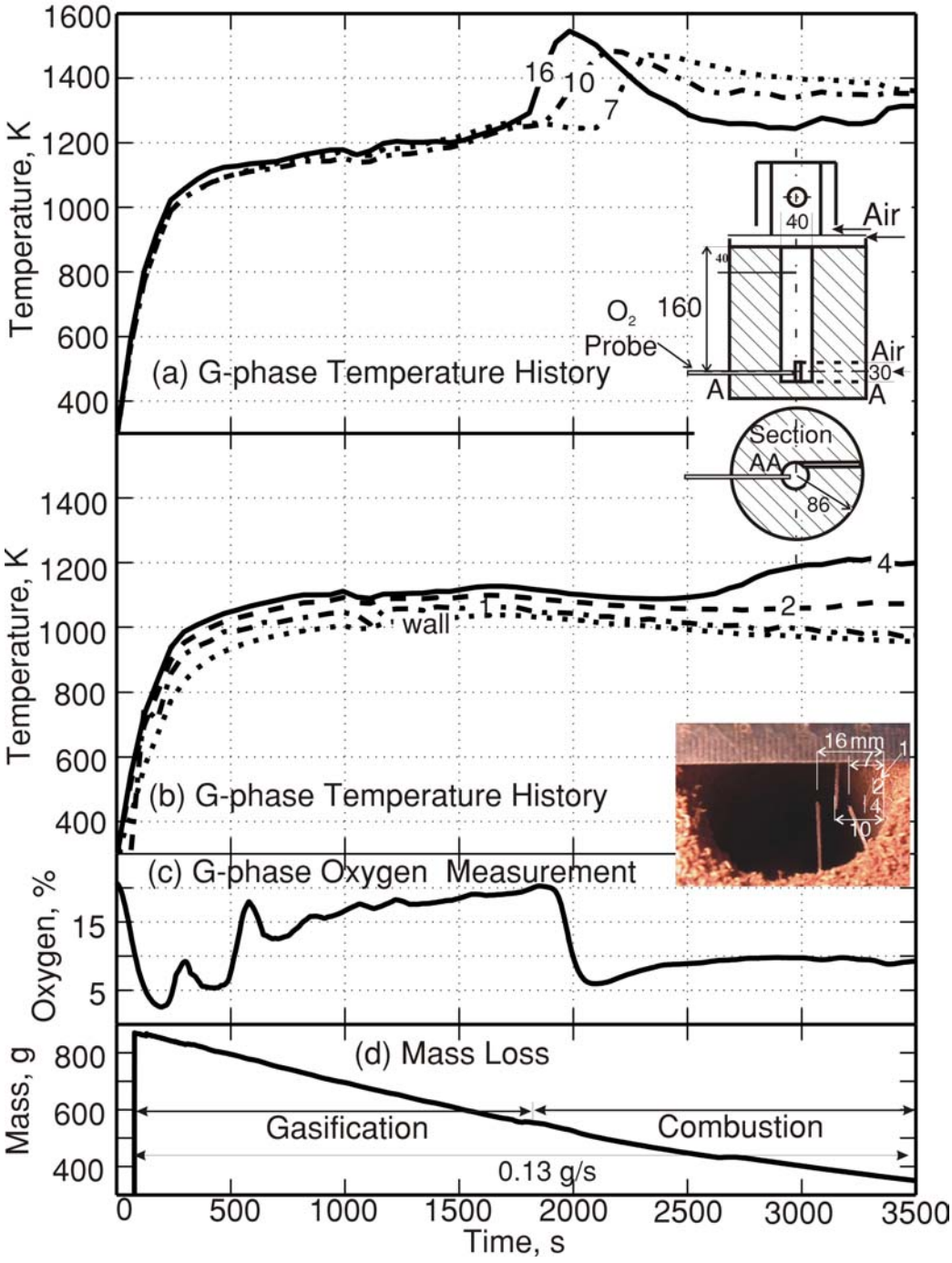

Figure 3.14: G-phase temperature and oxygen measurement (Port diameter = 40 mm, AR = 4). Figures (a) and (b) show temperature histories at six R type 50 μm diameter thermocouple locations including one on wall as shown in the photograph. Figure (c) gives variation of oxygen volume fraction with time at location shown in schematic diagram. Figure (d) shows mass loss pattern.

in this sketch. The radial location of thermocouples used for temperature measurement is shown in the pictorial view of Fig. 3.14. Numbers on the plots indicate distances of thermocouple measuring junctions from port wall. These distances are also shown in the pictorial view of the port shown inset to Fig. 3.14.

Figures 3.14 (a) and (b) show the temporal temperature distribution in the g-phase at the measured locations. Measured oxygen concentration is shown in Fig. 3.14 (c). Weight loss during the experiment is shown in Fig. 3.14 (d).

The flash back occurred after 30 minutes of stove operation indicated by sharp increase in temperature at a location 16 mm from port wall (4 mm radius) as seen in Fig. 3.14 (a). Firstly, it is also important to recognize that the thermocouple at the wall never recorded any rise in temperature (see Fig. 3.14 (b)) indicating that the flash back phenomenon *gets started at the centre of the port.* In fact the temperatures at outer locations show up sharp rise at later instants. The difference in time between the instants at which temperature rise has started to occur from that at the centre is defined as a delay period. These data are set out as t_{FB} vs. port radius at which the event has occurred is plotted in Fig. 3.15. It is interesting to see that the process of transition is very long — as much as 20 minutes.

The oxygen record in the bottom region at the measured location shows a quick drop in oxygen at the beginning of stove operation. During gasification mode operation, it increased gradually and flash back occurred when it had built up to near ambient levels. Flash back resulted in quick depletion of oxygen to low values. This indicates to the possibility that as long as the oxidation processes taking place in side inlet and bottom region are able bring down oxygen level of the incoming air the gasification mode operation might proceed. To confirm these observations one more experiment was conducted in the same fuel block geometry. This time, fuel block density in the bottom region was kept high in order to ensure volatile release from bottom region for a longer duration, though average density of fuel block was comparable to previous experiment. Oxygen measurements at bottom region as well as in the region below the fuel block exit were made along with radial temperature distribution. Experimental details are shown in #34 of Table. 3.4 (Page 61).

Figures 3.16 (a) and (b) show the temporal temperature distribution in the g-phase at the measured locations. Numbers on the plots indicate distances of the measuring points from the port wall im mm. Locations of measuring junctions are also shown in the pictorial view of the port with thermocouples in position. Measured oxygen concentration is shown in Fig. 3.16 (c). Weight loss during the experiment is shown in Fig. 3.16 (d).

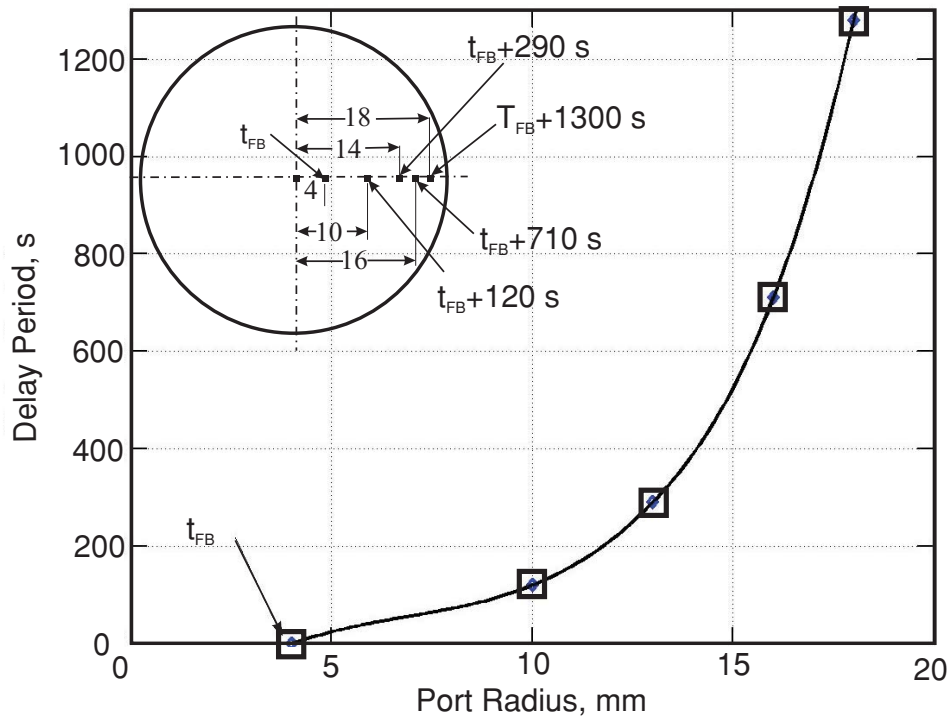

Figure 3.15: Progress of flame front in g-phase at a location 40 mm below port exit during stove operation. The times at which the flame was sensed at various physical locations in the port are shown in the inset with the reference time being the time of flash back (t_{FB}).

Flash back occurred across the entire port cross section in the 39^{th} minute of stove operation as seen by the sharp rise in g-phase temperatures at all the measured locations (shown in Figs. 3.16 (a) and (b)) including port wall simultaneously.

The above two results imply that flash back might occur in two different ways depending upon the conditions that prevail in the fuel port. That is the flame might flash back into the port only through that region around axis where the mixture conditions are favourable. Once this happens, there is a gradual increase in air flow through the port caused by higher temperature gases in the port resulting in widening of flame core within the fuel port which would have caused the temperature of gases at outer radii to go up at later instants as seen in Fig. 3.14 (a). The other possibility is flame might flash back into the fuel port grazing the port surface if the air fuel mixture over the entire cross section of the upper region of port is uniform, which might have happened during the experiment whose results are presented in

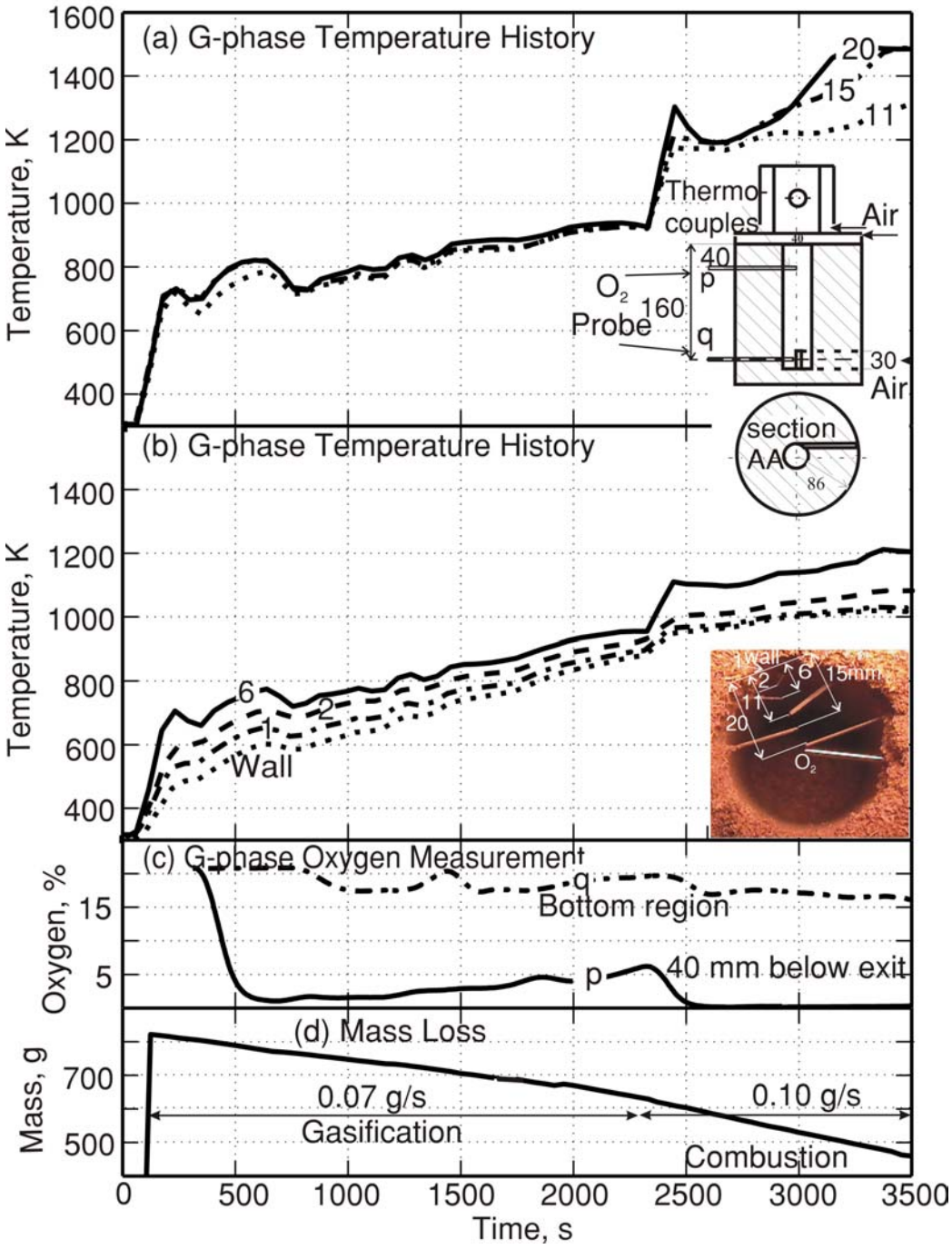

Figure 3.16: G-phase temperature and oxygen measurement (Port diameter = 40 mm, AR = 4). Figures (a) and (b) show temperature histories at seven radial locations of R type 50 μm diameter thermo-couples including one on wall. Oxygen volume fraction is plotted in Figure (c) as a function of time at two locations shown in schematic diagram. Figure (d) indicates mass loss rate and gasification and combustion durations. In Fig. c, q is the data at the bottom region and p is at 40 mm below the top

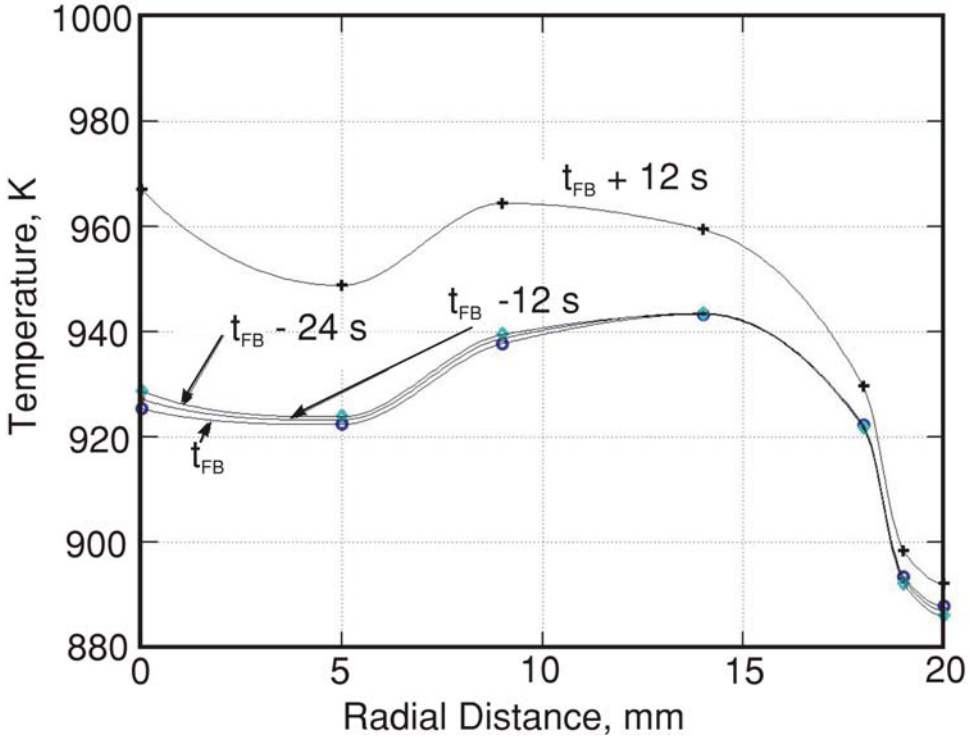

Figure 3.17: G-phase radial temperature distribution at flash back and few instants before and after flash back are shown in the figure. (t_{FB}, $t_{\mathrm{FB}} - 12$ s, t_{FB} - 24 s and $t_{\mathrm{FB}} + 12$ s)

Fig. 3.16 (a).

The radial temperature distribution within the fuel port at flash back, 12 and 24 seconds before flash back and 12 seconds after flash back is shown in Fig. 3.17. It can be seen that temperatures at locations nearer to centre show a decreasing trend with time before flash back probably due to increased influx of air from gasification port. After flash back gas temperatures over entire g-phase are seen to increase due to presence of g-phase reactions. Fig 3.16 (c) shows the variation of oxygen concentration within the fuel port at inlet and near port exit. The sampling was started a few minutes after ignition to prevent the sampling probe from getting clogged during ignition period at the beginning. Plot p of Fig. 3.16 (c) shows the oxygen variation in the upper region of the port. Oxygen concentration in the exit region went to near-zero value at the beginning of the gasification mode operation. During gasification mode operation, the oxygen fraction gradually increased until flash back ocurred. Further, combustion mode operation continued with zero-oxygen near the port exit.

Table 3.5: Specifications and performance of selected tube stoves of AR = 6

Sl	Date	d	AR	ρ	m_i	0-30 mins		0-60 mins		t_g	Data[a]
No	'01/'02	mm		$\frac{kg}{m^3}$	kg	% Mass	Power kW	% Mass	Power kW	min	
38	31/7	40	6.0	240	1.06	20.0	1.7	40.0	1.7	30	T 3.19
43	26/9	40	6.0	225	1.0	24.0	2.0	52.0	2.2	30	T O_2 3.21
45	30/9	40	6.0	225	1.0	30.0	2.5	55.0	2.3	30	T 3.20
47	5/10	40	6.0	225	1.0	25.0	2.1	50.0	2.1	30	T 3.18

[a]Numbers in the data column indicate figure reference numbers where the acquired data is presented.

Oxygen concentrations recorded at inlet level during this experiment were similar to the previous experiment, but values recorded were higher. These differences might possibly be due to minor geometric variations in positioning the side air inlet relative to the fuel port and the sampling probe inlet caused during the set-up of the experiment. In this experiment oxygen at inlet level went down to 18.4% at the beginning of gasification mode operation and showed an increasing trend. At flash back it had reached ambient concentrations.

Higher AR stoves for the same port diameter were explored for the possibility of longer gasification duration operation. These were expected to work at a higher power level implying larger fuel release rates. As inlet size was maintained the same, it was expected that air to fuel ratio near the port exit might remain low long enough in these stoves to prevent flame flash back within the required burn duration. Therefore studies were conducted in stoves with AR = 6.

Consider the results of a typical g-phase temperature measurement in an AR = 6 stove. Temperature measurement was made at a single location in a stove with port dimensions shown in the schematic diagram inset to Fig. 3.18. The measurement location, shown in the sketch, corresponds to the same vertical level of the earlier reported measurements in AR = 4 stoves. The experimental details are shown in #47 of Table. 3.5.

It is seen that flash back had occurred after 30 minutes of stove operation indicated by a sharp increase in g-phase temperature at the measured location. During gasification mode operation g-phase temperatures were about 1000 K. After flash back gas temperature at the measured location went up by about 300 K.

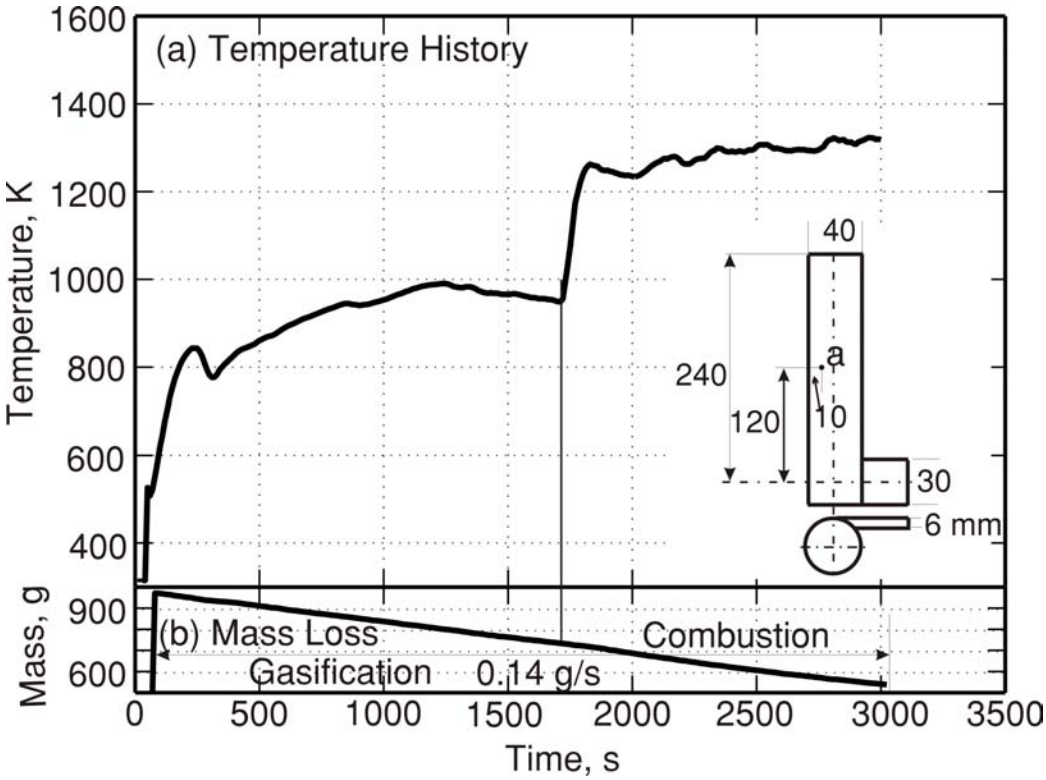

Figure 3.18: Temperature history in the port of an AR = 6 stove at the location 'a' shown in the schematic diagram inset to (a). Fig. (b) shows the mass loss details during the experimental run.

In an other experiment, g-phase temperatures at several radial locations were continuously monitored. A schematic diagram of the stove used is shown inset to Fig. 3.19 which shows the location of thermocouples also. Experimental details are given in #38 of Table 3.5.

The temporal temperature distribution at the measured locations is given in Fig. 3.19 (a). Weight loss data is shown in Fig. 3.19 (b). During that experiment also flash back occurred 30 min after ignition. The temporal temperature distribution is indicative of a flash back initiated only in the central region of the stove as the port wall temperature had not recorded step rise in temperature.

Another measurement of g-phase temperatures at several radial locations in an AR = 6 stove is presented in Fig. 3.20. Port dimensions and locations of thermocouples are shown in the schematic diagram inset to Fig. 3.20. A picture of the thermocouple bank used for the measurements is also shown inset to Fig. 3.20. As seen from Fig. 3.20, (a) and (b), flash back took place

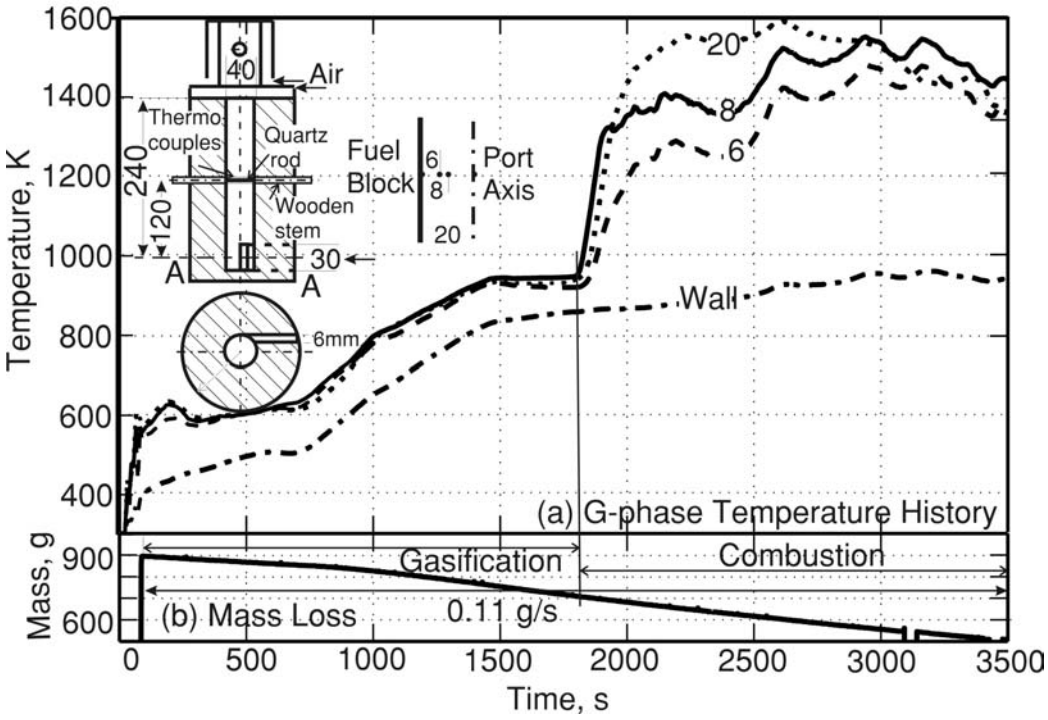

Figure 3.19: G-phase temperature measurement (AR = 6). Figure (a) shows g-phase temperatures at 4 radial locations of R type 50 μm diameter thermo-couples as indicated in the schematic diagram. Figure (b) shows corresponding mass loss.

across the entire port cross-section as indicated by step rise in temperatures at all measured locations *including the wall*. The event is indicated as 'c' on the weight loss record. This indicates flash back took place in both the known modes in AR = 6 stoves also.

During this experiment flame in the port was extinguished by closing the air inlet using ceramic wool. This resulted in dropping of g-phase temperatures. However, opening of inlet at the instant 'd' brought back combustion mode operation. It is also noted that at in earlier instant, 'b' the fuel block had to be reignited due to flame blow off. The issues related to reignition will be discussed subsequently.

The port oxygen was monitored simultaneously at several vertical locations along the port axis to determine vertical oxygen distribution. During this experiment, gas temperatures at the sampled locations was also monitored.

The locations where measurements were carried out are given in the schematic diagram of the port shown inset to Fig. 3.21. Experimental details

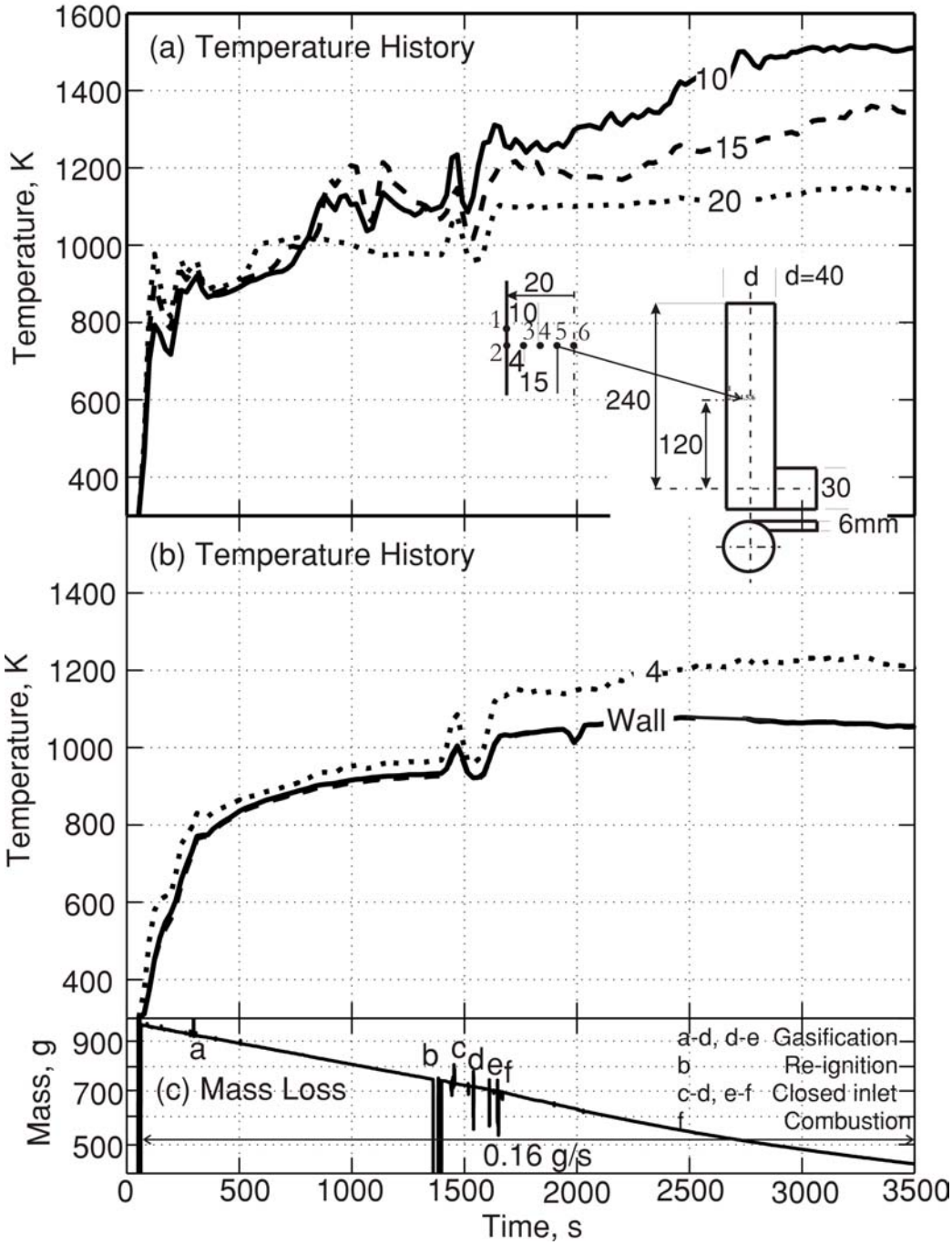

Figure 3.20: Figures (a) and (b) show temperature history in 40 mm diameter AR = 6 stove port measured using R type 100 μm thermo-couples whose locations are shown in schematic diagram. Figure (c) shows the corresponding mass loss.

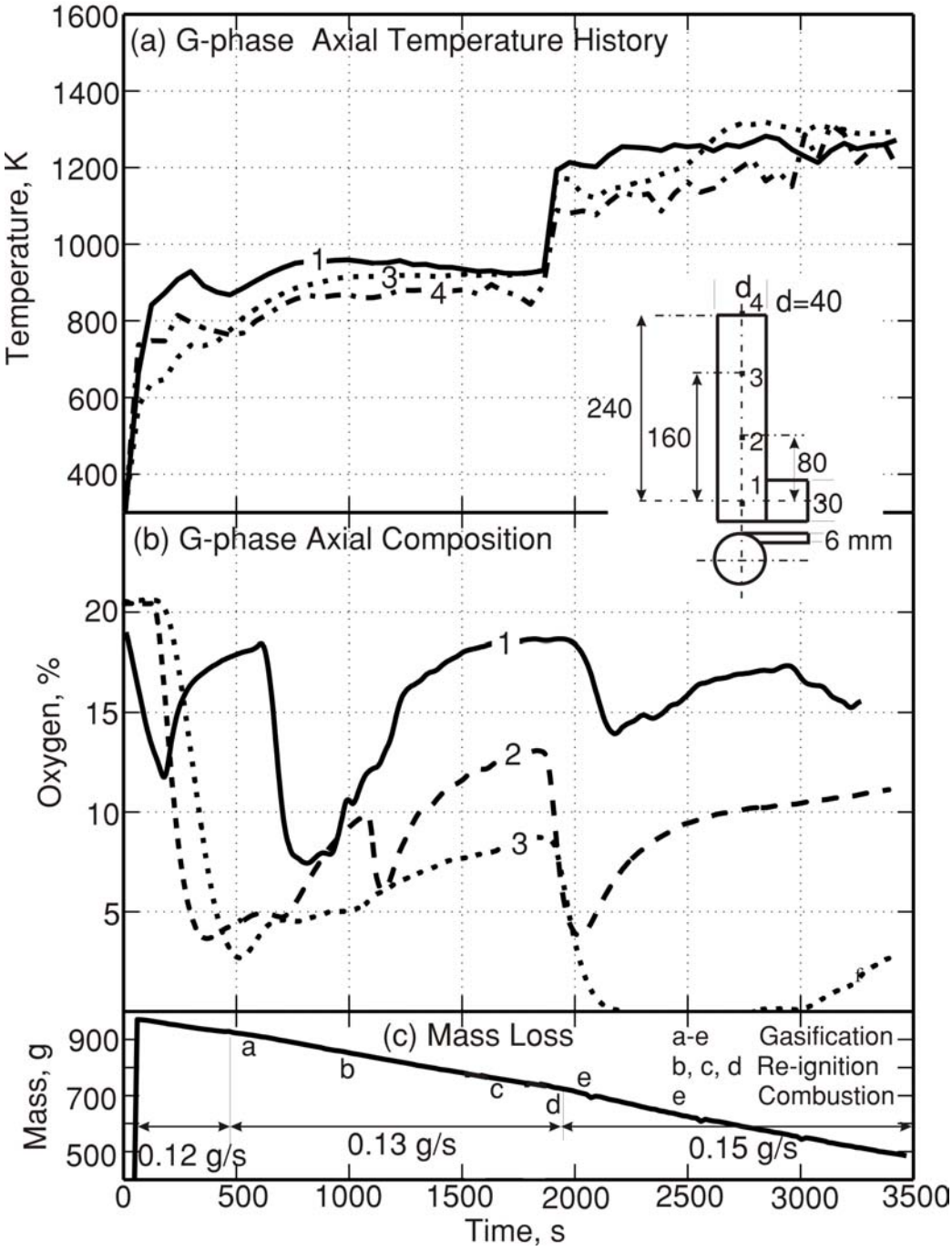

Figure 3.21: Temperature and oxygen in the fuel port at four axial locations. Port diameter =40 mm, AR = 6. Figure (a) indicates temperature history measured using K type 100 μm diameter thermo-couples at locations 1-4 shown in schematic diagram. Figure (b) shows oxygen volume fraction at the same locations. Figure (c) gives the mass loss of stove during experiment.

Table 3.6: Thermocouple measuring junction locations for the results presented in Fig. 3.22

Label	Location of measuring junctions [a]
1	Flush with port wall, 185 mm below exit
2	Flush with port wall, 145 mm below exit
3	Flush with port wall, 105 mm below exit
4	Flush with port wall, 65 mm below exit
5	Flush with port wall, 25 mm below exit

[a]Same locations were employed for both gasification and combustion modes.

are given in Table 3.5.

Temperature measurements shown in Fig. 3.21 (a) indicate that flash back has taken place after about 30 minutes of stove operation. Oxygen measurements at locations 1, 2 and 3 are indicative of progressive depletion of oxygen levels along the vertically upward direction as shown in Fig. 3.21 (b). Higher oxygen level at the port exit may be due to influx of air along the top surface of fuel block due to draft created by flame and the combustion device. The variations in the oxygen record at location 1 may be due to movements in the eye of the swirl, that is created in the bottom region due to ambient disturbances.

Since flash back was present in most of the cases of AR = 6 stove, it was decided to increase the AR to 6.5 and test the performance. Port size and inlet geometry used for AR = 6 stove were retained.

Fuel port surface temperature measurements at several vertical locations were made in a stove with 40 mm port diameter. Single tangential inlet of size 30 mm × 6 mm, used in earlier experiments was retained. It was decided to make surface temperature measurements in the stove when it was operating in gasification mode and combustion mode for the complete operational duration to understand the differences between both the modes of operation. Temperature measurements were made with thermocouples placed flush with the port surface. This resulted in the junction getting uncovered during the operation of stove since port surface receded due to char oxidation. Therefore the surface temperature records for the stove operation unavailable beyond initial period.

Fuel port surface temperatures were recorded at five equally spaced vertical locations with measuring junctions located as indicated in the inset to Fig. 3.22. The coordinates of measuring junctions are shown in Table. 3.6. Temporal distribution recorded during runs are presented in Fig. 3.22 (a) and (b) when the stove is functioning in combustion mode and gasification

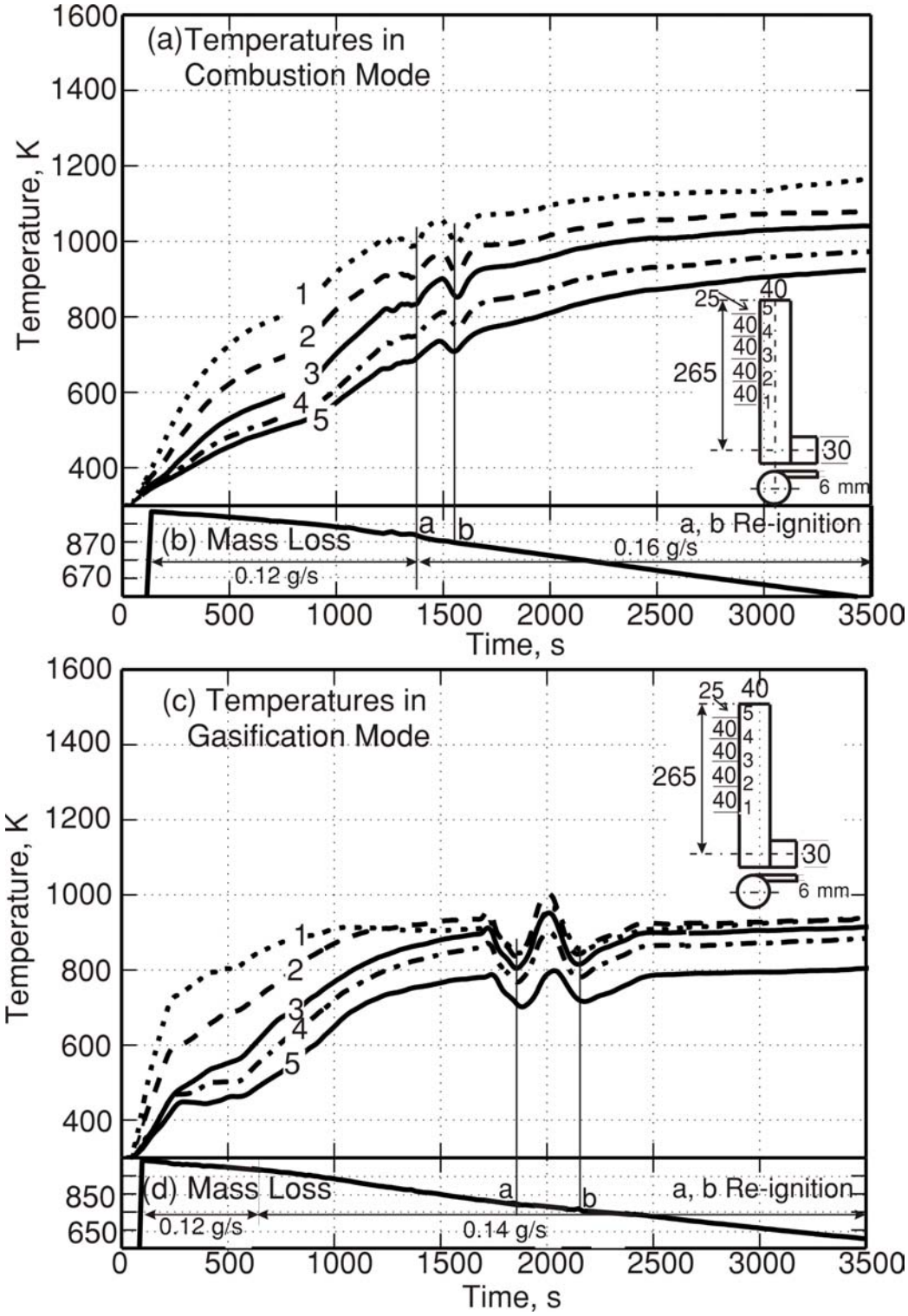

Figure 3.22: Temperature measurement (Port diameter = 40 mm, AR = 6.5). Figure (a) shows wall temperature histories at five axial locations (shown in schematic diagram) measured using K type 100 μm diameter thermo-couples with the stove operating in combustion mode. Figure (b) shows the corresponding mass loss. Figure (c) shows similar temperature measurements with the stove operating in gasification mode. Figure (d) indicates the corresponding mass loss. The temperature records indicate surface temperatures for the initial duration of stove operation.

Table 3.7: Specifications and performance of selected tube stoves of AR = 6.5

Sl No	Date '01/'02	d mm	AR	ρ $\frac{kg}{m^3}$	m_i kg	0-30 mins % Mass	0-30 mins Power kW	0-60 mins % Mass	0-60 mins Power kW	t_g min	Data[a]
36	10/7	40	6.5	240	1.07	23.0	2.0	50.0	2.2	0	T 3.22 (a)
37	12/7	40	6.5	235	1.05	23.0	2.0	47.0	2.1	60	T 3.22 (b)

[a]Numbers in the data column indicate figure reference numbers where the acquired data is presented.

mode respectively. The readings represent port surface temperatures only during initial period of stove operation. Experimental details are presented in Table 3.7. During these experiments combustion mode operation was achieved by using large amounts of liquid fuel for ignition which ensured that conditions in the port never became favourable for the onset of gasification mode.

In gasification mode operation of the stove flame flash back was observed after about 30 min of operation as seen in Fig. 3.22 (b). However, it was possible to stop combustion in the port by momentarily closing inlet using ceramic wool. After this the fuel block had to be reignited. The stove operation continued in gasification mode for about an hour.

Two important observations are made from this comparison experiment. (i) During the initial phase, port surface temperatures of stove functioning in gasification mode were higher than that of combustion mode at corresponding times as seen in temporal temperature distributions presented in Fig. 3.23 (a) and (b). This difference was larger in location 1 which was nearer to inlet compared to location 5 near port exit. In the gasification mode the surface temperature is a consequence of a surface reaction between the char and the oxygen diffusing to the surface. In the case of combustion mode, the oxygen at the surface is very low since it is consumed at the flame itself and hence the temperature realised at the surface is a consequence of the heat transfer to the surface from the flame. (ii) Surface temperature profiles shown in Fig. 3.23 (c) and (d) indicate a sharper temperature gradient in axial direction during gasification mode operation compared to combustion mode operation at corresponding times. This implies port surface temperatures were more uniform in combustion mode operation.

Since flash back was present in AR = 6.5 stoves also, AR = 8 stove were tried. Port diameter was retained at 40 mm. The inlet geometry was also maintained same.

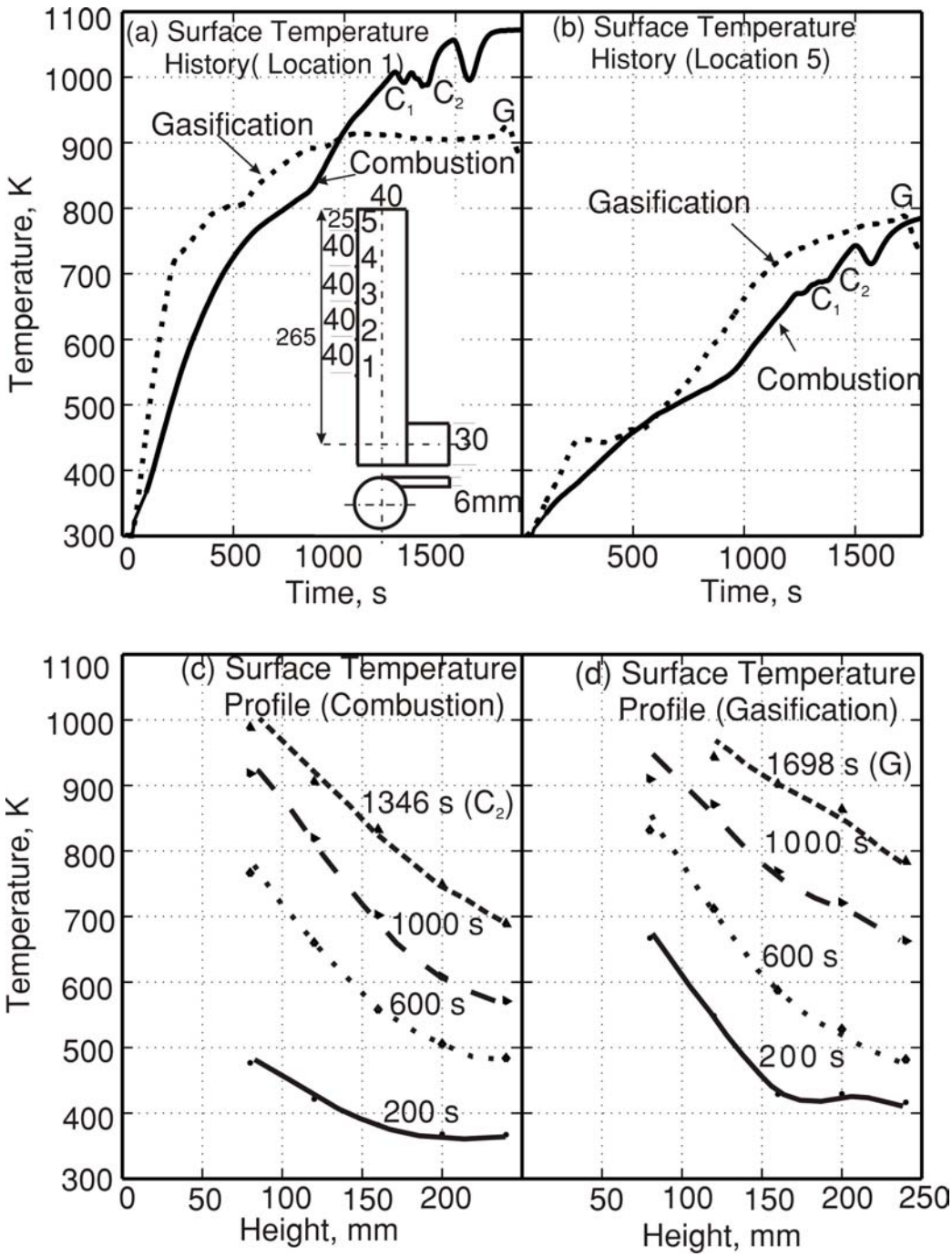

Figure 3.23: Comparison of gasification and combustion mode. Figures (a) and (b) indicate surface temperature histories at locations 1 and 5 respectively during stove operation in combustion mode and gasification mode. Figure (c) shows thermal profile of the surface during combustion mode operation at various times. Figure (d) shows a similar plot when stove is functioning in gasification mode.

Table 3.8: Specifications and performance of selected tube stoves of AR = 8

Sl	Date	d	AR	ρ	m_i	0-30 mins		0-60 mins		t_g	Data[a]
No	'01/'02	mm		$\frac{kg}{m^3}$	kg	% Mass	Power kW	% Mass	Power kW	min	
48	16/12	40	8.0	225	1.3	26.9	2.9	46.2	2.6	30	T 3.24
49	19/12	40	8.0	235	1.3	29.2	3.1	53.8	2.9	35	T η

[a]Numbers in the data column indicate figure reference numbers where the acquired data is presented.

The schematic diagram of the stove is shown in Fig. 3.24. During this test the surface temperature at a location 25 mm below the port exit was monitored. Wall temperatures at several vertical locations were also monitored to assess the rate of progress of pyrolisis front into c-phase at various levels. These data are shown in Fig. 3.24 (a) and (b). The fuel block details and stove performance is presented in no #48 of Table 3.8. The surface temperature record is presented as plot 's' in Fig. 3.24 (a). During the operation of stove fuel block had to be reignited twice as indicated by letters a and b in the mass loss record shown in Fig. 3.24 (c).

These events were reflected as temperature drops in the surface temperature records. During the operation of that stove flash back took place after 30 minutes of stove operation. The event was not reflected on the surface temperature record implying flash back occurred only through the central region of the port.

The fuel block wall temperature records indicate that at the end of gasification period fuel block wall temperature at location # 2 had reached 400 K indicating volatalization had commensed in this region. This implied pyrolisis front was close to wall which also meant fuel release rates through this zone might have come down considerably. This strengthens the view point that higher fuel release from the bottom region is essential for gasification mode operation. Also The temperature rise in the 5^{th} and 6^{th} diameters during the first hour of stove operation was close to nill.

Since single inlet stoves had exhibited flash back phenomena at all the aspect ratios tried it was decided to find the effect of modification in inlet configuration on the flash back. The alternative inlet configuration tried was axial inlet stove of the type shown in Figs. 3.25. The reason for this choice arose from the consideration that it would be possible to concieve of a stove design without a side leg, no matter how commonly used it might be and it was decided to try out this configuration. Several experiments were done

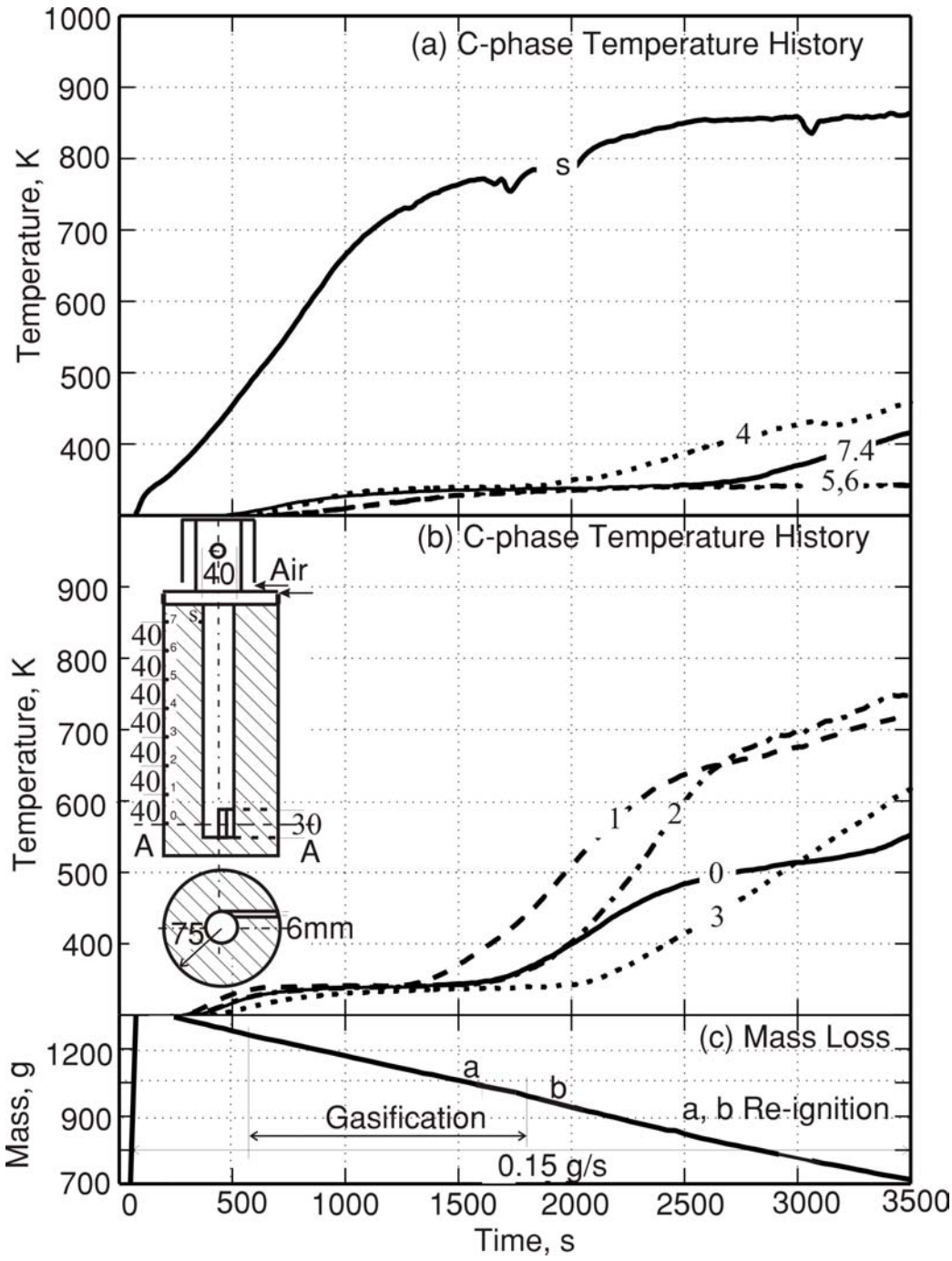

Figure 3.24: C-phase temperature measurement (Port diameter = 40 mm, AR = 8). Figures (a) and (b) show condensed phase temperature history at the locations indicated in the schematic diagram. Numbers on the plot indicate the axial position of thermo-couples with reference to inlet level in terms of number of port diameters. Plots refers to surface temperature 25 mm below port exit. R type 50 μm diameter thermo-couples are used. Mass loss as a function of time is shown in Fig.(c).

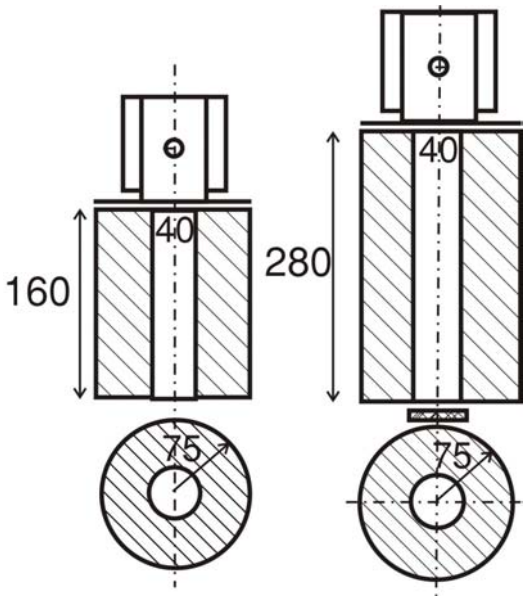

Figure 3.25: Figure shows axial inlet stove configurations tested.

Table 3.9: Specifications and performance of tube stoves with axial air inlets

Sl	Date	d	AR	ρ	m_i	0-30 mins		0-60 mins		t_g
No	'03	mm		$\frac{kg}{m^3}$	kg	% Mass	Power kW	% Mass	Power kW	min
70	16/02	40	4.0	180	0.7	36.2	2.1	–	–	05
71	16/02	40	7.0	235	1.0	25.2	2.1	–	–	20

for AR in the range 4–7, two of which will be reported. The experimental geometries of the selected experiments are presented in Figs. 3.25 (a) and (b).

Figure. 3.25 (a) shows an axial inlet stove with AR = 4. This stove had inlet area equal to port area. A gasification duration of about 5 minutes was observed. This is probably due to low packing density chosen. During the operation of stove, flame at port exit was frail with large amounts of air at the core. This could be detected by observing the flame at the exit which had a hollow structure with the central region beyond certain flame height devoid of reactions. Experimental details are presented in #70 of Table. 3.9. It was decided to check out the gasification performance at AR = 7. The fuel block is shown in Fig. 3.25 (b). During this trial also,

Table 3.10: Consolidated summary of experiments made on determination of causes of flash back

Port Dia. mm	AR	Inlet Area mm^2	Flash Back min
32	4.0	270	30
32	4.0	270	30
32	4.0	270	35
40	4.0	180	30
40	4.0	180	40
40	6.0	180	30
40	6.0	180	30
40	6.0	180	30
40	6.0	180	30
40	6.5	180	60
40	8.0	180	30
40	8.0	180	35
40	4.0	1250 (Axial)	05
40	7.0	1250 (Axial)	20

large amount of air was observed in the core and therefore the inlet geometry was modified to prevent excess air entry through the core of the port. Using ceramic wool, a gap whose area along the circumference of the inlet was equivalent to port cross section was created at the bottom air entry. This arrangement permitted air along the circumference of the inlet only and reduced the amounts of air traversing the core. The gasification duration during this experiment was about 20 minutes. The fact that gasification was achieved at all was contrary to expectations since earlier experiments were all made with restricted air inlets to achieve gasification. Gasification might have occurred in axial inlet stoves due to the cold air at inlet which gave a chilling zone near bottom allowing no flame in the port at the beginning of stove operation which permitted the gasification mode of functioning.

The experiments made with axial inlet stoves with the gasification mode of functioning had opened up new possibilities which were utilized in multi-port operation to be discussed in next chapter.

Experiments at various aspect ratios and inlet configurations have revealed that flash back is an inevitable part of tube stove operation. Table 3.10 consolidates information on the experiments made earlier and shows that in single port stoves flash back occurs beyond 30 minutes of stove operation.

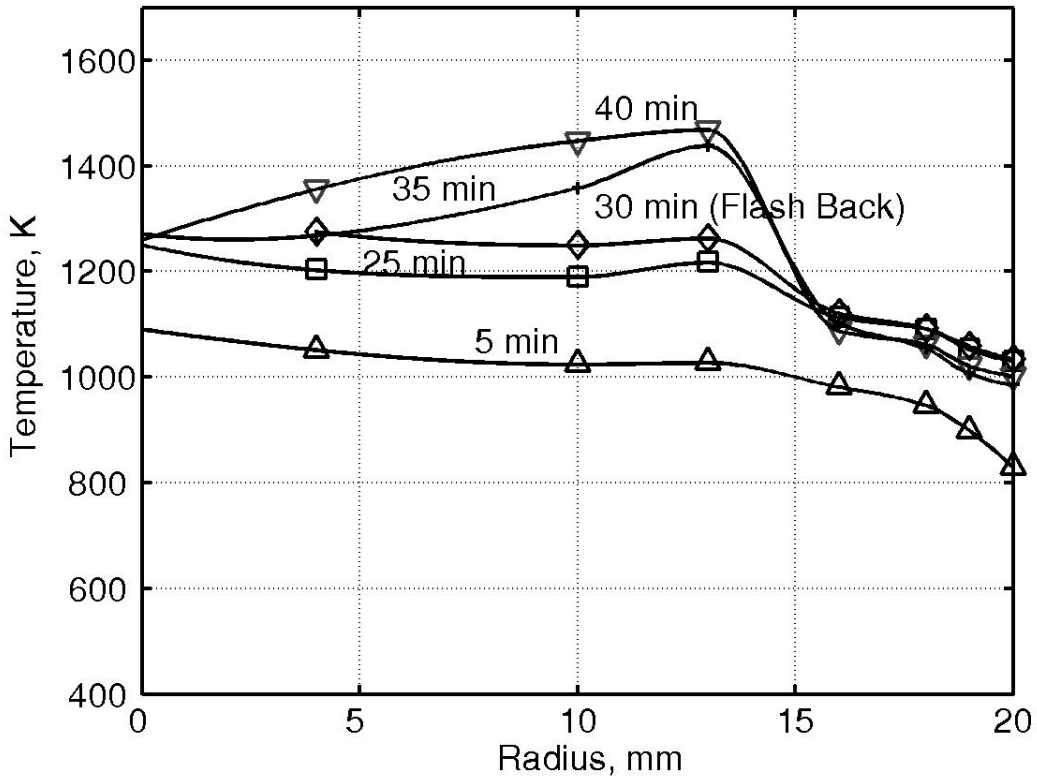

Figure 3.26: Radial temperature distribution in the fuel port 40 mm below port exit at various times for high power level operation.

The radial temperature distribution in g-phase at several times using data presented in Figs. 3.14 and 3.16 is presented in Figs. 3.26 and 3.27. The plots indicate that g-phase temperatures in the port are in the range of 600 to 1200 K. No other conclusions can be drawn from these plots as these were one off experiments and experiments were not repeated. Table 3.11 gives a comparison of time for peak gas temperatures from several experiments at a measuring plane 40 mm below port exit.

3.5 Miscellaneous Experiments

In order to determine the generality of the conclusions obtained from earlier studies, experiments were made at 63 mm port size in AR = 8 stoves. The air inlet used in these experiments was 75 mm $\times$ 6 mm to maintain same area ratio between port cross section and inlet cross section as that used in single inlet flash back studies. Table 3.12 shows the experimental details of

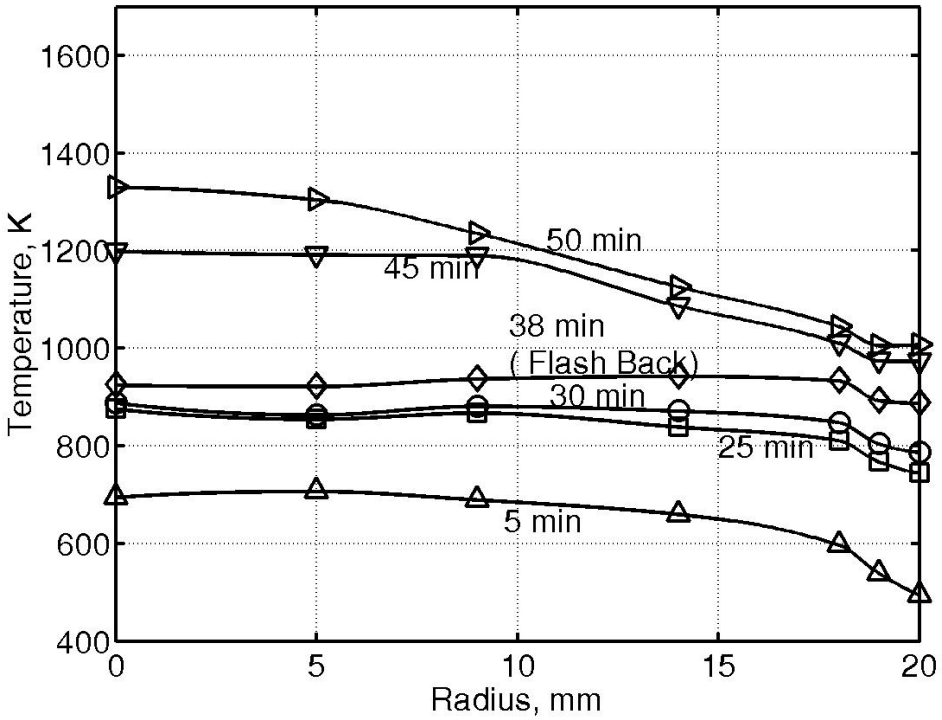

Figure 3.27: Radial temperature distribution in the fuel port 40 mm below port exit at various times for low power level operation (Higher density bottom region)

Table 3.11: Comparison of time for peak g-phase temperatures from several experiments

Sl	Time (600 K)	Time (800 K)	Time (900 K)	AR	ρ
1	120 s	600 s	1000 s	4	240
2	125 s	225 s	300 s	4	240
3	225 s	600 s	230 s	4	240
4	200 s	1000 s	1800 s	6	240
5	150 s	250 s	1500 s	6	225
6	125 s	250 s	800 s	6	225
7	50 s	800 s	900 s	6	225

Table 3.12: Specifications and performance of selected tube stoves of 63 mm port AR = 8

Sl	Date	d	AR	ρ	m_i	0-30 mins		0-60 mins		t_g	Data
No	'01/'02	mm		$\frac{kg}{m^3}$	kg	% Mass	Power kW	% Mass	Power kW	min	
50	25/12	63	8.0	250	3.0	26.0	6.6	50.0	6.3	0	T
51	26/12	63	8.0	266	3.1	24.4	6.6	47.0	6.3	0	T
52	26/12	63	8.0	275	3.2	22.8	6.0	40.6	5.5	10	T

the experiments carried out. These stoves operated in combustion mode for almost the entire duration of operation. It was decided to attempt to induce gasification in these stoves by increasing density in the bottom region. Outer diameter of the fuel block was kept same as that of the previous tests so that effect of reduced fuel web thickness on conversion percentage could be studied. The size of device at the exit was increased to enable it to handle higher mass through puts generated in 63 mm port. This stove operated in combustion mode from a few minutes after the lighting.

In an other experiment it was decided to use higher overall packing density with bottom region packed to density as high as 300 kg/m^3 and the upper region at 275 kg/m^3 as this fuel block also functioned in combustion mode.

Thus all experiments with port size larger than 40 mm and sawdust have resulted in combustion mode. The reason for this condition is inferred to be that the reactive zone in the port has such a large thermal release even with gasification mode that the surface temperatures near the top region attain quickly the minimum critical values ($\sim$950 K) so that combustion mode is unavoidable.

A stove configuration with high packing density (about 300 kg/m^3) in the radially outward region towards the stove wall and low packing density (230 kg/m^3) in the region around the fuel port as shown in the Fig. 3.28 was tried. This arrangement was made so that lower packing density around the port region would facilitate easy ignition and quick establishment of gasification mode functioning of the stove. The pyrolisis front encounters higher packing density fuel around the time combustion mode sets in. This strategy has resulted in a longer duration of gasification mode operation of 50 minutes compared to normal packing technique.

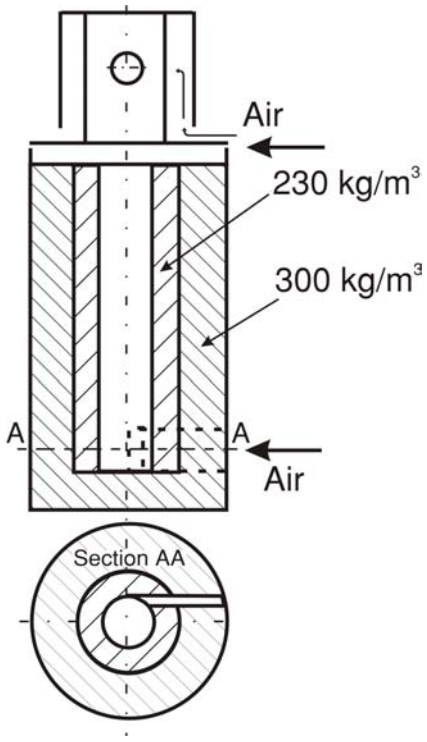

Figure 3.28: Schematic diagram of stove with higher fuel packing density in the outer region and lower density in the region around the fuel port.

3.6 Propagation Rates, Efficiency and Emissions

During the studies conducted on flash back phenomena information regarding position of pyrolisis front at various times was obtained. C-phase temperature histories at known locations were also determined. These data could be used to determine the rate of pyrolisis front movement into c-phase, called the propagation rate. Experimentally determined data along with theoretical comparisons will be presented in this section.

Most of the studies made on the flash back phenomena seen in tube stoves were made with the stove operating such that the products escape to the ambient and the flow through the port is unobstructed by the presence of the vessel. The presence of the vessel at the exit of the stove may also have an effect on flash back and consequently gasification duration. To quantify this and also evaluate the performance of the stove as an energy extraction system, the performance studies were conducted. Stove with 40 mm port

and AR = 6 was used for the determination of performance of tube stoves. A photograph of this stove in operation is shown in Fig. 3.29. This stove has prospects of high heat utilization efficiency as it delivers focussed energy which was one of the primary reasons for the selection of this stove for study in the first place. Performance of this stove in terms of efficiency and quality of combustion will also be presented in this section.

3.6.1 Propagation rates

Studies were conducted to determine the propagation rates of the pyrolisis front in the c-phase of the stove experimentally and two different sets of data were used to determine propagation rates in the c-phase of the stove at different vertical levels. They are

1. Pyrolisis front position at various times trapped on paper sheets (see Fig. 3.11)

2. Radial temperature distribution (see Fig. 3.12)

Average propagation rate was determined as distance moved by pyrolisis front in a known time. In case 1 position of pyrolisis front after known duration of operation was available as interface between char zone and unburnt paper. Pyrolisis zone, indicated by the yellowed region in the paper sheet shown in Figs. 3.11 (a) and (b) of page 58 was found to be 2–3 mm thick.

In case 2, the attainment of a temperature of 580 K within the c-phase was assumed to signify location of the middle region of pyrolisis activity. From the known temperature distribution at all times and known thermocouple locations, propagation rates were calculated.

Propagation rates were also computed based on energy balance at the pyrolisis front for unsteady one dimensional heat conduction.

Considering energy balance at the pyrolisis front shown in Fig. 3.30,

Enthalpy of pyrolisis Products	+	Product Heat Gain	=	Enthalpy of Biomass	+	Biomass Heat Gain

Products of pyrolisis, volatiles and char, gain heat from char bed and wood gains heat from the front.

$$\rho_p \dot{r}(f h_v + (1-f) h_c) \quad + \quad k_c \frac{dT}{dr}\bigg|_c \quad = \quad \rho_p \dot{r} h_w \quad + \quad k_w \frac{dT}{dr}\bigg|_w$$

Figure 3.29: A photograph of 40 mm diameter AR = 6 stove functioning at 2.3 kW power level.

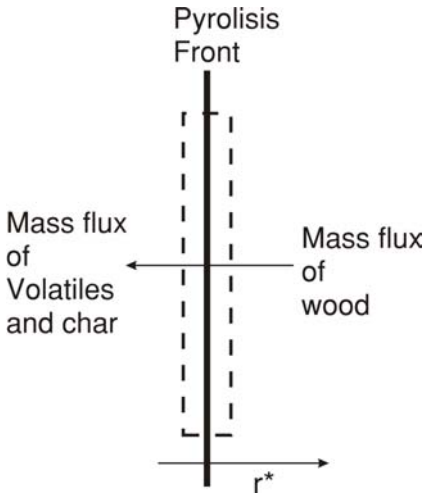

Figure 3.30: Mass balance at the pyrolisis front

Where, ρ_p is the loading density of the pulverised fuel kg/m^3, $\dot{r}$ is the pyrolisis front propagation rate m/s, f is the fraction volatilized, h_v is the enthalpy of volatiles, h_c is the enthalpy of char, J/kg and h_w is the enthalpy of wood, J/kg, k_c is the conductivity of hot char, W/m K and k_w is the conductivity of wood. Subscript c denotes char and subscript w is used for wood. Subscript c denotes char and subscript w is used for wood. This is simplified to

$$\rho_p \dot{r}(f h_v + (1-f)h_c - h_w) = k_w \left.\frac{dT}{dr}\right|_w - k_c \left.\frac{dT}{dr}\right|_c$$

Therefore

$$\rho_p \dot{r} \Delta H = k_w \left.\frac{dT}{dr}\right|_{w,r=r^*} - k_c \left.\frac{dT}{dr}\right|_{c,r=r^*} \tag{3.3}$$

ΔH is the heat of reaction of pyrolisis of wood J/kg. Superscript * is used to denote position and properties of pyrolisis front.

The temperature gradients are evaluated as follows. Consider the char zone. The products of pyrolisis at temperature T^* move across the porous char zone radially inwards, absorbing heat from char zone to get released into the port at T_s. Neglecting the temperature dependance of conductivity the conduction equation for char zone becomes

$$\frac{1}{r}\frac{d}{dr}\left(r\frac{dT}{dr}\right) + \frac{\dot{m}c_p}{2\pi r k_c}\frac{dT}{dr} = 0 \tag{3.4}$$

Where $\dot{m}$ is the mass loss rate per unit height of the bed kg/m.s and c_p is the specific heat J/kgK of hot char. The boundary conditions are at $r = a$,

$$h(T_g - T_s) = -k_c \frac{dT}{dr} \tag{3.5}$$

Where h is the free convection heat transfer coefficient W/m^{2}K, T_g is the gas temperature K within the port and T_s is the port surface temperature. At $r = r^*$, $T = T^*$. Temperature distribution in char zone is obtained as

$$T = C_2 - \frac{C_1}{r^c} \tag{3.6}$$

and temperature gradient in char zone is obtained as

$$\frac{dT}{dr} = \frac{C_1}{r^{1+c}} \tag{3.7}$$

Where

$$c = \frac{\dot{m}c_p}{2\pi k_c} = \frac{2\pi r^* \rho_p \dot{r} c_p f}{2\pi k_c} = \frac{f\rho_p c_p}{k_c}\dot{r}r^* = D\dot{r}r^* \tag{3.8}$$

Where f is the fraction of volatiles leaving the fuel bed.

$$C_1 = \frac{T^* - T_g}{\frac{1}{a^c} + \frac{k_c}{ha^{1+c}} - \frac{1}{r^{*c}}} \tag{3.9}$$

$$C_2 = T^* + \frac{C_1}{r^{*c}} \tag{3.10}$$

Similarly, the unpyrolised fuel region receives heat from pyrolisis front at location r^* and temperature T^* moving radially outwards. Let the radial coordinate for biomass region be r' so that $r' = r - r^*$. Therefore conduction equation for this region is written as

$$\frac{1}{r' + r^*}\frac{d}{dr'}\left((r' + r^*)\frac{dT}{dr'}\right) + \frac{\rho c_{pw}\dot{r}}{k_w}\frac{dT}{dr'} = 0 \tag{3.11}$$

Where c_{pw} is the specific heat of green biomass. The boundary conditions are at $r' = 0$, $T = T^*$ and at $r' = \infty$, $T = T_\infty$. The temperature distribution is given by

$$\frac{T - T^*}{T_\infty - T^*} = \frac{\int_0^{r'} \frac{\exp(-c_w z)}{r^* + z} dz}{\int_0^{\infty} \frac{\exp(-c_w z)}{r^* + z} dz} \tag{3.12}$$

The Temperature gradient is given by

$$\frac{dT}{dr'} = \frac{(T_\infty - T^*)\exp(-c_w r')}{(r^* + r')\displaystyle\int_0^\infty \frac{\exp(-c_w z)}{r^* + z} dz} \tag{3.13}$$

The integral in the denominator is re-written in terms of exponential integral as

$$\begin{aligned}\int_0^\infty \frac{\exp(-c_w z)}{r^* + z} dz &= \exp(c_w r^*) \int_1^\infty \frac{\exp(-c_w r^* y)}{y} dy \\ &= \exp(c_w r^*) E_1(c_w r^*)\end{aligned} \tag{3.14}$$

Where

$$c_w = \frac{\rho_p c_{pw}}{k_w}\dot{r} = D_w \dot{r} \tag{3.15}$$

Substituting 3.7 and 3.13 in 3.3 we have

$$\rho_p \dot{r} \Delta H = \frac{k_w (T_\infty - T^*)}{r^* \exp(c_w r^*) E_1(c_w r^*)} - \frac{k_c C_1}{r^{*1+c}} \tag{3.16}$$

Time taken for the front to travel between any two radial positions r_1^* and r_2^* is obtained as

$$t = \rho_p (\Delta H) \int_{r_1^*}^{r_2^*} \frac{r^* dr^*}{\frac{k_w (T_\infty - T^*)}{\exp(D_w \dot{r} r^*) E_1 (D_w \dot{r} r^*)} - \frac{k_c (T^* - T_g)}{(1 + \frac{k_c}{h a})(\frac{r^*}{a})^{D \dot{r} r^* - 1}}} \tag{3.17}$$

with $\dot{r}$ obtained from 3.16 for each value of r^*. The approximation for the function $E_1(x)$ where x is $c_w r^*$ is obtained from *Abramowitz and Stegun* (1964).

The packing density of biomass was $\rho_p = 250$ kg/m^3. The reported heat of reaction ΔH for wood pyrolisis is in the range -160 to -200 kJ/kg (*Mukunda et al.*, 1984; *Kanury and Blackshear*, 1970). A measurement of heat of reaction of the sample used for experiment was tested for heat of reaction using Digital Scanning Calorimetry (DSC). DSC Data is presented in Fig. 3.31. The data indicates pyrolisis to be exothermic with a heat of reaction of about 120 kJ/kg. The values of various physical constants used are as follows. $c_{p(char)}$=1250 J/kgK, k_{char} = 0.4 W/mK, $k_{gas,800K}$ = 0.04 W/mK, ϵ_{char} = 0.9. $c_{p(wood)}$=2400 J/kgK, $k_{biomass}$ = 0.168 W/mK, $k_{air,300K}$ = 0.02 W/mK, ϵ_{wood}=0.6. Porosity of pulverised fuel bed was approximated based on particle density of biomass used (∼600 kg/m^3) and packing density of fuel bed during experiment. Porosity of char bed was estimated based on intrinsic char density of 1600 kg/m^3, assuming 20% of initial biomass is left

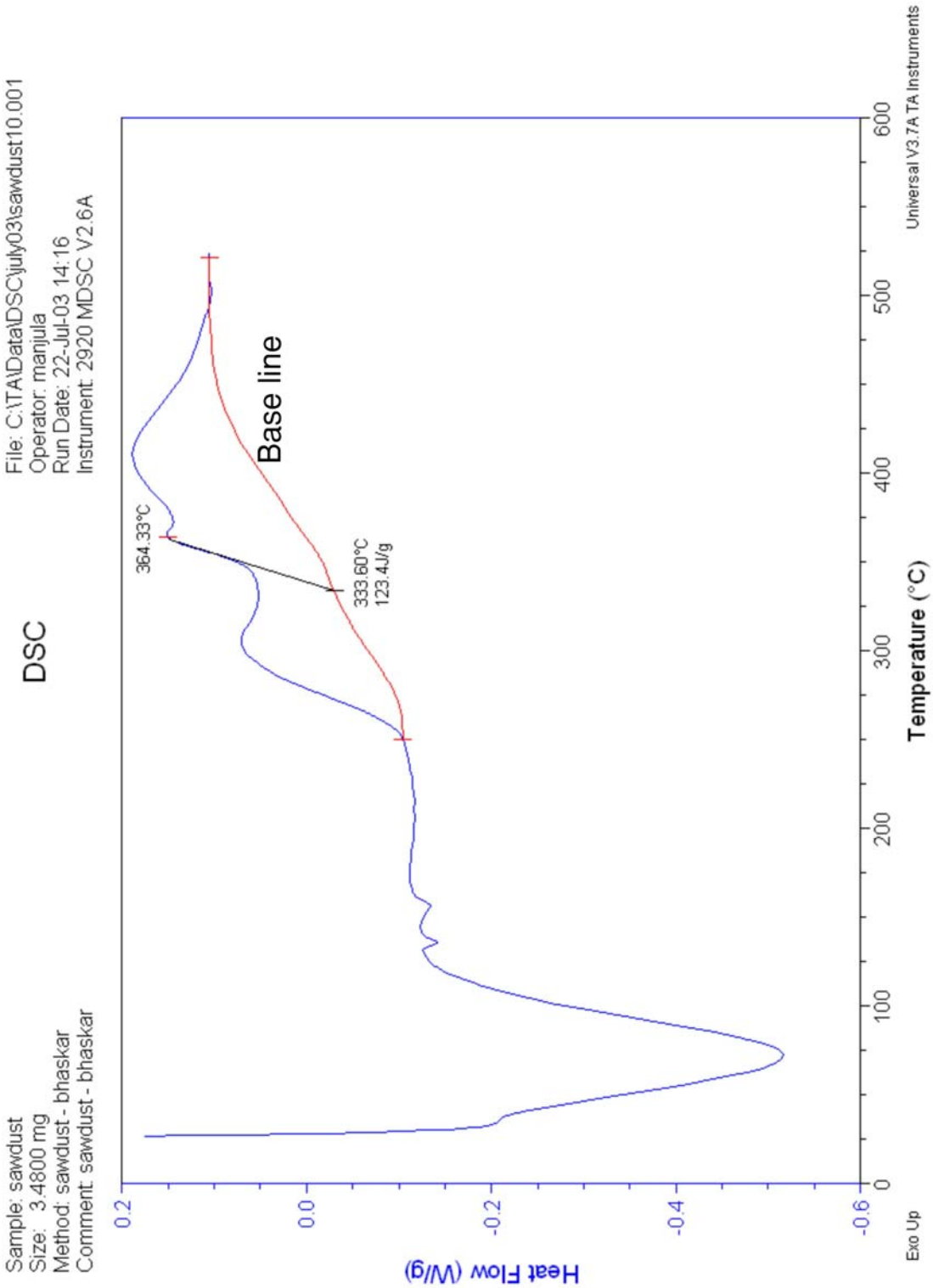

Figure 3.31: Heat flow rate W/g as a function of temperature for sawdust sample from Digital Scanning Calorimetry

behind as char. Most of parameters have been chosen from available sources (*Mukunda et al.*, 1984; *Holman*, 1989; *Perry and Chilton*, 1973). The average conductivity of porous bed is obtained from *Mukunda et al.* (1984) as

$$\bar{k} = k_c(1-\epsilon) + \epsilon k \tag{3.18}$$

Where k_c is the conductivity of solid, k is the conductivity of gas in the pores and ϵ is the porosity, the fraction of gas volume in total volume.

The free convection heat transfer coefficient was estimated from corelation for vertical plates.

$$\mathrm{Nu} = 0.59(\mathrm{GrPr})^{0.25} \tag{3.19}$$

Where Nusselt number $\mathrm{Nu} = hx/k$, x is the vertical distance, Grashoff number $\mathrm{Gr} = gx^3(T_f - T_\circ)/(T_\circ\nu^2)$ Prandtl number $\mathrm{Pr} = \mu c_p/k$ with fluid properties evaluated at mean fluid temperature. The convective heat flux to the port wall from g-phase is subjected to a blocking effect by the mass flux from the port wall (mass flux causes the boundary layer to thicken resulting in reduced gradients) This results in reduction of heat transfer coefficient. This reduction in heat transfer coefficient is taken into account in the following manner. Heat transfer coefficient, h is proportional to $(\ln(1+B))/B$ (*Mukunda*, 1989).

Therefore,

$$\frac{h}{h_o} = \frac{\ln(1+B)}{B} \tag{3.20}$$

where $B = \rho v c_p/h$. Let $B_o = \rho v c_p/h_o$ where ρv is the volatile mass flux $f\rho_p\dot{r}$. Equation 3.20 is rewritten in terms of $B_\circ$ as

$$\frac{h}{h_o} = \frac{B_o}{\exp B_o - 1} \tag{3.21}$$

From which heat transfer coefficient h at any given $\dot{r}$ can be obtained.

The experimental geometry is shown in Fig. 3.12 of page 59. Details of thermocouple locations and acquired data are also presented there. The radius of pyrolisis front r^* as a function of time t, obtained from equation 3.17, is plotted in Fig. 3.32 as the solid lines for the range of heats of reaction for wood pyrolisis reported in literature. The experimentally obtained position of r^* as a function of time is also shown. The experimental results are in agreement with theory. The burn rates with measured values of heat of pyrolisis of 120 kJ/kg is closest to the experimentally determined burn rates.

The radial temperature distribution in char region ($r/r^* < 1$) and in biomass region($r/r^* > 1$) obtained from equations 3.6 and 3.12 is plotted in Fig. 3.33 (a)—(e). with radial positions normalised by the radius of the

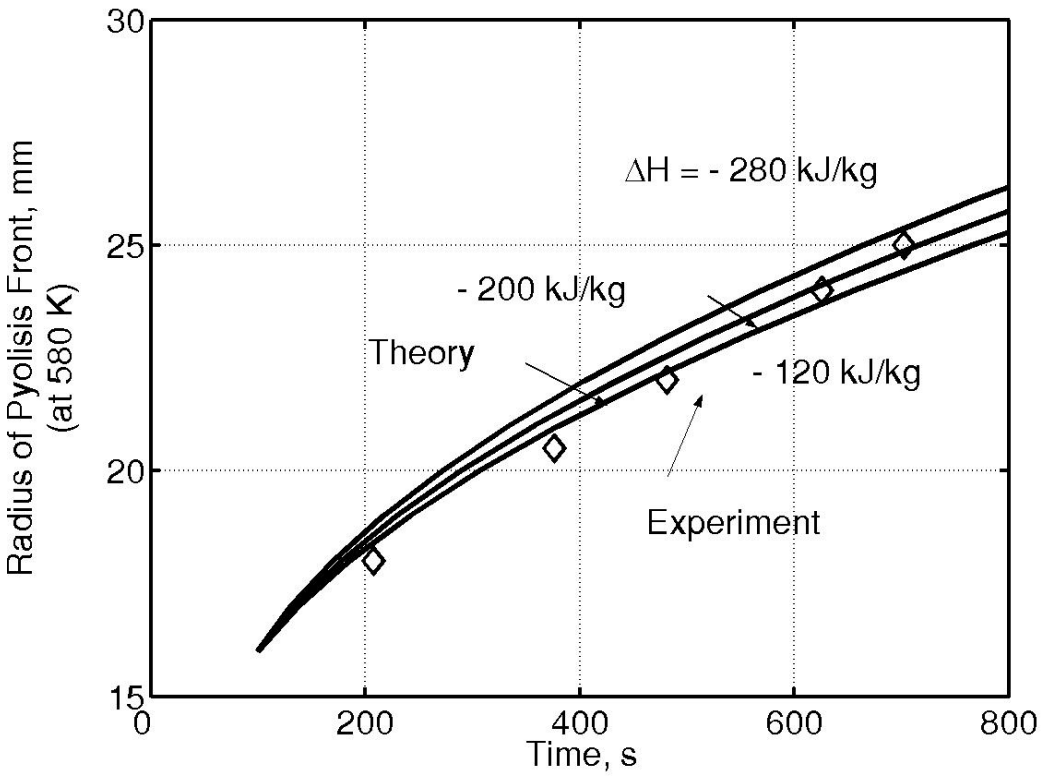

Figure 3.32: Radius of pyrolisis front as a function of time. Computed values are shown for three heats of reaction

pyrolisis front r^*. The experimental data plotted are for times corresponding to radius of pyrolisis front r^* indicated in Fig. 3.33 (a)–(e), obtained from Fig. 3.32. The experimental data concurrs with the theoretical predictions within experimental error.

C-phase temperatures as a function of time obtained from equation 3.17 at a location 2 mm into c-phase is plotted in Fig. 3.34. Experimental data linearly extrapolated from c-phase distribution 2 mm inside c-phase is also plotted for comparison. Measured surface temperature values are lower than the predicted values due to conduction loss from the measuring junction through thermocouple wires.

Regression rate at several vertical locations was also determined simultaneously using paper sheet experiments described earlier. This data is presented in Fig. 3.35. The average propagation rates obtained vary between 25 to 80 mm/hour. This variation is probably due to density variation of packed fuel. The swirl effects in the bottom region might also make a difference by causing particle erosion in the bottom region.

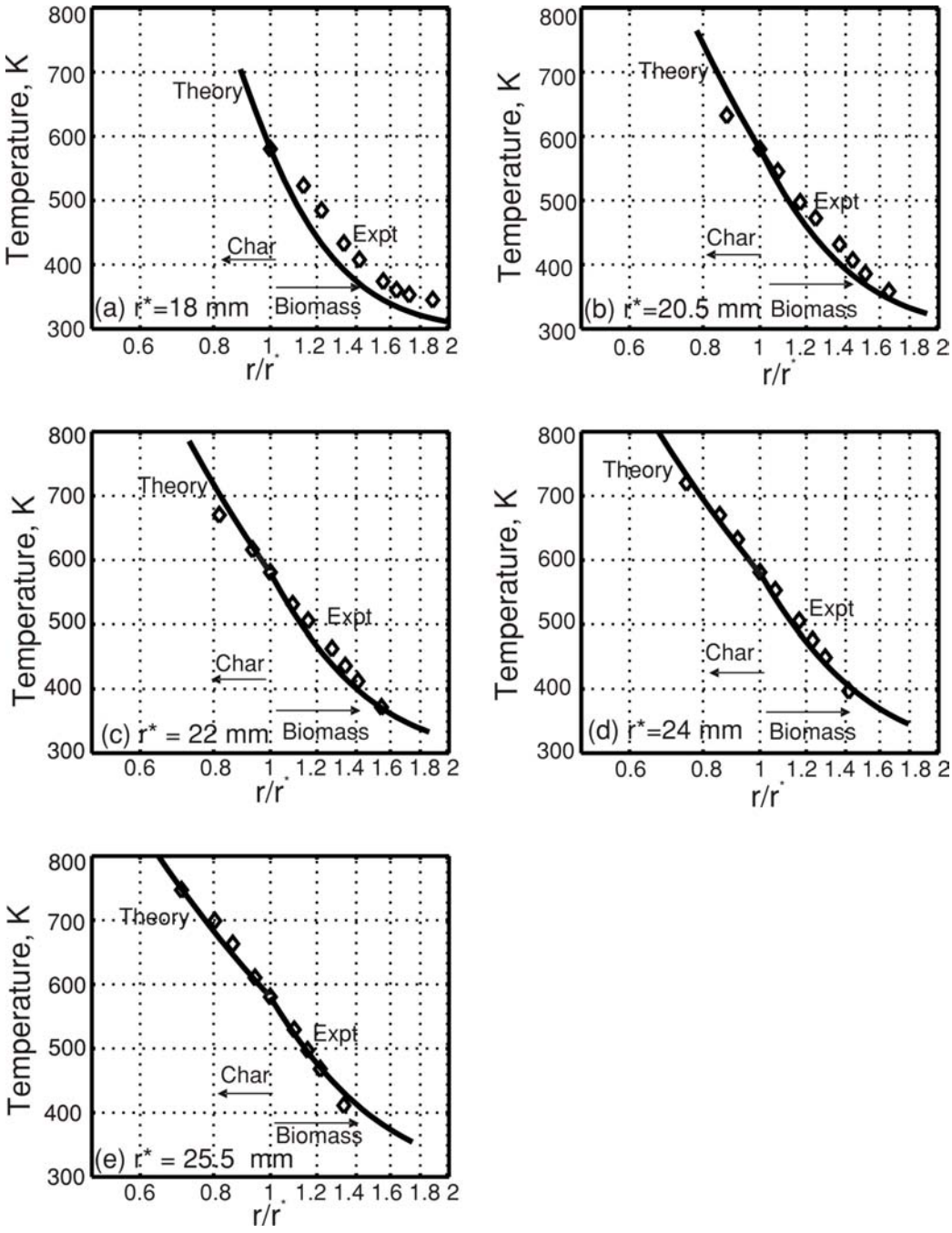

Figure 3.33: Radial temperature distribution at several positions of pyrolisis front

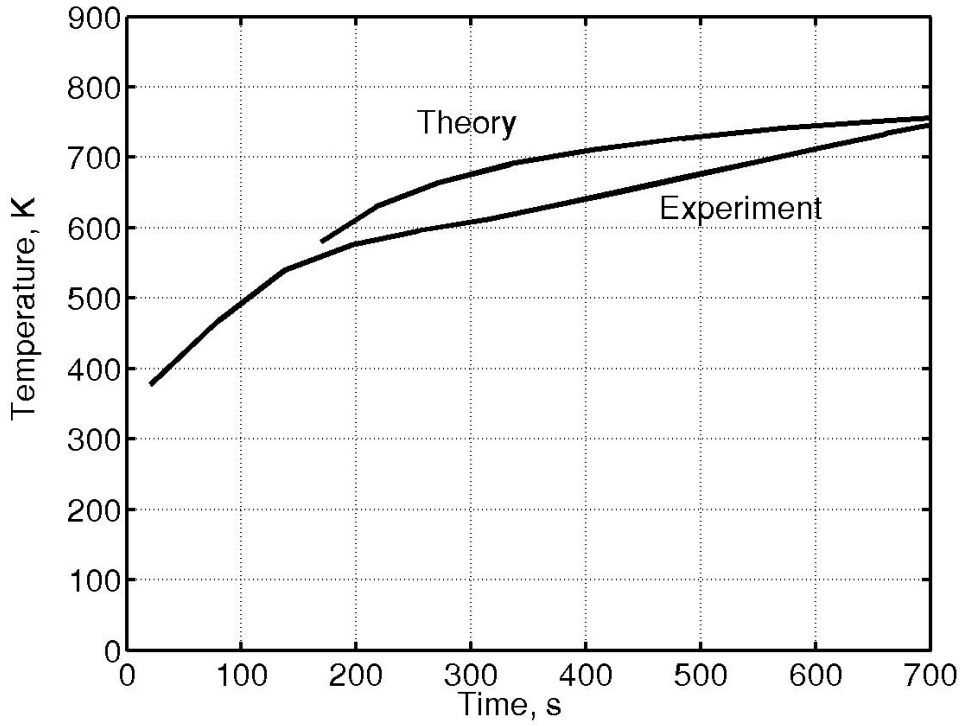

Figure 3.34: C-phase temperature as a function of time at a location 65 mm below the port exit and 2 mm into c-phase.

3.6.2 Efficiency

Studies on efficiency consisted of the determination of the effect of spacing between bottom of the vessel and the exit of the stove on the overall heat utilization efficiency of the stove. During this study effect of higher density bottom region on gasification duration of the stove was also studied. Efficiency was determined using standard procedures described in CIS 1315Z (part 1) 1991 of Beureau of Indian Standards (BIS). The vessel diameter for efficiency measurement for a particular power level is fixed as per BIS standards. The list of vessel diameters prescribed for various power levels is given in Appendix C The stove tested functioned at a nominal power level of 2.3 kW for which the prescribed vessel diameter is 200 mm and Water quantity for each heating was 2 kg.

The prescribed procedure consisted of repeatedly heating 2 kg of water at ambient temperature to a temperature 5°C below boiling point using two sets of vessels alternatively. The vessels were stirred once just before attainment

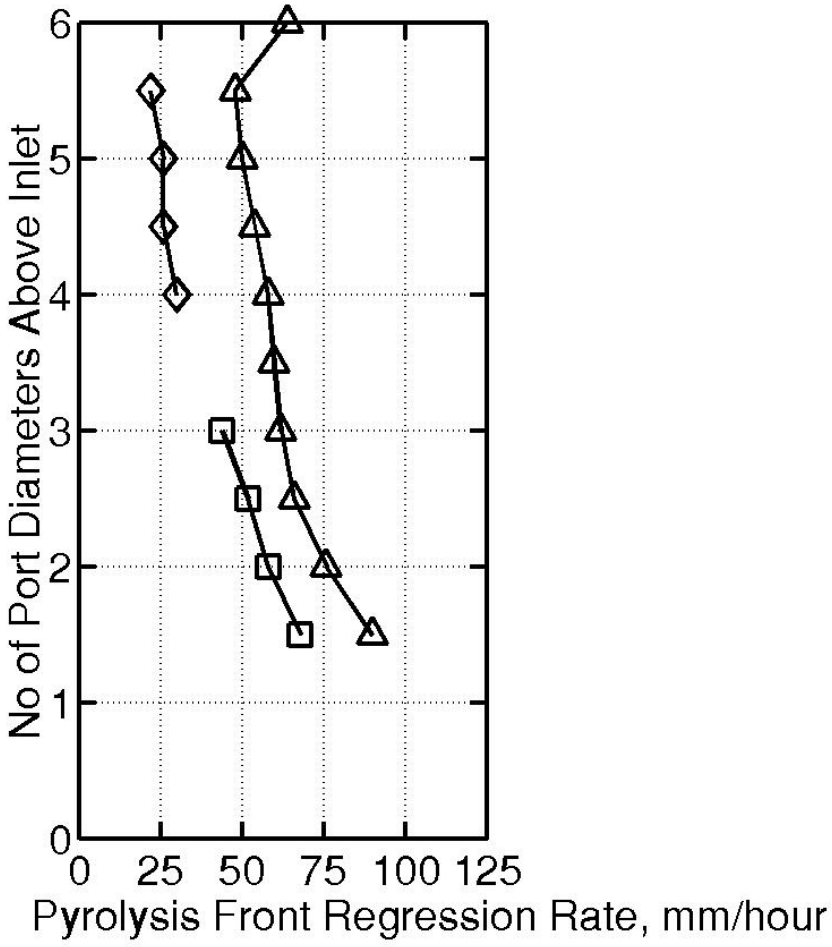

Figure 3.35: Pyrolisis front movement rates as a function of vertical distance

Table 3.13: Effect of spacing on water heating efficiency during first hour of stove operation. Initial biomass loaded is 1000 g. Average packing density is 225 kg/m^3. Inlet dimensions 6 mm x 30 mm

Spacing	Fuel converted		Power	IE[a]	OE[b]	η[c]	t_g[d]	Remarks
mm	g	%	kW	MJ	MJ	%	mins	
12	580	58	2.4	8.7	2.911	33.4	20	Lower Density
25	570	57	2.4	8.7	2.336	29.1	40	Bottom Region
12	460	46	1.9	6.9	2.544	39.8	25	Higher Density
25	440	44	1.8	6.6	1.963	29.7	50	Bottom Region

[a]IE = Input Energy
[b]OE = Output Energy
[c]η= Heat utilization efficiency
[d]t_g=Gasification duration

of required temperature. A total of 3 to 7 runs were required to completely extract useful energy present in the fuel block.

A special arrangement was made for mounting the vessel at various distances from device exit. This arrangement consisted mounting the vessel on a threaded support as shown in the schematic diagram inset to Fig. 3.36. Any desired gap could be obtained between the vessel and stove by adjusting the threaded support.

During the experimentation two sets of vessels were used. It was observed that increased gap brought down sooting tendency but heat utilization efficiency was also lower. A gap of 12 mm was found to be optimal for operation. Tests were conducted with graded packing densities. Fig. 3.36 shows the water temperature and the weight loss record. From water temperature record it is seen that stove is able to function effectively for a duration of 80 min. It was able to heat 2 kg of room temperature water to near boiling conditions in an average time of 13 min during the first hour of operation.

Results from these tests are presented in Table 3.13. The fuel block details and experimental summary of these experiments are presented in

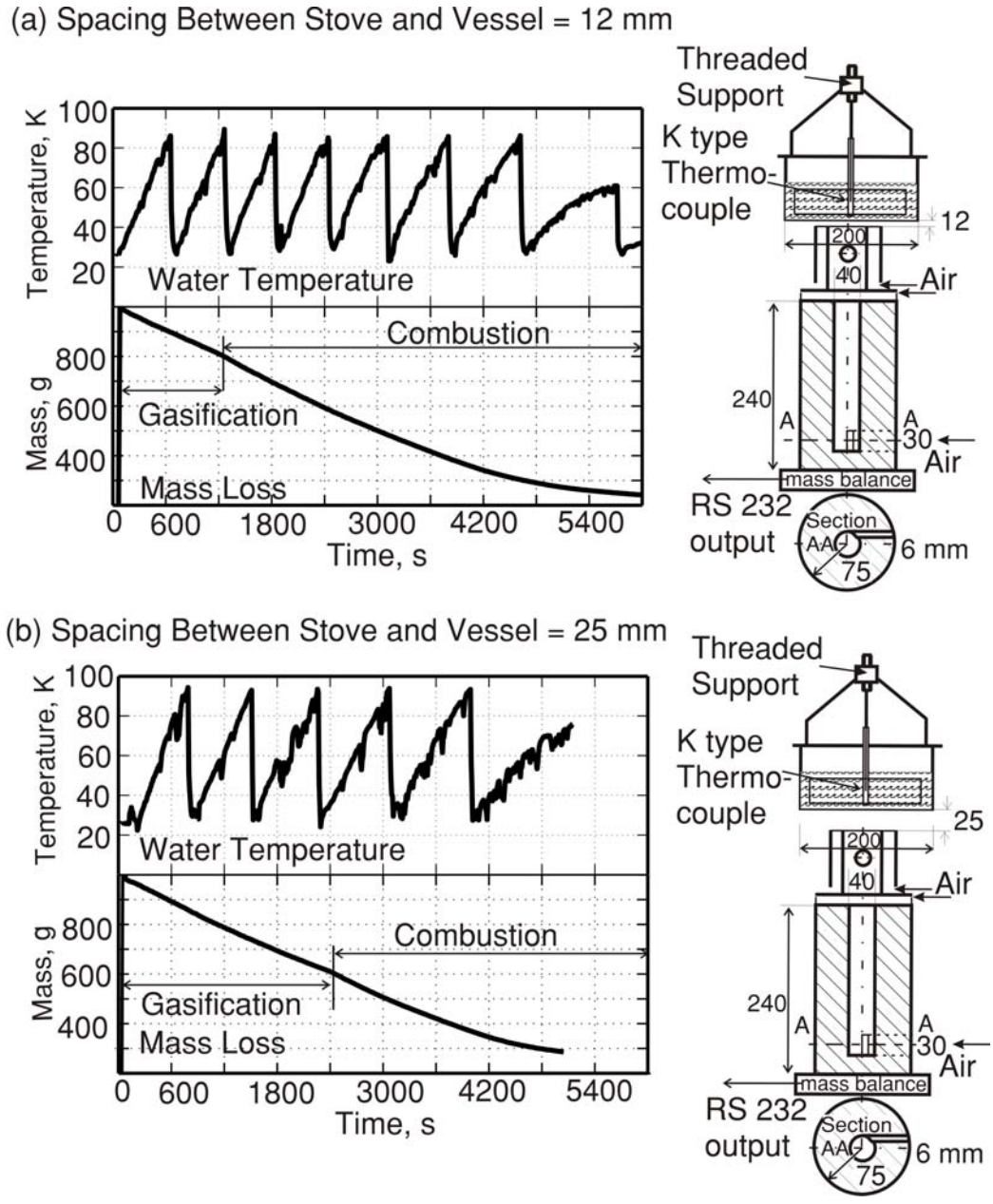

Figure 3.36: Effect of spacing between stove and vessel on water boiling efficiency for lower density bottom region of the stove. Figure (a) shows water temperature increase and corresponding mass loss of fuel for 12 mm spacing between stove and vessel. Figure (b) shows similar measurements for 25 mm spacing. Water content in vessel for each heating is 2 kg. Fuel loaded is 1000 g. Average packing density is 225 kg/m^3. Port diameter = 40 mm. Aspect Ratio = 6.

Table 3.14: Determination of efficiency

Sl No	Date '01/'02	d mm	AR	ρ $\frac{kg}{m^3}$	m_i kg	0-30 mins % Mass	0-30 mins Power kW	0-60 mins % Mass	0-60 mins Power kW	t_g mins	Data[a]
39	11/9	40	6.0	225	1.0	30.0	2.5	60.0	2.5	20	η 3.36 (a)
40	12/9	40	6.0	225	1.0	30.0	2.5	58.0	2.4	25	
41	13/9	40	6.0	225	1.0	30.0	2.5	58.0	2.4	40	
42	14/9	40	6.0	225	1.0	25.0	2.1	44.0	1.8	50	η 3.36 (b)
49	19/12	40	8.0	235	1.3	29.2	3.1	53.8	2.9	35	T η 3.37

[a]Numbers in the data column indicate figure reference numbers where the acquired data is presented.

Table 3.14. Experiments #39 and#40 were conducted with lower density bottom region while #40 and #41 were conducted higher density bottom region. The power level of operation for stove with lower degree of compaction was higher compared to the stove with higher degree of compaction as can be seen from Table. 3.13. Results presented in the table show lower density bottom region led to lower gasification duration. However, it is seen from Fig. 3.36 (a) that even with the presence of vessel the gasification duration of stove had remained around 30 min. Hence the result on the gasification duration is intrinsic to the operation of the stove.

In a separate experiment, efficiency of an AR = 8 stove was determined where the aim of experiment was to determine the effect of presence of vessel on the gasification duration. In that experiment, gasification duration was 35 min and the efficiency of operation was 26%. Lower efficiency was inferred due to higher input power level. Data from this experiment is presented in Fig. 3.37. This result supports the observations made by *Mukunda et al.* (1988) regarding the dependence of stove efficiency on the choice of power.

3.6.3 Emissions

Air quality in an enclosed space where stove is functioning was tested for carbon monoxide and Solid Particulate Matter (SPM). Sooting tendency of stove was also tested. CO measurements were made using Quintox analyser with probe positioned at a distance of 30 to 45 cm from the burning stove and at a height of 30 to 37.5 cm from the ground level of the stove. The CO emissions were less than the 9 and 35 ppm, limitation of national air quality standards (both primary and secondary) of USA as quoted by *Mukunda et al.*

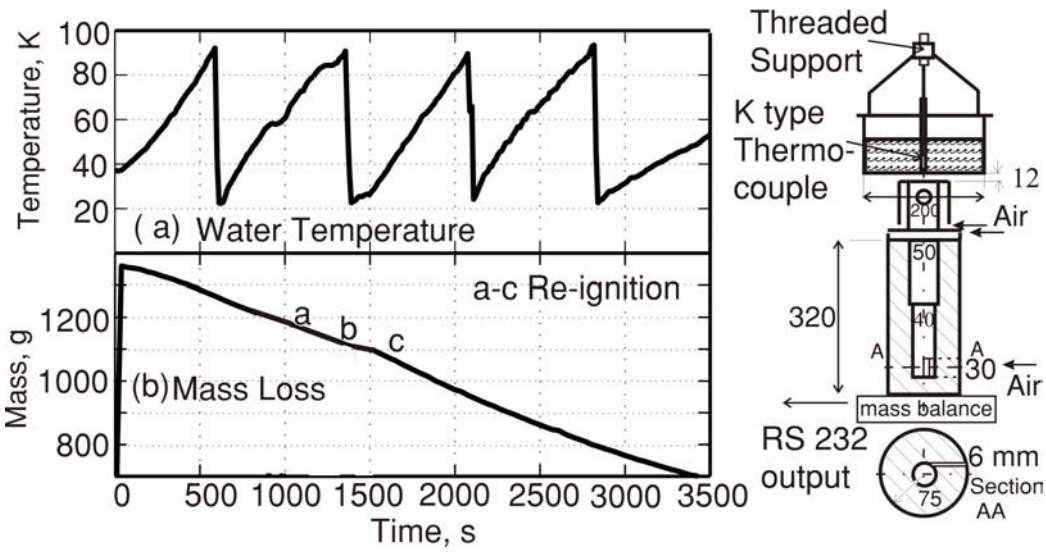

Figure 3.37: Determination of efficiency. Port Diameter = 40/50 mm Aspect Ratio = 8. Figures (a) and (b) show water temperature rise and mass loss respectively. Schematic diagram shown inset to figure shows the experimental arrangement.

(1988). The emission factors of CO, CO_2 and NO_x in terms for kg/kg fuel were also determined for tube stoves. *These studies were conducted for multi-port configuration of stoves and the results of these studies will be presented in Chapter 4.*

SPM in air surrounding stove was measured using an air quality meter which consisted of a vacuum pump with a flow meter connected to it. Ambient air in the enclosed space where stove was functioning was sampled from the same location described above, at the prescribed flow rate of 1 l/min through a desiccated whatman filter paper of known mass and of size 20 mm diameter (prescribed size). Mass of Particulate trapped in the given duration of one hour is found after weighing the dried filter paper. Since volume of gas flown across the filter paper was known SPM content could be determined. SPM content is found to be less than 2 mg/ m^3. This value is comparable to earlier measurements at 2.4 mg/m^3 reported by *Mukunda et al.* (1988).The actual kitchen SPM emission levels quoted by *Agarwal et al.* (1983) from their measurements in a number of kitchens are about 56 mg/m^3 maximum and 7 mg/m^3 average. The emission levels recorded in the present study is very low compared to these values.

Sooting tendency of the stove was also determined. This experiment was done in parallel with efficiency measurements. The soot collected at the bottom of the vessels used for water heating was cleaned using known mass

Table 3.15: Summary of single port studies

Sl. No	d	AR mm	No. of Expts	Density kg/m^3	% Converted	Avg t_g min	Expts with Reignition	m_i kg
1	40	4	5	240	44-54	30	None	0.8
2	40	6	10	225	40-60	36	5	1
3	40	6.5	2	240	47-50	0&60	1	1.05
4	40	8	2	230	46-53	30	2	1.3
5	63	8	3	260	40-50	0	0	3

of surgical cotton soaked in acetone. The soot collected is thus transferred to cotton. Cotton is dried in an oven and final mass is noted down to determine the mass of soot collected. Soot collected was about 2g/kg fuel. There is no comparison possible with earlier work on this subject as it appears that this parameter has not been a matter of concern in stove design or operations. Only study available on this subject was conducted by *Mukunda et al.* (1988) who have reported upper limit of soot ∼13g/kg fuel quantity for sun dry biomass with 12–15% moisture content.

3.7 Summary

This chapter has been concerned with single port operation with sawdust and other pulverised tree residues.

Lower density packing has led to stove operation with high power. Higher particulate emissions were also observed. Very high density packing in the stove has led to difficulties in ignition. High densities have resulted in low power operation. Occasional flame blow-off was also observed, possibly due to ambient winds. High density bottom region has also resulted in longer duration gasification mode operation. Average packing densities of 230–240 kg/m^3 was found to be most suitable for sawdust. This implies light packing is sufficient for proper stove operation. This guiding principle is found to be adequate for other fine fuels also.

Pyrolisis front propagation rate was determined using radial temperature distribution data. This data was compared with theory based on energy balance at the pyrolisis front for unsteady one dimensional heat conduction. The comparison of predicted propagation rates, temperature distribution and port surface temperatures with theory is excellent. Very extensive studies have revealed that the stoves function at 2.0 - 2.5 kW_{th} with a port diameter of 40 mm in gasification mode for about half the burn duration. Stove oper-

ation was characterized by low conversion percentages in the required burn duration and need for occasional re-ignition.

A summary of experiments made on single port stoves is presented in Table 3.15. From the table it is seen the percentage of fuel converted at the end of one hour, the chosen optimum operational duration, needs to be improved. Also except for the case of AR = 4 stoves fuel blocks have required reignition.

To overcome these two drawbacks multi-port stove designs with axial inlets were employed. Studies on these stoves are the subject of the next chapter.

Chapter 4

Studies on Multi-Port Stoves

In this chapter experimental studies on multiple port stoves will be described. Studies on multi-port pulverized fuel stoves were taken up to overcome two major short comings of single port stoves. They were (a) re-ignition problems and (b) low fuel-to-energy conversion percentage in the required burn duration. The objective of the study was to determine the stove configuration which would ensure no-loss-of-flame and high fuel utilization criteria along with power level, burn duration and low emission requirements stated in Chapter 3.

The reasons for expecting that multi-port stoves will help overcome the problems of single port design are as follows:

1. During multi port operation of the stove it was expected that the flames at the exit of the port would demonstrate a co-operative effect which would eliminate the need for re-ignition through external assistance, since at any given point of time, the probability of all the ports from an operational stove getting extinguished due to minor ambient disturbances was minimal making sure an ignition source in the form of at least one active port was always available for continued stove operation.

2. In multi-port stoves the progress of pyrolisis fronts originating from different ports took place towards each other which resulted in their shorter approach paths to unpyrolised biomass. This would contribute to higher conversion percentages within the required burn duration.

3. Since gasification mode operation took place for about half the burn duration, only biomass close to port wall got volatilized during gasification mode operation while the portions of fuel farther away from the port wall, especially in the top region of the stove, got oxidized in

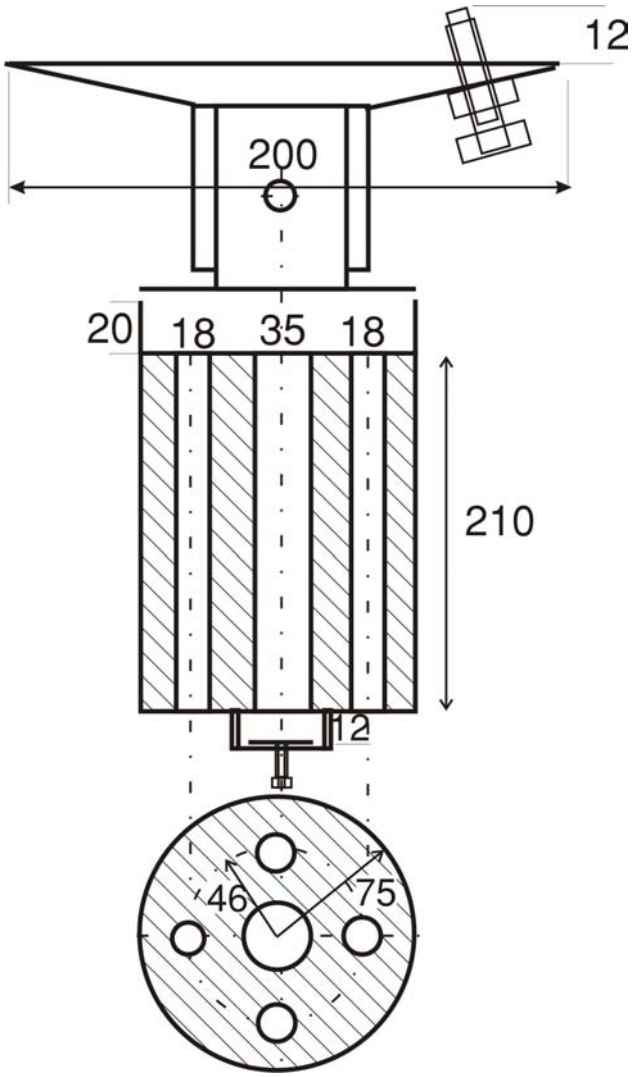

Figure 4.1: A multiport stove

combustion mode. Thus, overall combustion quality of a multi port stove was not inferior to that of a single port stove.

For these studies, axial inlet port design was selected. This choice was based on the consideration that in the side inlet configuration, minor collapse of loose biomass from the upper region, if left unattended, led to increased restriction or even blockage of side air inlet resulting in the non-optimum stove performance. Where as in axial inlet configuration of the type shown in Fig. 4.1 the loose biomass always fell through with no possibility of blockage.

4.1 Operation of Multi-Port Stove

The typical structure of a fuel block having multiple fuel ports with axial inlets is shown in Fig. 4.1. In this configuration there is a central main port of larger diameter with 4 auxiliary satellite ports of smaller diameter. A flat plate with an arrangement for varying the distance from the bottom of the fuel block was provided as a control area to vary the possible air-to-fuel ratio for cheiving gasification. This was helpful for placing a burning wick to facilitate ignition. Top of the fuel block was covered with a thin layer of ash which prevented indiscriminate lateral communication of ignition from the main port to side ports along the fuel block surface. A plenum volume vertically above the fuel block gave free passage to hot gases coming out of auxiliary ports into the device. The device shown at the exit in Fig. 4.1 is similar to the one used in single port studies. The conical perforated plate placed above the device was used to carry out emission studies with a flat bottomed vessel placed over it. Three adjustable threaded supports shown in figure were used to optimise the spacing between the vessel and the plate.

Only the central port was ignited at the beginning of stove operation. A few drops of kerosene were sprinkled around the circumference of central port and also on to the small pile of fine fuel on the plate below the axial air inlet. Ignition was performed at the top first to create the draught and then on the pile of fine fuel at the bottom. Then the top cover is placed above the stove. By the time the pilot fuel was burnt up this process taking 3–5 minutes, the bottom region of the port became red hot and started generating volatiles allowing the stove to operate in the gasification mode. Gasification mode operation continued for about 20 minutes beyond which flame was observed within the main port. Operation of stove during this period was similar to single port stove.

Based on the pyrolisis front propagation data from single port studies, the auxiliary ports were so located that the pyrolisis front would reach these ports by 20 minutes of operation. Auxiliary ports were at a greater aspect ratio and delivered fuel rich gases which burnt at the exit in a stable diffusion mode. The partly burnt fuel streams from the auxiliary ports got drawn into the device due to the draft created by existing region. A space between fuel block and the top device facilitated the free passage of gases from auxiliary ports to the device inlet. The excess fuel in the device region received part of the air necessary for oxidation through the central port as well as from the device. A small portion of the fuel also burnt beyond the stove exit. The port structure remained intact for almost entire flaming combustion duration. Towards the end of flaming combustion the structure around the central port was seen to disintegrate. By this time most of the biomass

present in the stove was charred. This is indicative of the high conversion percentages achieved in multi-port stoves.

4.2 Exploratory Studies

Various multiport configurations were tried before selection of suitable stove geometry for optimization. Of these, two will be discussed. They are

- small ports of same size distributed over the fuel block
- Central main port of larger diameter and auxiliary satellite ports of smaller diameter.

Smaller ports were experimented with the idea that they gave lower fuel delivery per port which implied the air available around the port exit might be sufficient for combustion. This would improve the quality of combustion at the port exit. A fuel block of this type is shown in Fig. 4.2. The other configuration consisted of central main port and satellite ports discussed earlier while describing the operation of stove shown in Fig. 4.1.

Two types of combustion devices were used during this phase of experimentation. For multi-port arrangements with ports distributed across the fuel block, it was thought necessary to create a plenum volume vertically above the fuel block with possibility of transport of air from sides into this volume. Hot product gases could escape from the top through a centrally located exit of small diameter. This device, which consisted of a perforated MS sheet cylinder about 50 mm high with a covered top, is shown in Fig. 4.2. During the operation of the stove with this device, it was found that product gases would leak out from the sides through top rows of perforation. This problem was solved by closing 1–2 top rows with a strip of sheet metal. This device has the advantage of long life since perforated sheet always gets maintained at lower temperature ($\sim 400^{\circ}$C) due to continuous air influx across it and also, the product gases made only edge contact with the device.

The second device tried was the device of the kind used in single port studies shown in Fig. 3.3 of page 47 and elsewhere. This device was more suitable for multiport configurations with central main port. In this device, only the inner metallic cylinder, which is in direct contact with the flame during stove operation, could be made replacable to achieve long life operation.

Both the devices performed well as far as quality of combustion at the exit of the port is concerned. The second device was preferred due to its capability to create a little extra draft which made sure all the product gases

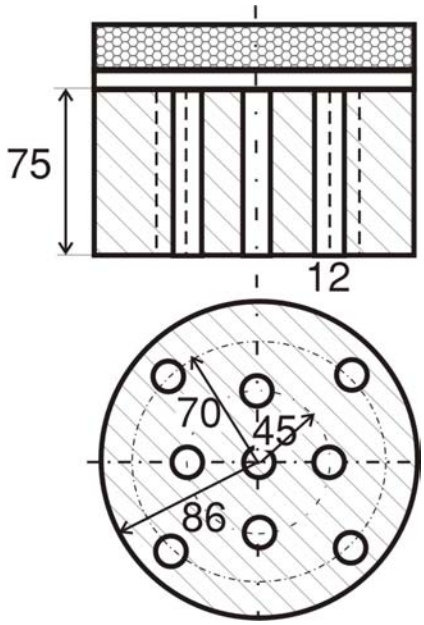

Figure 4.2: A perforated sheet device

were drawn through central region of the port with provision for addition of air from the sides giving an arrangement that ensured complete combustion.

Also the central main port configuration was preferred to distributed port configuration since ignition in this arrangement was more convenient as it was found that ignition of larger diameter central port was all that was required to start the stove operation. The remaining smaller ports started delivering fuel on their own once pyrolisis front moving radially outwards, reached them. Ignition of one auxilliary port was sufficient to maintain continuous flaming combustion. Distributed port configuration involved ignition of at least 2–3 small ports to achieve threshold power levels. Ignition of multiple smaller dia ports took slightly longer duration to catch on than single main port.

4.3 Optimization of Port Geometry

During the course of optimization, fuel block geometry was modified to obtain the required power level and conversion fraction. Different main port and auxiliary port configurations were obtained by using a replacable bottom plate with holes of required size drilled at desired position. Various combinations of sizes of main port and auxiliary ports were tried. In all those trials the combustion device of the kind used in single port studies was employed.

Table 4.1: Optimization of port geometry

Sl	Date	Main Port	Aux. Port		AR[a]	ρ	m_i	Power	Conv.	Burn time
No	'03	Dia.	Dia.	No		$\frac{kg}{m^3}$	kg	kW	%	min
1	26/02	35	18	3	6	230	0.7	3.0	68	40
2	27/02	35	18	4	6	230	0.7	3.2	72	40
3	19/02	40	18	6	5	265	0.75	3.5	73	38

[a]based on main port diameter

Experiments were made at various fuel port heights and main port and auxiliary port sizes. Number of auxiliary ports was varied between 3 to 6 to observe the effect on conversion percentage and power level of operation. The methodology adopted for arriving at the final stove configuration and two results high lighting the effect of number of auxiliary ports will be reported.

The initial mass of pulverized fuel was decided based on expected conversion percentage of ∼75%. Loading density was taken to be ∼230 kg/m^3 based on the experience from single port studies. A burn duration of about 40 min was considered acceptable for this study using the same hardware as was used for single port studies. The stove operation could be extended to any required burn duration by varying the outer diameter of the fuel block. At the specified conversion percentage, an initial fuel load of about 700 g would be sufficient to obtain a consistant power level of 3 kW for 40 minutes which corresponded to a mass conversion rate of 0.75 kg/hour.

A main port size of 35 mm with AR = 6 was considered for study. For this port configuration fuel block outer diameter of 150 mm would give the necessary initial fuel mass at the required loading density.

In the first test, a configuration with three auxiliary ports was considered. The geometry is shown in Fig. 4.3 (a). The mass loss during this test is presented in Fig. 4.1 (c). Experimental details are shown in #1 of Table. 4.1.

In the next test, the number of auxiliary ports was increased to 4. During this trial, peak power level was higher but at the same time conversion was better. This is probably due to the fact that four port configuration provides more circumferentially uniform approach to the fuel. Experimental details are presented in #2 of Table. 4.1.

Observation of the mass vs time data in Fig. 4.3 (c) show that in both the experiments the auxiliary ports became active by the end of 20 min of operation. This event is symbolized by the increase in mass loss rate around this time.

It was also seen that six auxilliary port configuration gave conversion

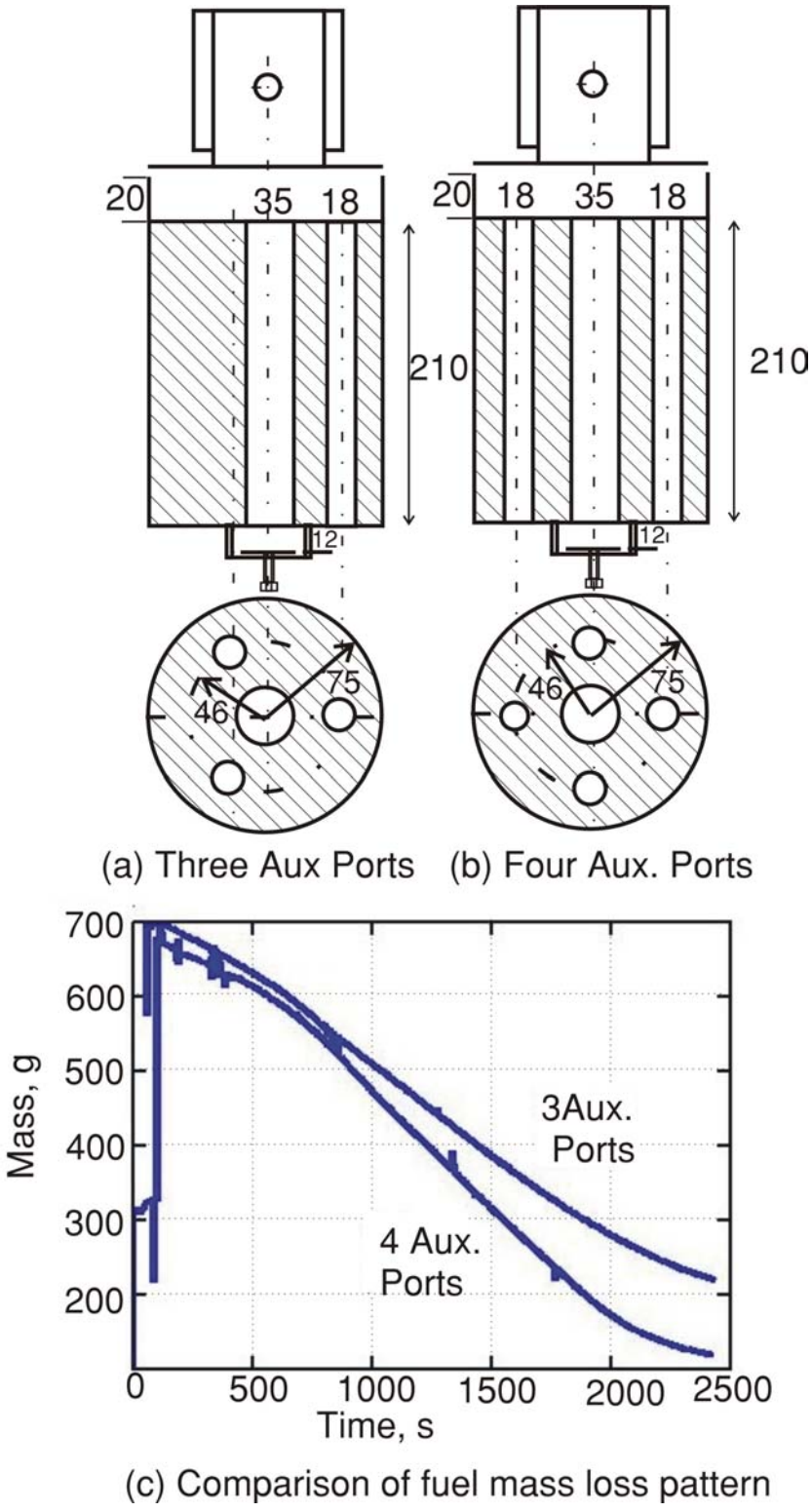

Figure 4.3: Comparison of performance of 3 aux. port and 4 aux. port stoves. (a) shows the 3 aux. port geometry. (b) shows the 4 aux. port geometry. The power levels of operation from these stoves are compared in (c).

percentage of 73% in 38 min burn duration as seen by the result presented in #3 of Table. 4.1. Usage of 6 auxilliary ports gave very high peak powers which would result in lower overall heat utilization efficiencies as discussed in 1.2. Usage of 4 auxiliary ports appears to be an acceptable compromise between achievable conversion percentages and uniformity in power delivered.

4.4 Emissions

The products of combustion from multi-port stove were tested for emissions of carbon monoxide and oxides of nitrogen. For emission studies, four auxiliary port configuration of the kind shown in Fig. 4.1 was employed. Standard hood method described in section 2.4 was used for emission measurements. Moisture free sample gases were analysed for CO, NO_x and O_2. From this data, the emission factors of pollutants in kg/kg fuel of known composition, were calculated using the method described in Appendix B.

It was found that emissions were higher when the spacing between the vessel and the stove was low. This was probably due to flame quenching due to larger portion of reacting gases coming in contact with colder metal. Similar observations were also reported by *Zhang et al.* (2000); *Ballard-Trameer and Jawurek* (1996). Lower spacing is preferable from the point of view of achieving higher efficiency. Therefore, a study was conducted to optimise the spacing at which acceptable efficiency and emission levels are achieved by varying the spacing between stove and vessel. This indicated that at a spacing of 12 mm between the vessel bottom and perforated guide plate at the bottom will have acceptable efficiency and emission levels. A comparison of the results of emission performance at some optimum spacing between vessel and the stove with the available data from literature is presented in Figs. 4.4 and 4.5.

The data from literature was presented and discussed earlier in 1.2.

CO emission factors of less than 17 g/kg fuel have been recorded during present study. The results of present study have demonstrated that lower emission at higher efficiencies is possible by adopting better combustion strategy in the form of phased air addition to the combustion zone. The hot product gases leave the stove through a narrow opening which results in focussed delivery of energy that not only ensures complete combustion as the exit region is generally kept hot but also improves downstream heat transfer efficiencies.

NO_x emission factors recorded from tube stoves are about 1 g/kg fuel. This value is higher than those obtained by *Bhattacharya et al.* (2002a) but falls in the mid range of the scattered values reported by *Zhang et al.* (2000)

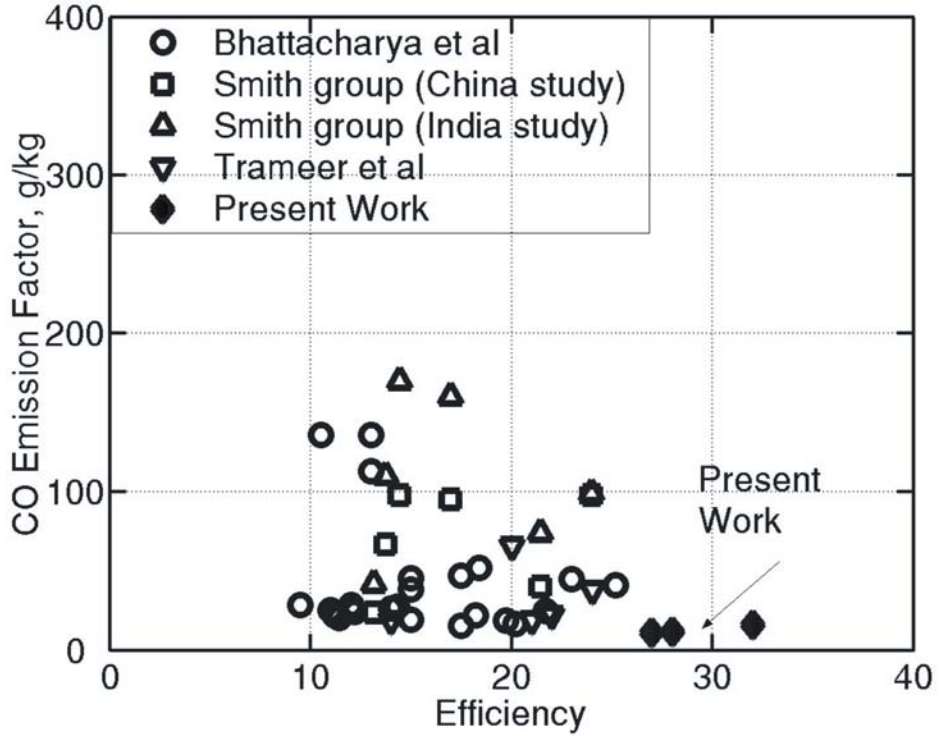

Figure 4.4: Comparison of results from present work with CO emissions reported in literature

as seen in Fig. 4.5.

4.5 Summary

Over 25 experiments were conducted on multi-port stoves with varying configurations and it was found that the combustion was continuous without any flame-out during multi-port operation. Fuel-to-energy conversion was in the range of 66% to 73%. Higher conversion efficiencies were observed in fuel blocks with larger number of auxilliary ports. The increase in conversion efficiency between 4 and 6 ports was not appreciable. It appears multi-port tube stoves which are relatively simpler to construct and operate are viable options to obtain "clean" combustion coupled with high efficiencies using pulverised fuels.

Trials were conducted to assess the performance of tube stoves using pulverised fuels obtained from leafy droppings. These studies will be described

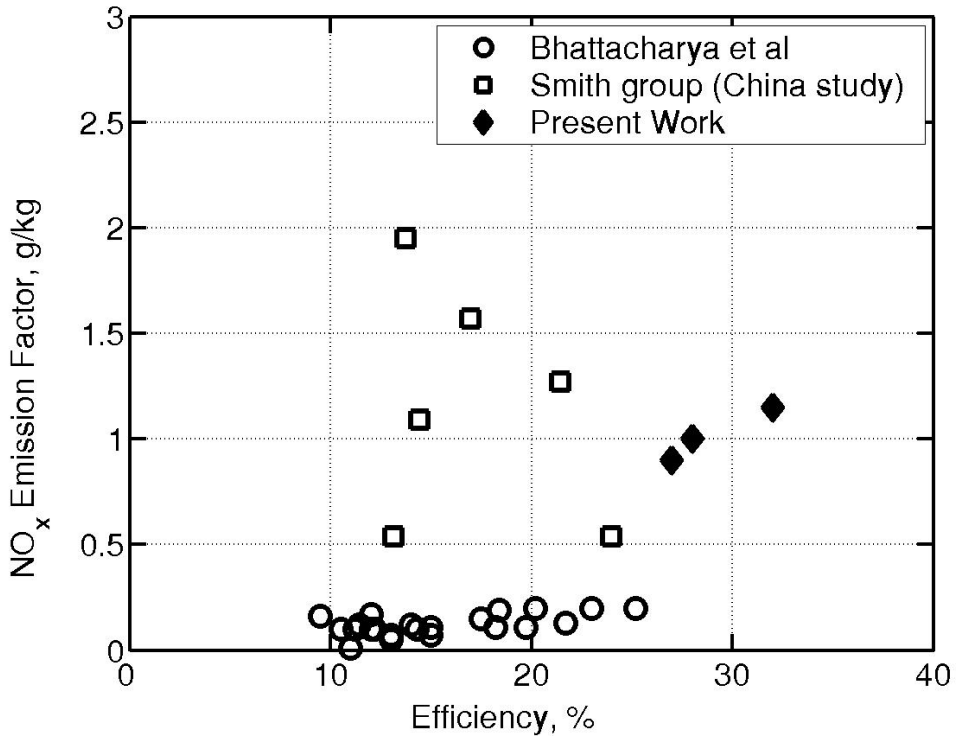

Figure 4.5: Comparison of present work with NO emissions reported in literature

in the next chapter.

Chapter 5

Studies with Other Pulverized Fuels

This chapter is concerned with the studies on extending the utility of a tube stove to other fine fuels generated by pulverising leafy biomass. The objective is to evolve a strategy for the selection of a suitable port geometry for biofuels with different characteristics.

Studies have been conducted in both single port and multi-port configurations to determine the power levels achieved in similar configurations as well as the port configurations that were suitable for proper functioning with various fuels.

5.1 Single Port

The performance of tube stove has been studied with varieties of pulverised leafy droppings in single port configuration. Of these, a comparative study of power levels from sawdust and pulverised acacia leafy droppings made at AR = 4 is reported. Under normal loading conditions the packing density of acacia was over 400 kg/m^3. This was due to high intrinsic density of fuel material (1000 kg/m^3) compared to sawdust.

A comparison of stove performance with similar configuration using acacia and sawdust as fuels is shown in Fig. 5.1. Experimental details presented in Table 5.1. The power level of operation was found to be 70% of sawdust stove (1.1 kW $_{th}$ instead of 1.6 kW$_{th}$) at comparable degree of compaction. This was puzzling since the only recognizable difference from sawdust stove at that juncture was the difference in loading density of the fuel and expected behaviour was denser pulverised fuel should still generate comparable power output as mass flux from pyrolisis front, given by $\rho_p \dot{r}$ was expected to remain

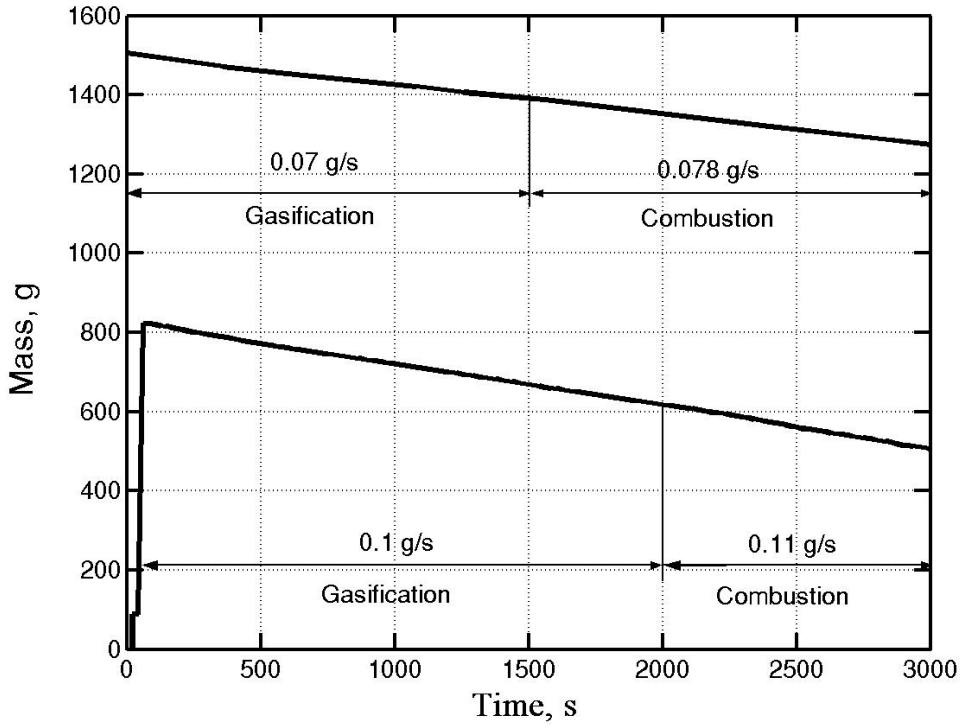

Figure 5.1: Comparison of mass loss profiles from single port stoves (Port Dia. = 32 mm AR = 4) with acacia and sawdust as fuels

Table 5.1: Comparison of Acacia and sawdust

Sl	Date	d	AR	ρ	m_i	0-30 mins		0-60 mins		t_g	Data
No	'01/'02	mm		$\frac{kg}{m^3}$	kg	% Mass	Power kW	% Mass	Power kW	min	
19	6/1	32	4.0	425	1.50	10.4	1.0	17.7	1.1	.	Acacia
25	24/2	32	4.0	240	0.82	21.7	1.6	44.7	1.6	.	Sawdust

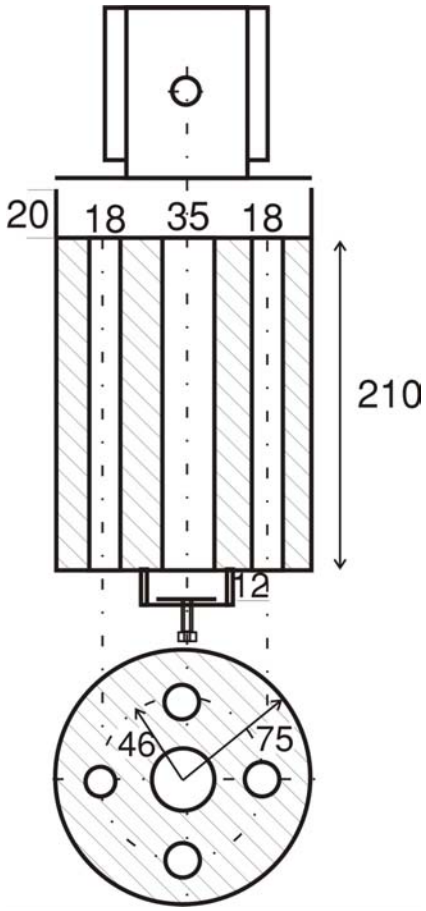

Figure 5.2: Multiport stove configuration used for comparison of leucaena and sawdust.

same, with increase in ρ_p getting compensated by decreased $\dot{r}$ (this is because all thermal balance equations have $\rho_p \dot{r}$ as the term; therefore, the surface heat balance allows one to get $\rho_p \dot{r}$, for instance, see *Mukunda* (1989)).

5.2 Multi-Port

A similar comparative study between performances of tube stove with pulverised leucaena pod and sawdust in a multi-port configuration was also conducted. The geometry employed for this study is shown in Fig. 5.2. Mass loss comparison is shown in Fig. 5.3. Experimental details are presented in Table 5.2. It is seen that the power levels obtained with leucaena as fuel is about 75% of the power level obtained in a similar geometry with sawdust as fuel as seen in Fig. 5.3.

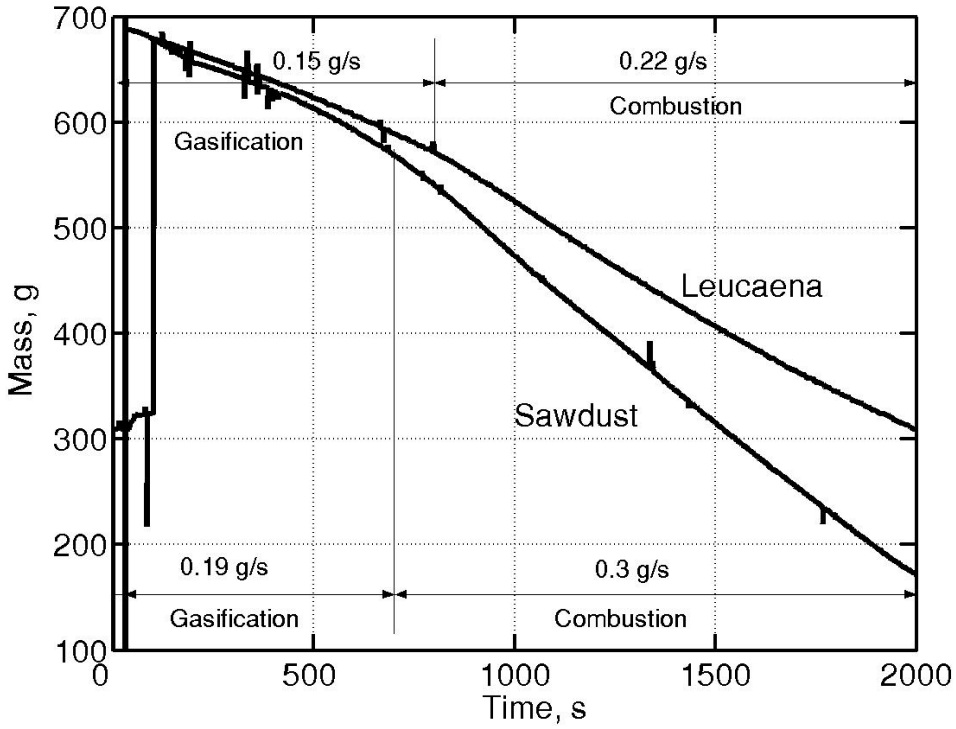

Figure 5.3: Comparison of mass loss profiles in a 4 aux. port stove with leucaena and sawdust as fuels

Table 5.2: Comparison of 4 Aux. port stoves with leucaena and sawdust as fuels

Sl	Date	Main	Aux. Port		AR[a]	ρ	m_i	Power	Conv.	t_b	Fuel
No	'03	Dia	Dia	No		$\frac{kg}{m^3}$	kg	kW	%	min	
1	27/02	35	18	4	6	230	0.7	3.2	72	40	Sawdust
2	23/02	35	18	4	6	230	0.7	2.4	72	55	Leucaena

[a]based on main port diameter

Table 5.3: Results of TGA study on selected pulverised leafy fuels at heating rate of 10°C/min

Sample	ρ_p	Volatilization				Ash	Rel. Power[a]	
	$\frac{kg}{m^3}$	% Mass	Range °C	Rate %/min	Rel. Rate	(Dry) %	Gasif.	Comb.
Leucaena	230	87	235–490	3.4	0.75	5.18	0.79	0.73
Acacia	430	79	235–520	2.7	0.6	9.52	0.7	0.71
Sawdust	230	86	260–450	4.5	1.0	3.11	1.0	1.0

[a]Relative to sawdust

In case of pulverised leafy fuels, the port size on extraction of the tube around which the fuel block formed, became slightly smaller than the diameter of the tube used to construct the port due to readjustment of particles. This tendency was also present in sawdust but to a lower extent. This resulted in reduced size fuel ports for pulverised leafy biomass fuels. Initially it was thought the reduction in power level was due to this reduction in port size. Therefore to offset this, the tube used to form fuel port was chosen to be slightly larger than the required port size. This did not appreciably increase the power level of operation.

Therefore, it was decided to conduct a Thermo Gravimetric Analysis of different pulverised fuels used in the stove to determine the thermo chemical behaviour of these fuels. The results of this study is presented in Fig. 5.4. A constant heating rate of 10°C/min was employed for all fuels. Ash content of the fuel was also seperately determined. These values are also presented in Table. 5.3.

It is seen that volatilisation rate of pulverised leucaena pod is 75% of sawdust (See Fig. 5.4). Packing densities of both fuels are similar. The relative power level obtained from leucaena fuel block compared to sawdust fuel block of similar geometry was 79% during gasification mode operation and 73% during combustion mode operation. From this it was inferred that low average volatilization rates were responsible for the lower power level operation of leucaena compared to sawdust.

Volatilization rate of acacia is 60% of sawdust as seen from Fig. 5.4. The power obtained from acacia fuel block was 70% of a similar sawdust fuel block during gasification mode operation and 71% during combustion mode operation. The relative power from acacia fuel block is higher than the relative volatilization rate. Packing density of acacia fuel is 430 kg/m^3.

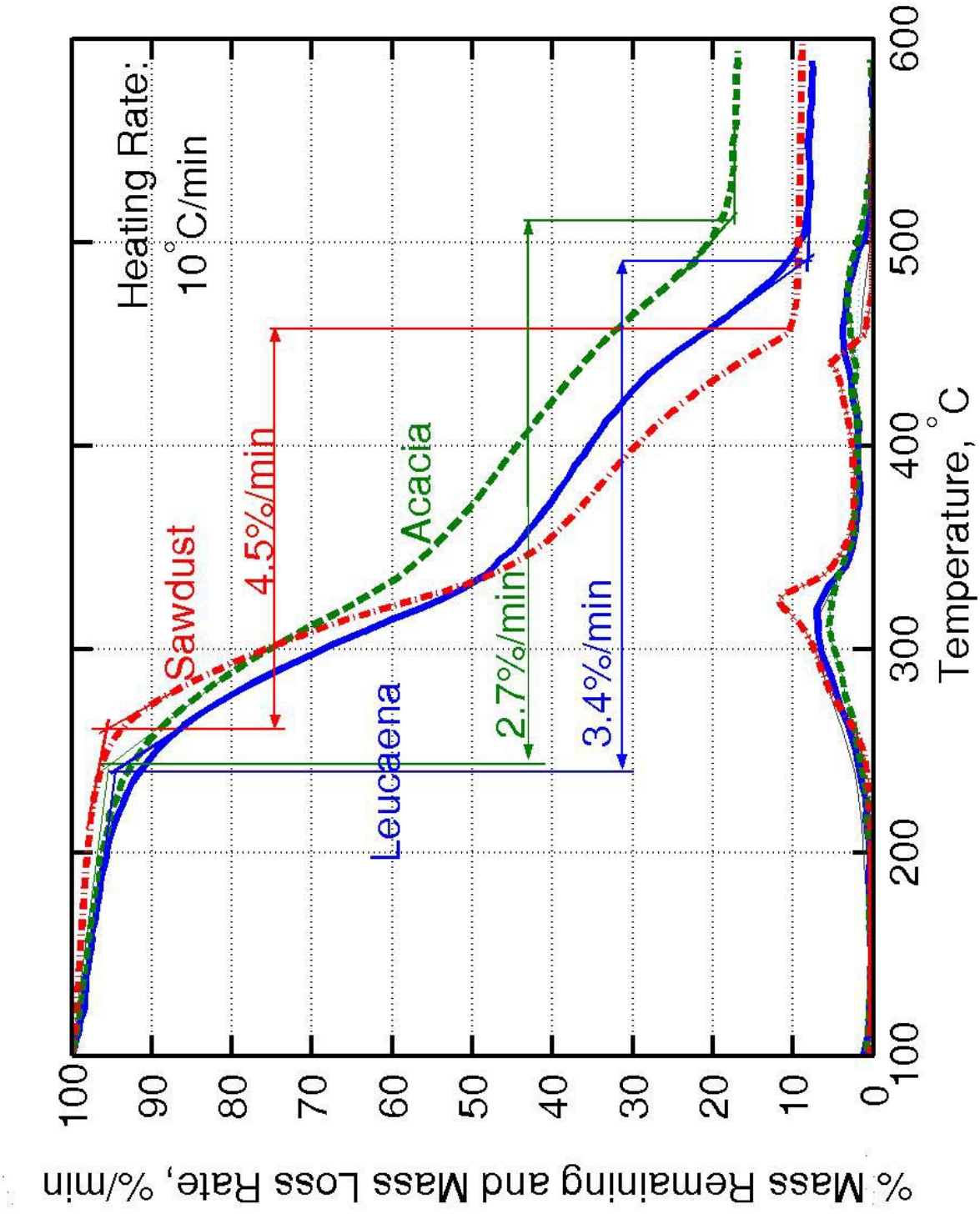

Figure 5.4: Thermo Gravimetric Analysis of selected pulverised leafy fuels.

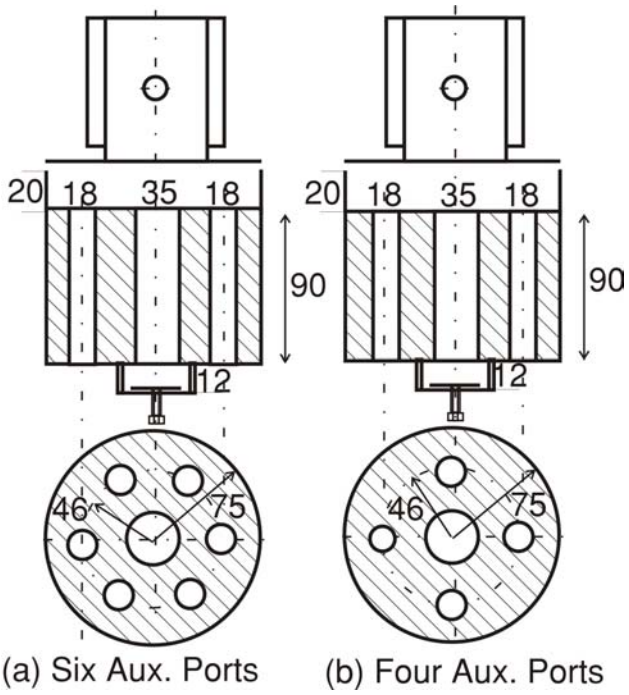

Figure 5.5: 4 aux. port and 6 aux. port stove configurations used with acacia as fuel.

Particle density of acacia leafy fuel is 1000 kg/m^3. This resulted in a fuel bed with higher porosity compared to sawdust with intrinsic density 560 kg/m^3 packed to 230 kg/m^3. The effect of lower degree of compaction is to increase power level of operation as discussed in subsection 3.6.2 of Chapter 3. Due to larger porosity, stove with acacia fuel has exhibited a relative power level higher than the relative volatilization rate compared to sawdust.

A comparative study of performance of stove with pulverised acacia as fuel using 4 and 6 aux. ports has also been made. For this study lower AR was selected. This was done for two reasons. The combustion of pulverised acacia, with AR based on main port greater than 4, was in a fuel - rich regime. Therefore an AR = 2.5 (based on main port) was selected for this study. It was found that at this AR, stable clean combustion could be established as most of the fuel port was active and the head causing air flow was also lower.

The studies were made using configurations shown in Fig. 5.5. The mass loss details recorded during the experiment is shown in Fig. 5.6. Experimental details are presented in Table. 5.4.

It is seen that power level of operation of 6 auxilliary port configuration was higher than 4 auxilliary port. Also the conversion fraction of 4 aux. port (48%) was low compared to 6 aux. port (58%) configuration. This must be

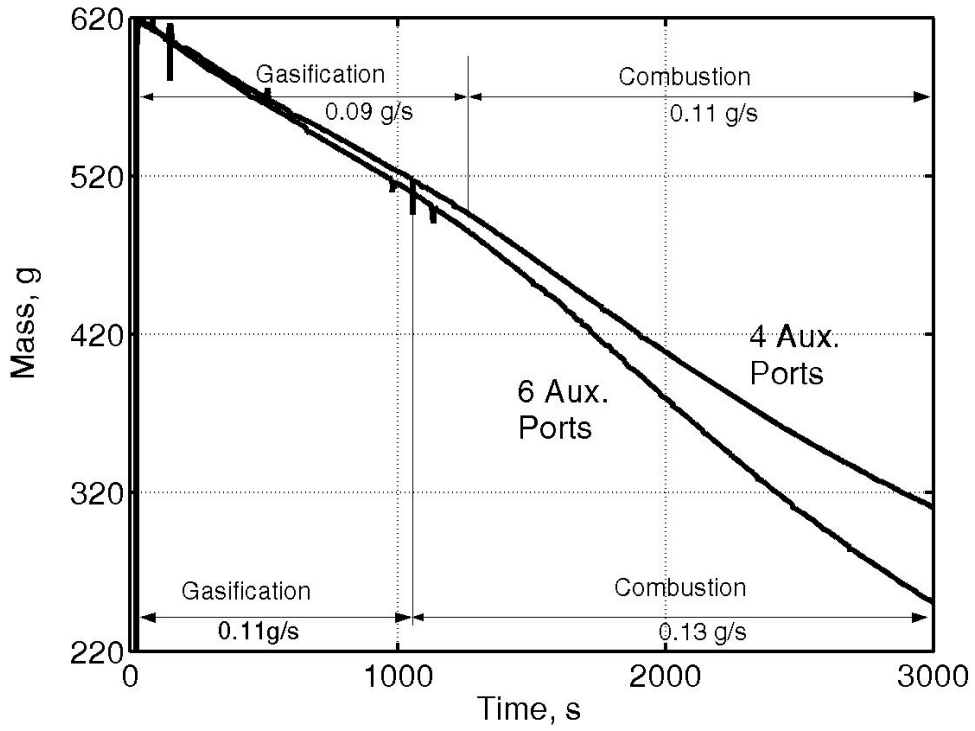

Figure 5.6: Comparison of mass loss rates of 4 aux. port and 6 aux. port tube stoves with acacia as fuel.

Table 5.4: Comparison of 4 Aux. port and 6 Aux. port stoves with acacia as fuel

Sl	Date	Main	Aux. Port		AR[a]	ρ	m_i	Power	Conv.	t_b[b]	Fuel
No	'03	Dia	Dia	No		$\frac{kg}{m^3}$	kg	kW	%	min	
1	27/02	35	18	4	2.5	230	0.62	1.5	48	50	Acacia
2	23/02	35	18	6	2.5	230	0.62	1.8	58	50	Acacia

[a]based on main port diameter, all dimensions in mm
[b]burn time

compared with the increase in conversion percentages obtained between 4 and 6 port configurations with sawdust as fuel which was just by 1 percent. This implies provision of larger fuel surface areas would lead to higher conversion fractions in case of fuels with lower average volatilization rates.

5.3 Summary

It is found that veriety of pulverised fuels can be used in tube stoves in single port and multi-port configurations. Pulverised fuels of leafy origin have low volatile content and low volatilization rates and hence exhibit lower power level operations in comparable geometries. Also, in multi port configurations at higher AR with axial inlets, the combustion at exit tended to be smoky due to partial flame outs caused by larger amounts of air traversing the core. Therefore lower AR geometries were successfully employed to achieve clean combustion. Required power levels of operation could be achieved by increasing the port diameters.

Chapter 6

Computational Study

This chapter presents the study on modeling the g-phase of tangential inlet single port tube stove with an aim to understand the processes that take place and to examine the gasification and combustion modes of functioning of the stove. A commercial CFD code *CFX-TASCflow* was used for this study.

6.1 Problem Definition

A port of a tube stove with 40 mm diameter and AR of 6 was chosen for modeling. The region selected included the fuel port, the tangential air inlet, secondary air inlet and the combustion device of a single port tangential inlet stove. To ensure proper simulation of exit conditions certain extra region over the port exit was also included in the computation. The 3-D reactive flow with natural convection in this domain was modeled. Figures 6.1 (a) and (b) show the schematic of the computational domain used for combustion mode and gasification mode simulations respectively.

The boundary conditions used for the computation are also shown in the figures. It was assumed that the g-phase was subjected to steady boundary conditions for the purpose of computation in both the simulations.

The two air inlets - primary (bottom) and secondary (shown in Figs. 6.1 (a) and (b)) were treated as constant total pressure inlets. Gasification air inlet was 6 mm wide $\times$ 30 mm high and was provided such that air enters the port in a tangential direction similar to inlet structure used during experimentation. The secondary air inlet was essentially the gap between the combustion device and the top surface of the fuel block which was about 10 mm. The circumferential region 10 mm high above the fuel port wall was treated as secondary air inlet.

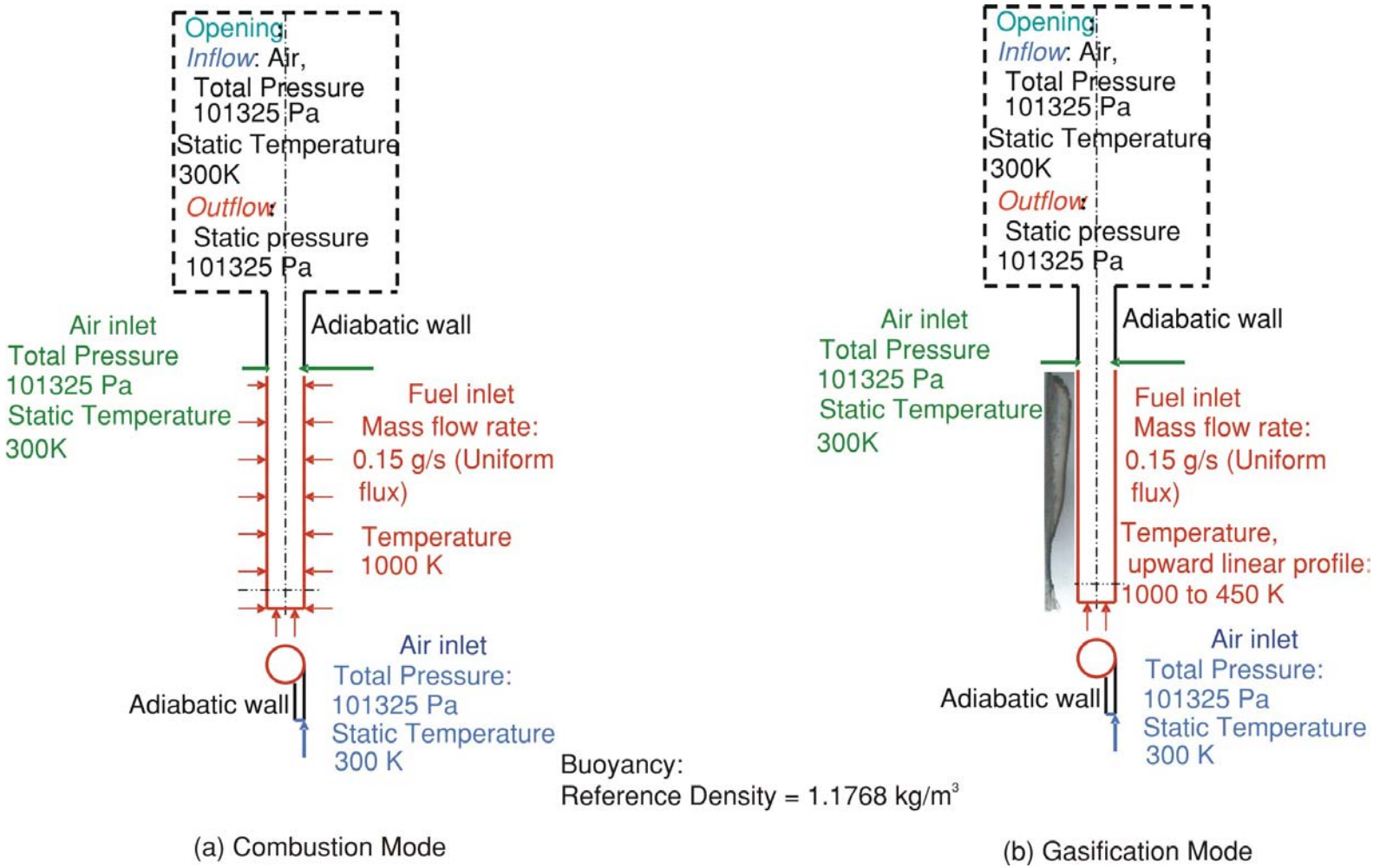

Figure 6.1: The computational domain along with boundary conditions and initial conditions used during combustion and gasification mode computations are shown in Figs. (a) and (b).

The boundary of entire region simulated above the fuel port was treated as an opening subjected to mixed flow boundary condition. That is, for inflow the fluid was assumed to be air at a total pressure of 101325 Pa and static temperature 300 K while the products went out at a static pressure of 101325 Pa.

The circumferential region above secondary air inlet up to fuel port exit was treated as adiabatic wall (See Figs. 6.1 (a) and (b)).

The entire fuel port wall was treated as fuel inlet with fuel flux directed radially inwards. The experimentally observed typical mass loss rate for the port configuration chosen (40 mm diameter, AR = 6) was ∼0.15 g/s. The mass loss rate during gasification mode operation was about 10% to 15% lower. For the purpose of simulation it was assumed during both combustion and gasification mode operations the fuel mass flow rate was constant at 0.15 g/s.

The mass flow distribution in the vertical direction was not uniform during gasification mode operation. It was experimentally determined that the mass flux from bottom region of the stove was larger. This can be seen by the photograph of the profile of the pyrolysis front at the end of 30 minutes of stove operation shown in Fig. 6.1 (b). From this profile it was possible to estimate the fuel flux as a function of vertical distance. Total mass loss rate during this period was determined experimentally to be 0.15 g/s which remained uniform for the complete duration of 30 min. Mass loss at any given vertical position is directly proportional to the depth of penetration of the pyrolisis front into the fuel block. The depth of penetration was measured from the char profile at discrete vertical intervals of 5 mm. The total mass loss rate was distributed in the same proportion as the depth of penetration. From this, fuel flow rate from each 5 mm section is known. Using this fuel flow rate, fuel flux from the port wall was determined. This was incorporated into the boundary condition during gasification mode operation with fuel inflow given as a profile matching with the experimentally observed mass flux. Fig. 6.2 shows the experimentally determined fuel flux profile.

For combustion mode operation, whose onset took place beyond 30 minutes of stove operation it was observed that fuel flux distribution in the vertical direction was more uniform since the entire port surface was active. The flux distribution determined from pyrolisis front data shown in Fig. 3.11 is presented in Fig. 6.2. The flux distribution is found to be nearly uniform. Therefore uniform vertical fuel flux of 0.0045 kg/m^{2}s which corresponds to a fuel mass flow rate of 0.15 g/s from the port wall was employed.

It was observed that port surface temperature distribution in the vertical region was such that temperatures in the bottom region was higher during the beginning of stove operation. Experiments have indicated tem-

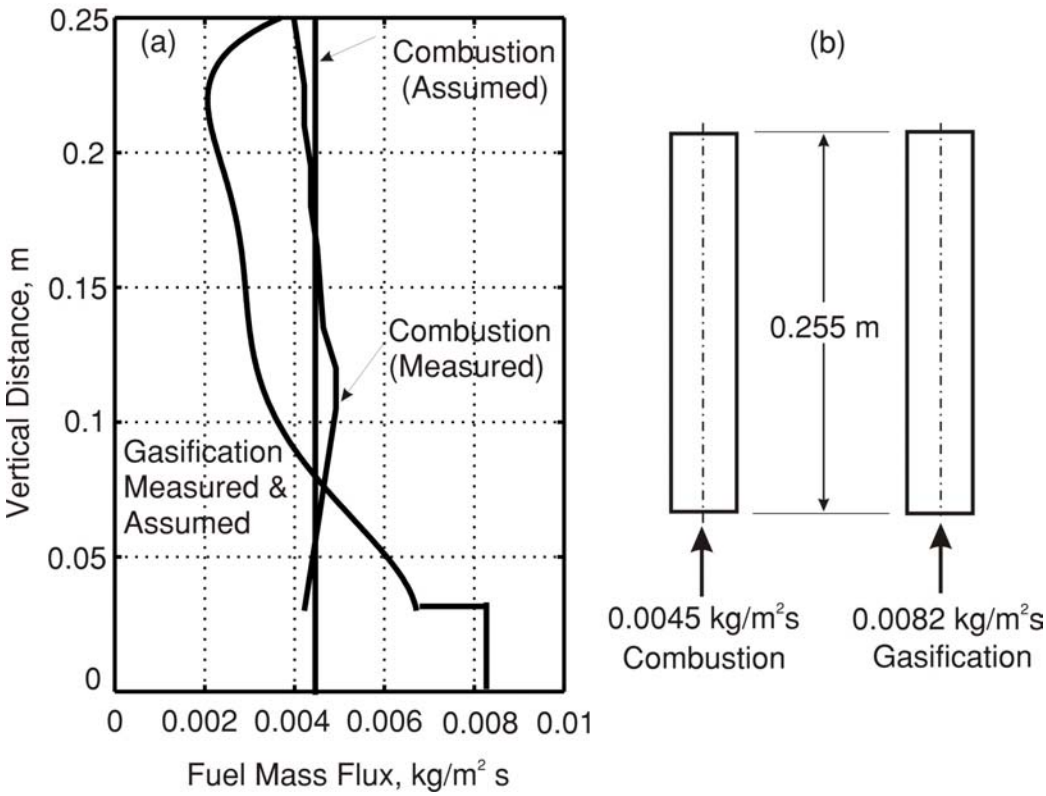

Figure 6.2: The fuel mass flux distribution during simulation of combustion and gasification modes of operation. Figure (b) shows the fuel flux from the bottom plane.

perature variation in the vertical direction as shown in Fig 3.23 during this period of stove operation when gasification mode functioning was observed. Port surface temperatures were assumed to vary linearly from 450 K to 1000 K during gasification mode functioning. During the experiment measuring junction of thermocouple was placed flush with the port surface. It was observed that during stove operation, port surface receded uncovering the measuring junction to g-phase. Thus information on surface temperatures during combustion mode was not available. For simplicity, it was assumed that the port surface was at a uniform value of 1000 K during combustion mode operation.

The composition of biomass is $CH_{1.4}O_{0.58}N_{0.001}$ (*Mukunda*, 1989) on ash free basis. For computational purposes nitrogen content was ignored. During the stove operation volatiles generated during pyrolisis entered the port. Volatiles constitute about 80% of total ash-free fuel mass with 20% carbon left behind. Thus one mole of volatiles generated from the biomass with

molecular composition defined above would contain ∼7.46 g (0.62 mole) carbon ∼1.4 g (1.4 mole) hydrogen and ∼9.28 g (0.58 mole) oxygen. From this, volatile molecule could be estimated to contain $CH_{2.2}O_{0.93}$. For computation, the approximate composition of fuel was chosen as CH_2O.

The energy content of volatiles was estimated based on total energy content of biomass and energy content of carbon that was left behind. The energy content of sun dry biomass is about 16 MJ/kg and energy content of char is about 32 MJ/kg (*Mukunda et al.*, 1984). This means, of 16 MJ of energy present in a kg of biomass 6.4 MJ will be left behind in 0.2 kg char. Therefore heat of combustion of volatiles would be 12 MJ/kg. Corresponding to this heat of combustion, heat of formation of volatiles is determined as follows. For any reaction,

$$\sum a_i A_i \longrightarrow \sum a_i' A_i \tag{6.1}$$

Where a_i and a_i' are stoichiometric coefficients, and A_i refer to species, heat of combustion H_c is given by

$$H_c = \sum (a_i - a_i')[h_{fi} + h_{si}(T) - h_{si}(298.16)] \tag{6.2}$$

Where h_{fi} is the heat of formation and h_{si} is the sensible enthalpy of i^{th} species. Consider combustion of CH_2O.

$$CH_2O + O_2 \longrightarrow CO_2 + H_2O \tag{6.3}$$

For this reaction, $a_1 = a_2 = 1$, $a_3 = a_4 = 0$, $a_1' = a_2' = 0$, $a_3' = a_4' = 1$, $A_1 = CH_2O$, $A_2 = O_2$, $A_3 = CO_2$, $A_4 = H_2O$. Therefore heat of combustion of CH_2O at 298.16 K is given by,

$$H_c = h_{f,CH_2O} + h_{f,O_2} - h_{f,CO_2} - h_{f,H_2O} \tag{6.4}$$

H_c = 12 MJ/kg (360 MJ/kmol CH_2O), h_{f,O_2}=0, $h_{f,CO_2} = -394$ MJ/kmol, $h_{f,H_2O} = -242$ MJ/kmol. Substituting in 6.4, heat of formation of volatiles is found as $h_{f,CH_2O} = -276$ MJ/kmol.

The reference density of surrounding medium, air, was assumed to be 1.18 kg/m^3 for calculation of buoyancy.

6.2 Aspects of Modeling

The computation was performed using the penta block structure shown in Figure 6.3. This structure ensures near-uniform distribution of nodes in the

central region of computational domain with closely spaced nodes nearer to wall. Grid skewness and aspect ratio were also checked and it was made sure that population of skewed flux elements (skew less than 20°) and flux elements with large aspect ratios (greater than 75) were extremely small (less than 0.2%). Studies were made with 0.163, 0.2 and 0.215 million nodes.

The equations governing flow within the port are

Continuity:

$$\frac{\partial \rho}{\partial t} + \frac{\partial}{\partial x_j}(\rho U_j) = 0\,. \tag{6.5}$$

Momentum:

$$\frac{\partial}{\partial t}(\rho U_i) + \frac{\partial}{\partial x_j}(\rho U_i U_j) = -\frac{\partial P}{\partial x_i} - \frac{\partial \tau_{ij}}{\partial x_j} + \rho f_i\,. \tag{6.6}$$

Where

$$\tau_{ij} = -\mu_b \delta_{ij} \frac{\partial U_l}{\partial x_l} - \mu\left(\frac{\partial U_i}{\partial x_j} + \frac{\partial U_j}{\partial x_i}\right)\,, \tag{6.7}$$

where

$\mu_b = 2/3\mu$ is the bulk viscosity, μ is the dynamic viscosity and δ_{ij} represents the Kronecker delta ($\delta_{ij} = 1$, $i = j$ and $\delta_{ij} = 0$ for $i \neq j$). Let reference density ρ_r be the density at some far field free stream density which is constant. Then $\rho = \rho_r + \rho - \rho_r$ from which momentum equation can be written as

$$\frac{\partial}{\partial t}(\rho U_i) + \frac{\partial}{\partial x_j}(\rho U_i U_j) = -\frac{\partial}{\partial x_i}(P - \rho_r g_i x_i) + (\rho - \rho_r) g_i - \frac{\partial \tau_{ij}}{\partial x_j}\,. \tag{6.8}$$

Energy:

$$\frac{\partial}{\partial t}(\rho H) + \frac{\partial}{\partial x_j}(\rho U_j H) = \frac{\partial P}{\partial t} - \frac{\partial}{\partial x_j}(U_i \tau_{ij} + Q_j) + \rho U_i f_i\,. \tag{6.9}$$

From fouriers law,

$$Q_j = -k\frac{\partial T}{\partial x_j} \tag{6.10}$$

Where k is thermal conductivity. Total enthalpy H is given by

$$H = c_p T + \frac{1}{2} U_i U_i \tag{6.11}$$

Where c_p is the specific heat.

Species:

$$\frac{\partial}{\partial t}(\rho C) + \frac{\partial}{\partial x_j}(\rho U_j C) = -\frac{\partial J_j}{\partial x_j} + R\,. \tag{6.12}$$

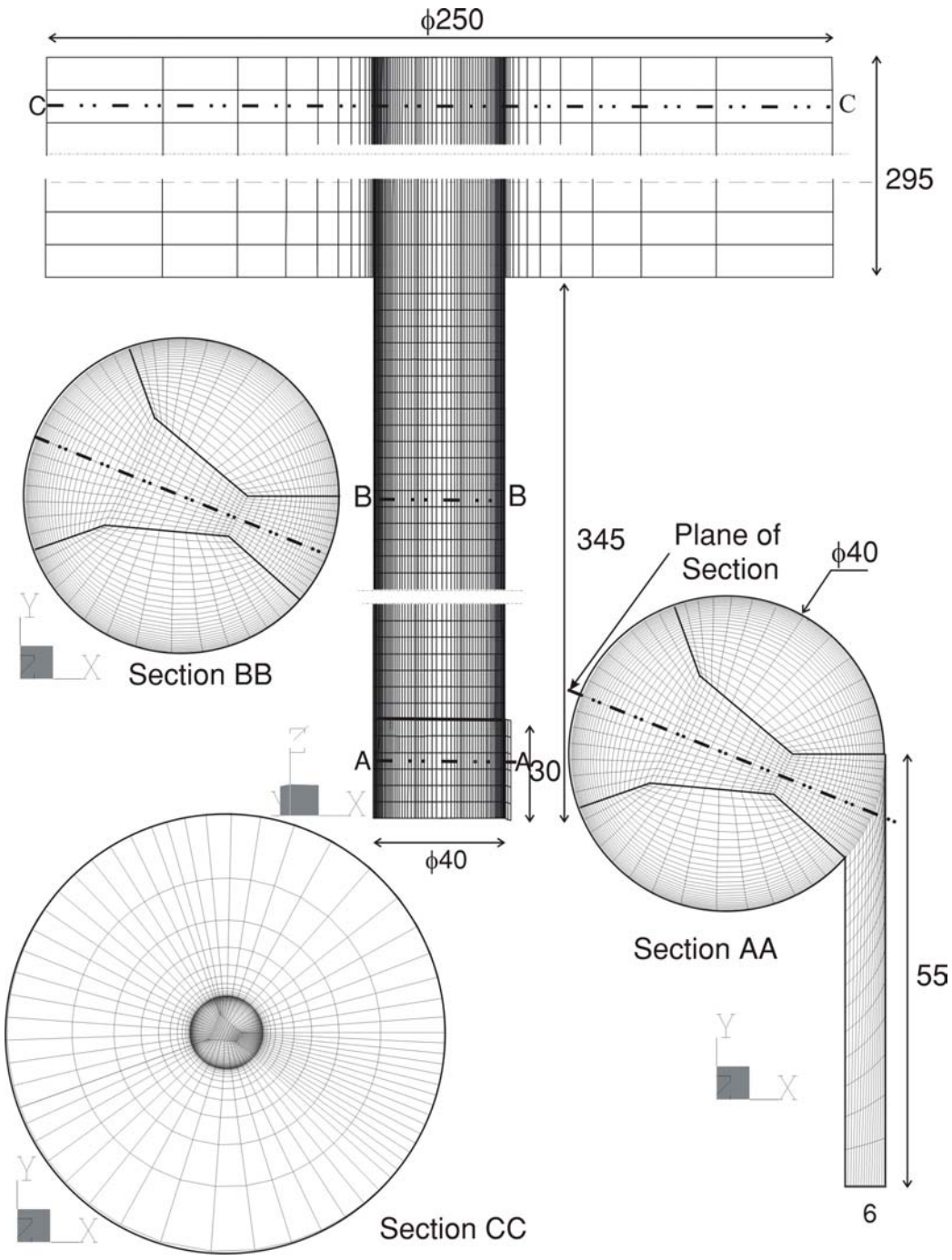

Figure 6.3: Discretisation of the computational domain

From Ficks second law

$$J_j = -D\frac{\partial C}{\partial x_j}\,, \tag{6.13}$$

Where D is the diffusion coefficient.

Combustion: Single step reaction with finite rate chemistry was used.

$$R_{kin} = -A_c[C_a]^n[C_b]^m \exp\left(-\frac{T_a}{T}\right) \tag{6.14}$$

The frequency factor used was A_c=10^{13} and activation temperature T_a was 15000 K, n=0.25 and m=1.5 (*Turns*, 2000).

Equation of State:

$$p = \rho RT \tag{6.15}$$

6.3 Numerical Scheme

CFX-TASCflow uses a finite element based finite volume method and involves the following steps. Integration of the governing equations of fluid flow over all the control volumes of the solution domain; the integrated equations with variable properties representing flow processes such as convection, diffusion and sources are discretized by substitution of the terms in the integrated equations with finite difference type approximation and there by converting them into algebraic equations. In the present study, a first order accurate upstream differencing algorithm was used for spatial discretization. The transient term used was a first order accurate backward Euler approximation (lumped mass approximation). This term affects the approach to the steady solution but not the accuracy of solution itself. A time step of 0.16 ms was employed. The set of algebraic equations obtained were solved by an iterative technique. The solution was deemed to have converged when RMS Residuals of flow went down by 4 orders of magnitude and the temperature field and scalar field remained unaltered after 2000 successive iterations. RMS residual plots as a function of simulation time are presented in Figs. 6.4 (a) and (b).

6.4 Results and Discussion

6.4.1 Numerical aspects

The numerical results were obtained with different node densities. A comparison of temperature and oxygen mass fraction with three different node densities is shown in Fig. 6.5. The results show that at 0.2 million nodes the

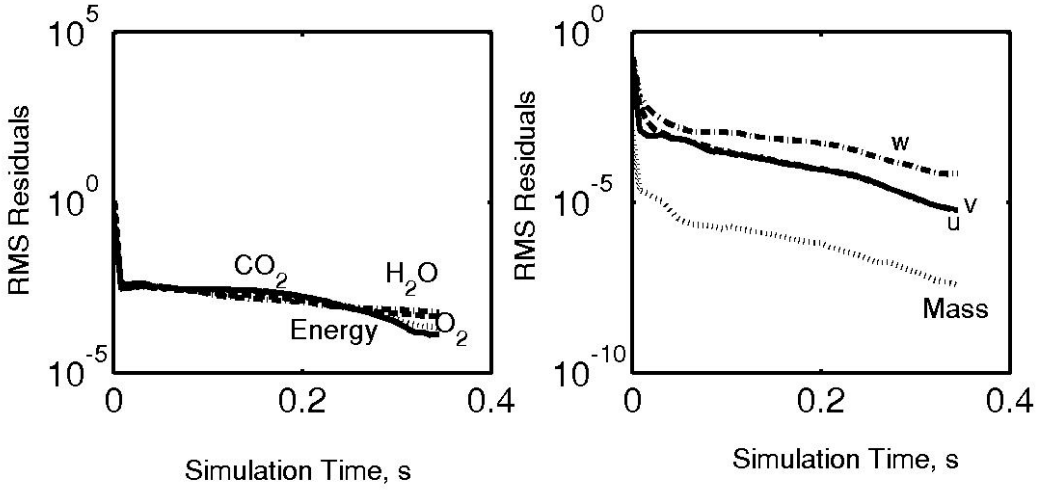

Figure 6.4: Residual plots of scalars during simulation

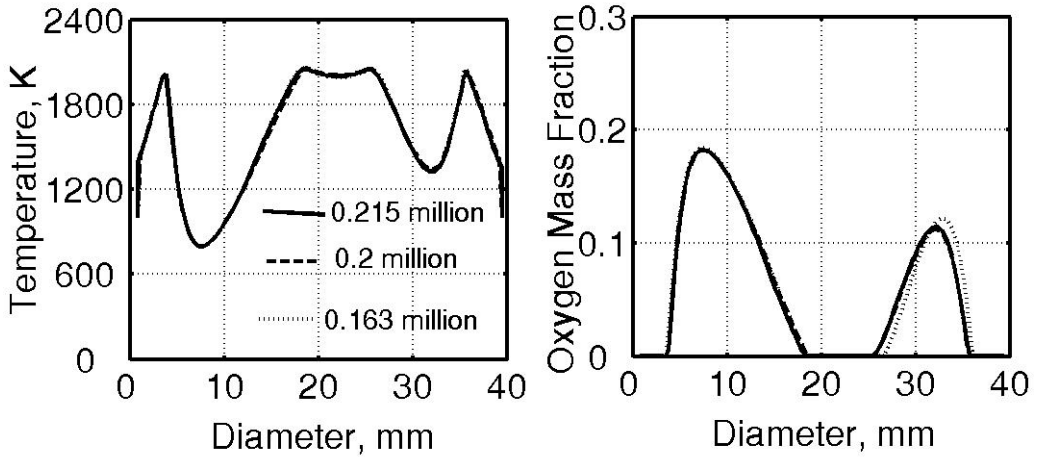

Figure 6.5: Comparison of temperature and oxygen at a vertical height of 50 mm from the bottom with different grids.

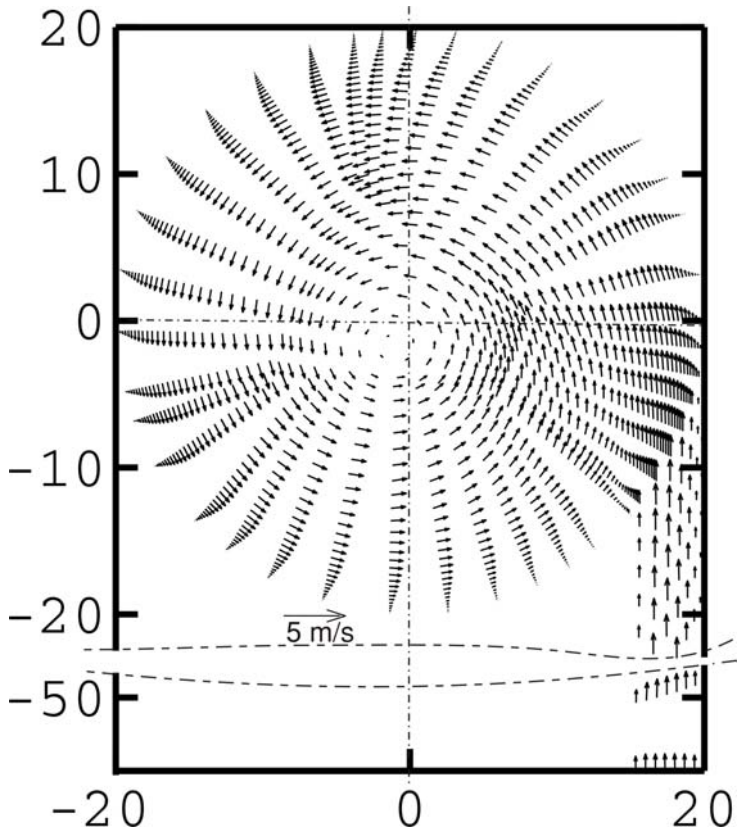

Figure 6.6: Computed velocity variation in radial plane during gasification mode operation. The dimensions indicated are in mm

results are grid independent. In this section the flow field is described first followed by a comparison of integrated mass flow parameters during combustion and gasification modes of operation. Then a comparison of radial distribution of temperature and composition at four vertical positions within the fuel port during both the modes of operation will be presented. A comparison of radial temperature profile and axial oxygen profile will be made with experimental results. Only steady state results are addressed here.

6.4.2 Flow field

Figure 6.6 shows a vector plot of flow field in a plane across the air entry at the bottom of the port. The swirl created by tangential air entry is evident from this figure. Typical maximum tangential velocity in the flow field is about 1.5 m/s. The velocity vectors in axial plane are presented in Fig. 6.7. The vectors are indicative of swirl about axis (r=0) in the flow. Due to

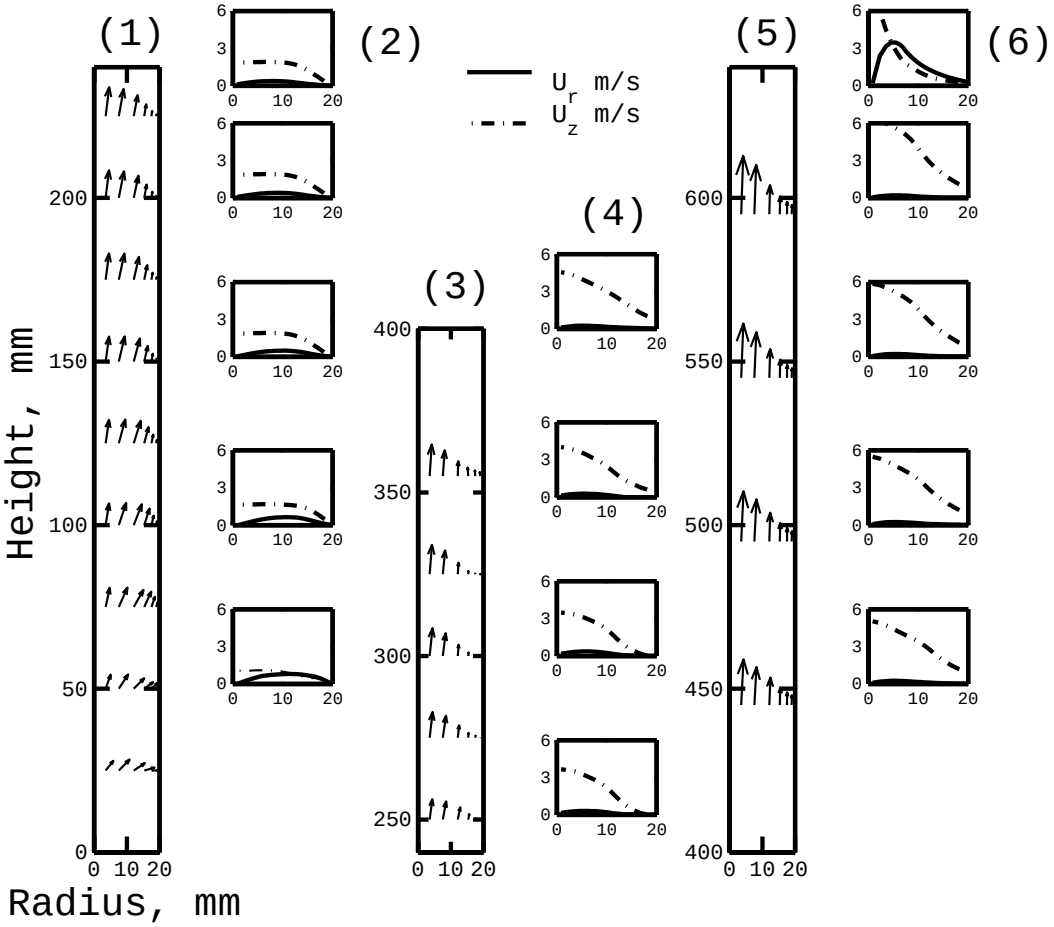

Figure 6.7: Computed velocity variation in axial plane during gasification mode operation. (1) shows vector plot in the axial plane in the port region. (2) shows radial distribution of radial (U_r) and axial (U_z) components of velocity at selected vertical distances indicated by their position. (3) shows velocity vectors at selected vertical positions in the combustion device region. (4) shows corresponding radial distribution of U_r and U_z. (5) and (6) show velocity vectors and radial velocity distributions at selected locations in the region above the device exit

the presence of swirl the flow in the bottom region has radial component U_r shown by solid line in Figs. 6.7 (2), (4) and (6). Radial component is maximum at mid-radius with its value becoming zero at centre (r=0) as well as at wall (r=20 mm). The peak magnitude of radial component at 50 mm height is 1.2 m/s. Peak U_r decreases in the direction of flow. At port exit (255 mm height) its value is about 0.3 m/s. Beyond device exit (345 mm) radial component becomes negligible.

Axial component of velocity U_z is shown using dash-dot line in the velocity plots of Fig. 6.7 (2), (4) and (6). The axial component, U_z is uniform in the central region of the port till the exit of fuel block (255 mm) as shown in Fig. 6.7 (2). The magnitude of peak U_z increases in the direction of flow. At 50 mm height peak U_z is 1.2 m/s. At port exit it is 2 m/s. In the region of the device, the radial distribution is non-uniform with with peak U_z occurring at r=0. as shown in Fig. 6.7 (4). At device exit peak u_z is 4 m/s. In the extra region computed, U_z as high as 6 m/s is observed as seen in Fig. 6.7 (6).

6.4.3 Flow parameters

The fuel flow, total flow and air-to-fuel ratios integrated over the area normal to flow direction (z direction) during gasification mode operation is presented in Fig. 6.8. The increase in total flow from 0–30 mm is due to air entry from gasification air inlet. The air-to-fuel ratio becomes stoichiometric (a/f = 6.3) at 25 mm height and drops continuously as the oxygen in flow stream is fully depleted by 100 mm height during gasification mode operation. Gasification air flow was 0.16 g/s. This corresponds to 17% of stoichiometric air requirement on overall basis. Secondary air flow was 0.15 g/s. This implies that complete combustion will need air from the atmosphere and the flame will stand much above the combustion device similar to the experiments.

Figure 6.9 shows the flow parameters total flow, fuel flow and air-to-fuel ratio as a function of vertical distance during combustion mode operation. The air-to-fuel ratio, integrated over port cross section during combustion mode operation, was very lean (a/f=48) in the inlet region. Air-to-fuel ratio became stoichiometric at 100 mm height and combustion continued in the port region.

The air inflow from gasification air inlet was 0.19 g/s. This is 20% of stoichiometric air requirement of the fuel supplied. The air inflow during gasification mode operation was about 15% lower than combustion mode operation. This may be because the fuel flux through the bottom region is relatively higher in gasification mode operation and part of the driving force due to buoyancy is utilized in transporting fuel from bottom region to the port exit resulting in reduction of air ingestion. Once the fuel flow

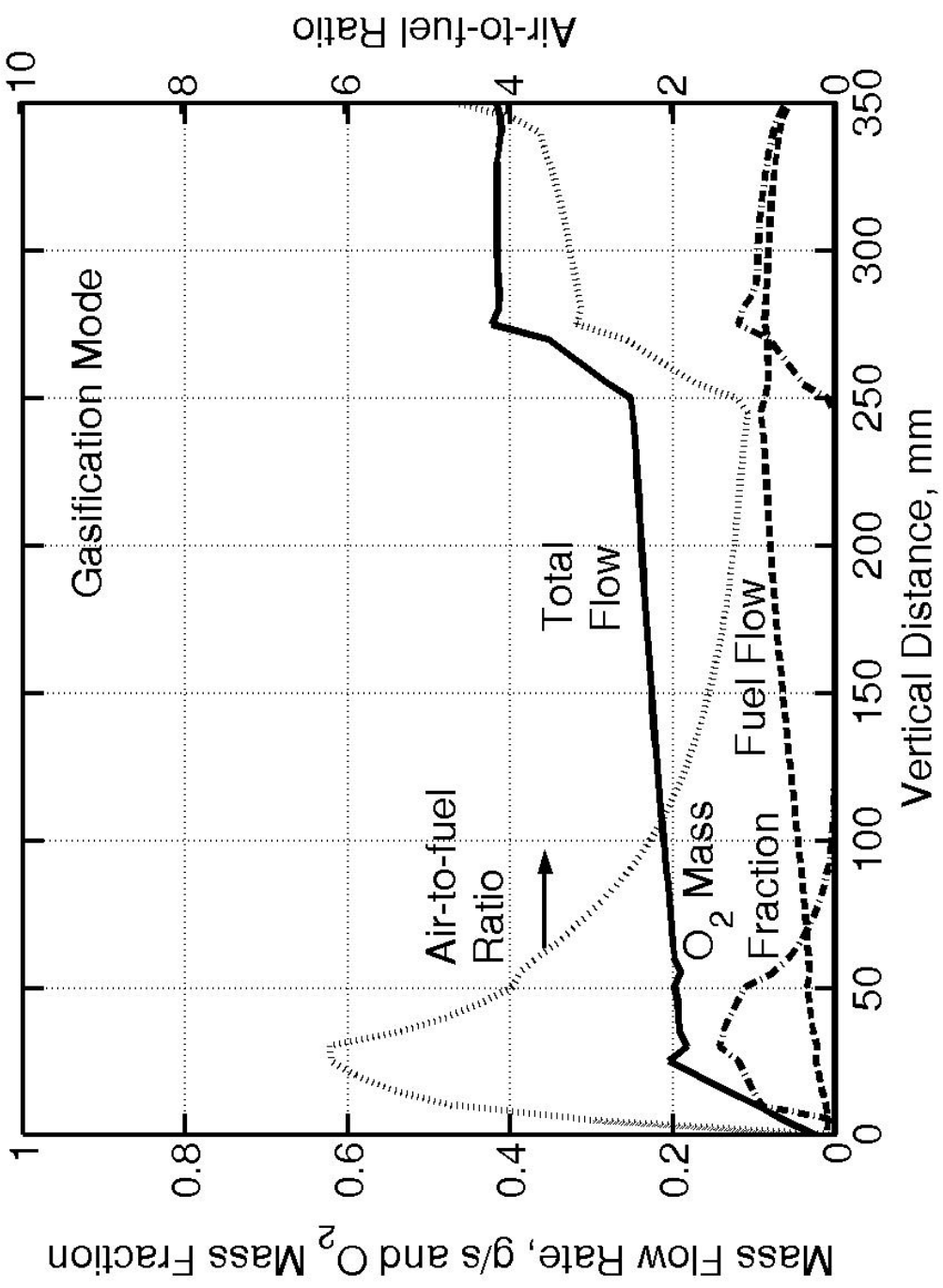

Figure 6.8: Total mass flow rate, fuel flow rate, air-to-fuel ratio and oxygen mass fraction averaged over flow cross section plotted during gasification mode operation

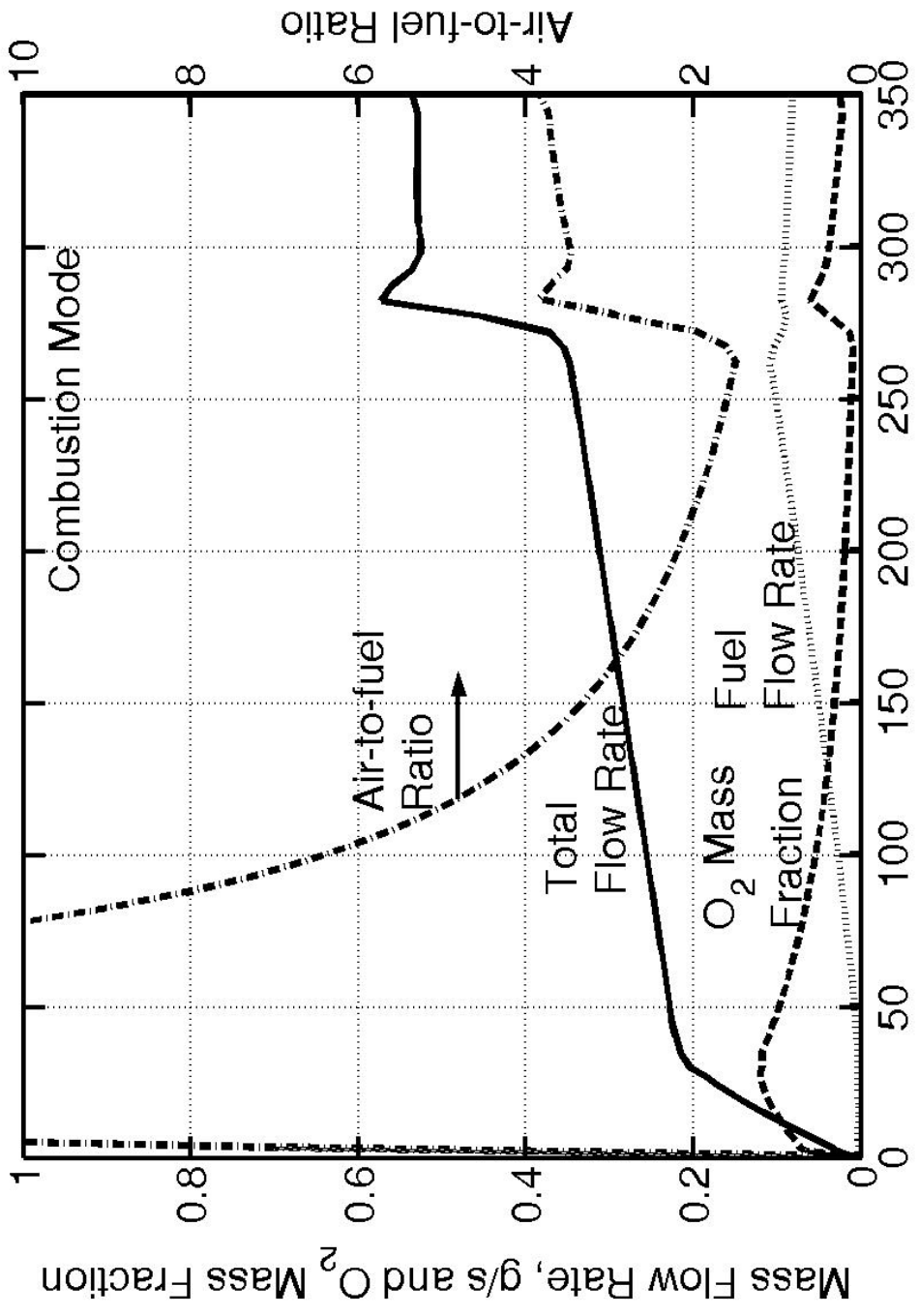

Figure 6.9: Total mass flow rate, fuel flow rate, air-to-fuel ratio and oxygen mass fraction averaged over flow cross section plotted during combustion mode operation

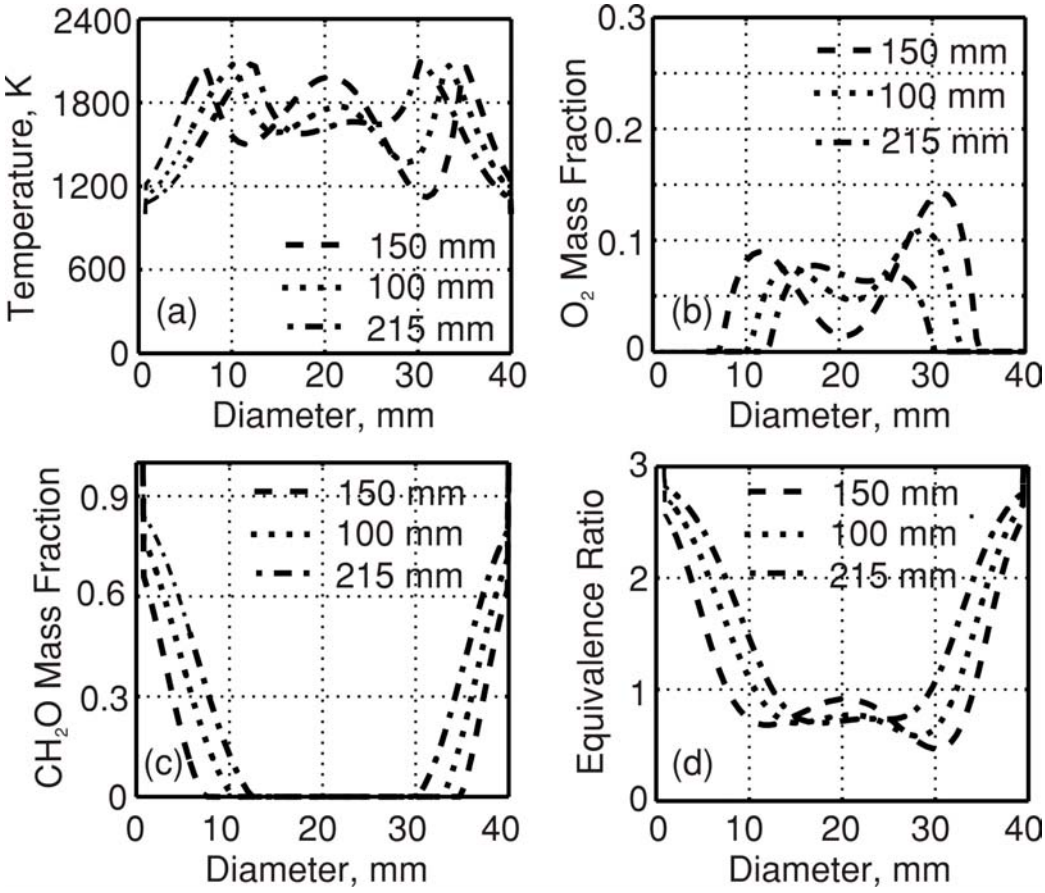

Figure 6.10: Variation of temperature and composition during combustion mode of stove operation. Fig. a shows the variation of temperature along the diameter of the fuel port at three vertical levels. Fuel and oxygen mass fractions are plotted in Figs. b and c. Equivalence ratio calculated from equation 6.17 is plotted in Fig. d

in combustion mode becomes more uniformly distributed, air inflow from bottom inlet increases since the available suction which was being utilized to lift fuel from bottom region is shifted to air inlet. Secondary air flow is nearly same in both the cases.

6.4.4 Temperature and composition

Temperature, fuel mass fraction, oxygen mass fraction and equivalence ratio at three vertical positions, 100 mm, 150 mm and 215 mm are presented in Fig. 6.10 a–d. Equivalence ratios of fuels with oxidizer present in it is

calculated as (*Gordon and McBride*, 1971)

$$\phi = \frac{\sum_i X_i (\sum_j N_{i,j} V_j)_f}{\sum_i X_i (\sum_j N_{i,j} V_j)_{ox}} \tag{6.16}$$

Where $N_{i,j}$ is the number of atoms of elements, fuel or oxidizer, V_j is the valencies of the specific elements and X_i is the mole fraction of the compound. For CH_2O combustion with only CO_2 and H_2O as products, equivalence ratio is given by

$$\phi = \frac{6X_{CH_2O} + 2X_{H_2O} + 4X_{CO_2}}{2X_{CH_2O} + 4X_{O_2} + 4X_{CO_2} + 2X_{H_2O}} \tag{6.17}$$

The temperature plot shown in Fig. 6.10 (a) is indicative of a thin flame structure in the fuel port with temperature peaks moving inwards as one goes upwards. This is similar to the flame structure experimentally observed in the port during the stove operation. Oxygen plot (see Fig. 6.10 (b)) shows that oxygen is present in the fuel port at all vertical levels but at magnitudes which are diminishing in the direction of flow. It is distributed such that the peak concentration is seen around mid-radius on either side of the axis. This occurs possibly due to presence of tangential entry which directs the air flow in such a manner. Fuel profile shown in Fig. 6.10 (c) shows that fuel concentrations, when seen along with oxygen profile of Fig. 6.10 (b) are indicative of classic diffusion flame structure. At 150 mm level (shown by dotted line) fuel and oxidizer concentrations are reduced to zero at 10 mm from wall which coincides with peak temperature location which also corresponds to ϕ=1 as seen from Fig. 6.10 (d). The composition in the central region of the fuel port is fuel lean with ϕ ranging from 0.5 to 0.9. Lower values of ϕ are seen to correspond to lower temperatures.

Temperature and composition profiles during gasification mode operation is presented in Figs. 6.11. Temperature profiles, shown in Fig. 6.11 (a) are seen to be spatially uniform in the mid region. Oxygen concentration profile in the port is shown in Fig. 6.11 (b). It can be seen that oxygen is reduced to zero beyond 100 mm height. During actual stove operation the bottom region vertically below fuel port is active in gasification mode. By the time combustion mode sets in this zone is nearly burnt out. The composition in the central region f the fuel port is fuel-rich with equivalence ratio in the range 1–1.5 as seen from Fig. 6.11 (d).

The rate parameters used for predicting the reaction rate, activation energy and pre-exponential factors depend upon the equivalence ratio (*Coffee et al.*, 1983). The present simulation was carried out with a constant reaction rate corresponding to stoichiometry. This has resulted in higher predicted g-phase temperatures in this region than that can be expected.

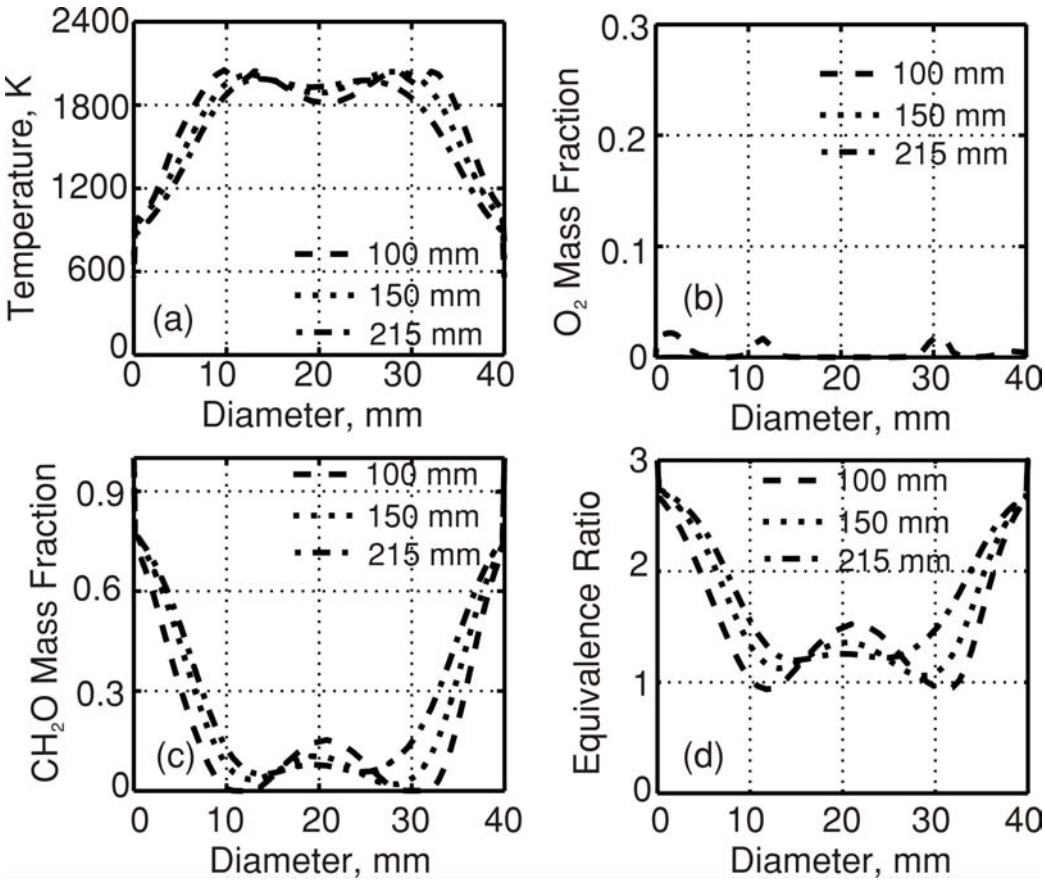

Figure 6.11: Variation of temperature and composition during gasification mode of stove operation. Fig.a shows the variation of temperature along the diameter of the fuel port at three vertical levels. Fuel and oxygen are plotted in Figs. b and c. Equivalence ratio calculated from equation 6.17 is plotted in Fig. d

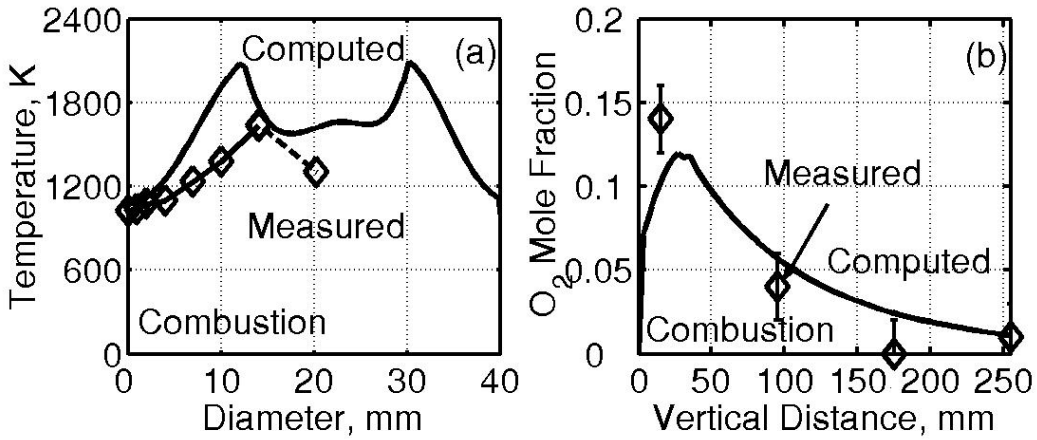

Figure 6.12: Comparison of computed and experimental temperature and oxygen fraction during combustion mode operation. Fig.(a) shows comparison of g-phase temperatures along the radius of the fuel port at a location 40 mm below port exit. Fig.(b) shows comparison of g-phase oxygen fraction along the axis of fuel port.

6.4.5 Experimental comparisons

The comparison of predicted and measured temperature and oxygen concentrations during combustion mode operation is presented in Fig. 6.12 (a) and (b). The predicted temperatures are in qualitative agreement with the measured values though the peak temperature is higher by 350 K. One clear reason is that during computation single step forward reaction without dissociation was considered. With dissociation the predicted temperatures will be lower. The measured oxygen concentration as shown in Fig. 6.12 (b) is in agreement with predicted values which implies that lower measured temperatures must be due to dissociation only. The comparison of predicted and measured temperature and oxygen concentrations during gasification mode operation is presented in Fig. 6.13 (a) and (b). In this case there are significant differences between predictions and measurements. As can be seen from Fig. 3.21 of page 71, the centre line temperature increases and oxygen fraction decreases when the flame flash back occurs. However the predictions show the opposite trend. It is clear from the experimental measurements that during gasification mode operation the g-phase reactions are nearly absent. There is no significant difference in surface temperature between gasification and combustion. The measured temperature profiles however indicate that the g-phase reactions are not totally absent since the temperature increases slightly with distance from the surface. The possible explaination for this behaviour is that the species such as hydrogen and to some extent carbon

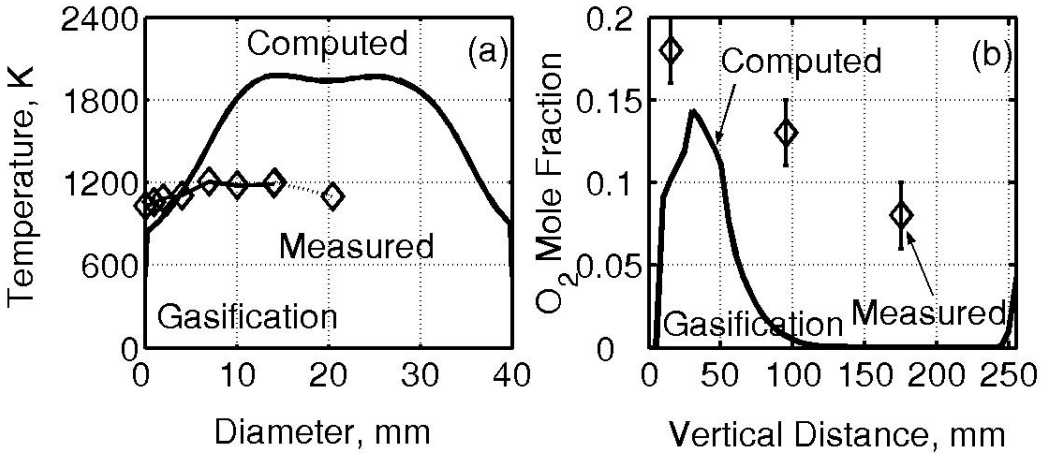

Figure 6.13: Comparison of computed and experimental temperature and oxygen fraction during gasification mode operation. Fig.(a) shows comparison of g-phase temperatures along the radius of the fuel port at a location 40 mm below port exit. Fig.(b) shows comparison of g-phase oxygen fraction along the axis of fuel port.

monoxide react while the large molecular mass pyrolisis products remain unreacted. The reactions between species such as hydrogen and oxygen have relatively low activation energy compared to those between large molecular mass pyrolisis gases and oxygen. Therefore, hydrogen and to certain extent carbon monoxide are oxidized while the high molecular mass campounds remain unreacted unless high temperature zone is present. These factors are not predicted in the numerical computations because of the use of single step forward chemistry model used in computations.

These observations are strengthened by the fact that in many cases the gasification mode is induced closing the inlet port and forcing the flame to quench in the port though there are cases where spontaneous transition from combustion to gasification mode has taken place. Once flame is blown off from the port only low activation energy reactions will proceed.

Further as can be seen from Figs. 6.12 (a) and 6.13 (a) the temperature gradient normal to the surface is significantly lower in the case of gasification mode compared to combustion. Yet the fuel consumption rate and the surface temperature are significantly different between the two cases in spite of the large change in heat flux to the surface. The possible explanation for this behaviour can be given from the fact that the oxygen concentration at the surface is large in the gasification mode while oxygen will be consumed in the flame in the case of combustion mode. Hence in gasification mode fuel consumption rate is sustained by the reaction between oxygen and char, while

in combustion mode the fuel consumption is sustained by heat flux from the flame. Fig. 6.14 shows a functioning stove along with computed temperature contours showing the flame intensity.

6.4.6 Conclusion

Two steady state calculations were made to simulate combustion and gasification modes of stove operations with several simplifying assumptions. The computational study confirms that gasification phenomena was due to larger fuel release that take place from the bottom region during the early part of stove operation.

As the stove operation continues in gasification mode, port surface temperatures become uniform with upper regions becoming active. Fuel flux from the bottom region is reduced, possibly due to exhaustion of volatile content. Under these conditions the stove will draw more air since available buoyancy force would get used to lift more air from gasification air inlet at the bottom causing combustion mode operation.

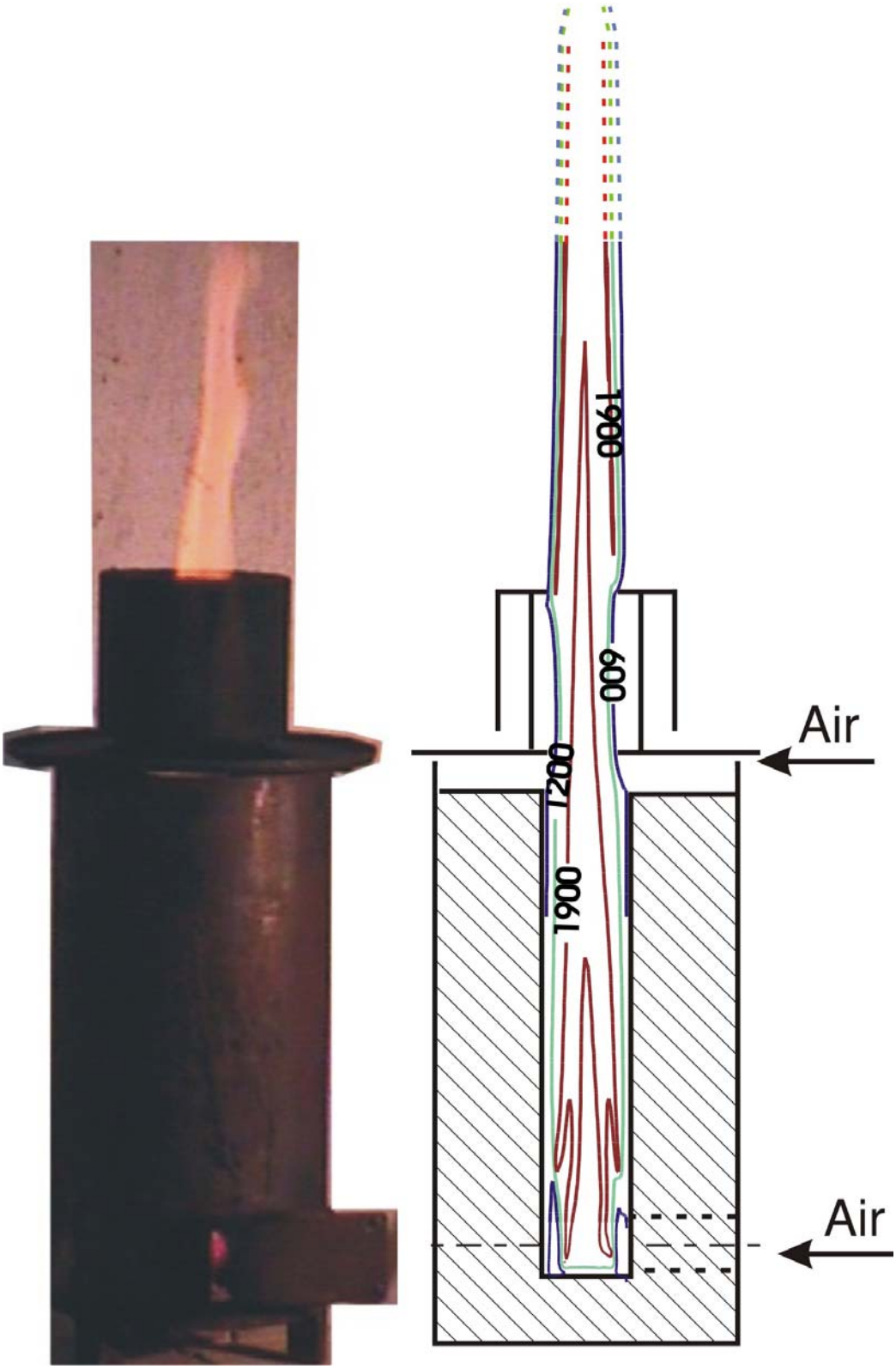

Figure 6.14: A functioning stove shown along with computed temperature contours showing the flame intensity.

Chapter 7

Overview

The present study was motivated by the recognition of the need for developing a stove for fine fuels. The starting point for the study was the conventional tube stove meant for sawdust on which the studies performed earlier had to be progressed. This stove was known to function in combustion mode quite well. The idea of the present study was to examine if the stove could function in gasification mode at all and if so, to determine the parameters that distinguish the functioning in gasification mode from combustion mode.

7.1 Gasification Mode and Alternate Configurations and Fuels

The first deviation from the conventional design that was attempted was to restrict the air entry area and examine if gasification mode of functioning could be obtained. This tube stove with a combustion device at the exit and a restricted inlet at the bottom functioned in the gasification mode for about 30 min of stove operation. Studies were conducted on this configuration with an aim to determine if the gasification mode operation could be extended and also to establish the causes for termination of gasification mode functioning through flame flash back into the fuel port. It was determined for the first time that *fuel density and packing density* have significant influence on the combustion and gasification process. From these studies, it has been determined that to obtain smooth ignition and approach to steady operation, a density of 230 to 250 kg/m^3 should not be exceeded. Several variants of experiments with different aspect ratios, densities were performed to examine the controlling parameters. Towards the end of the study, it was uncovered that h/d of 5 to 6 would be a good range for the gasification; it was also uncovered that if packing was done with inner region at 230 to 250 kg/m^3

and outer region (beyond a radius of 50 - 55 mm) at 500 to 700 kg/m^3, the gasification duration would get extended to 50 to 60 mins.

Alternate geometries of using a central port drawing air from the bottom region directly were also tried. These needed a multi-port design to ensure that intermediate extinctions do not occur. This change also helped in achieving high level of conversion in an hour that was set as a desired operational duration. Thus two competing designs for cook stoves were found meaningful.

Studies on leaf droppings and other wastes have shown that the above design does work with alterations in the choice of port diameter and h/d to achieve the desired power level and gasification mode of operation.

7.2 Performance

The stove has demonstrated excellent heat utilization capability with water heating efficiency in the range of 37% at an optimum spacing of 12 mm. The energy release in the form of a focussed stream of gases which is an inherent characteristic of these stoves represents a performance capability which is similar to conventional gas stoves. The conversion percentages obtained are in the range of 66% – 72% for the desired duration of operation of one hour.

7.3 Emissions

Emission performance of the stove was studied using standard hood design for CO and NO_x. CO emissions are about 12 g/kg fuel which is very low compared to the range of values (25 - 180 g/kg fuel) reported in literature presented in Fig. 4.4 of page 109 in Chapter 4. NO_x emissions from the stoves are in the range of 1 g/kg fuel which are comparable to other conventional biomass stoves. Considering the high efficiency of operation, this represents a significant performance indicator. The air quality in the region around the stove was monitored for CO and solid particulate matter. The values are below permissible levels of 9 ppm prescribed by primary national air quality standards of USA. The particulate matter emissions from the stove are are about 2.4 mg/m^3 which is much below the average levels of 56 mg/m^3 reported in literature. The stove has exhibited a significant reduction in the sooting tendency which is quantified by the amount of soot collected during stove operation. About 2 g of soot /kg fuel was collected during operation which compares favourably with reported values of 12 -13 g/ kg fuel (*Mukunda et al.*, 1994).

7.4 Analysis of Results

An analysis carried out on the c-phase thermal profile with moving pyrolisis front showed that the predicted temperature profiles and the pyrolisis front movement rates compared excellently with the measured data.

3D Modeling of the g-phase of tangential inlet single port tube stove was done using commercial software CFX TASCflow. The computational study confirms that gasification phenomena was due to larger fuel release that took place from the bottom region during the early part of stove operation.

To simulate gasification mode operation multi-step chemistry involving different sets of reactions for H_2, CO and other species need to be taken into account. This could be attempted as future work by using suitable reaction scheme taking into account the low activation energy hydrogen reaction.

Presently an experimentally determined fuel release pattern was employed to simulate the gasification mode functioning of the stove. This could be substituted to a fuel release pattern based on the results of c-phase analysis from which for a given position of the pyrolisis front it is possible to compute the magnitude of fuel flux and port wall temperature for a given heat flux from the g-phase to the fuel block.

7.5 Further Work

The current modeling effort has treated the g-phase and c-phase seperately. Coupling them would confirm and reveal the distinct reasons for switch from gasification to combustion mode in small systems (like 2.5 kW stove) and the inevitability of combustion mode throughout in larger systems (greater than 2.5 kW). Development work towards making the stove as a route to better utilization of biomass for cooking in locations where biomass is currently being used would be an important effort in times to come.

Appendix A

Measurement issues

A.1 Time constant determination of thermocouples

Assuming conduction and radiation heat losses from the thermocouple as well as any catalytic activity on its surface are negligible, the heat balance for a junction in hot gas stream gives:

> Heat accumulation rate in the junction = Convective heat transfer rate to it

$$\rho_w c_w V \frac{dT_w}{dt} = hA(T_g - T_w) \tag{A.1}$$

Where ρ_w = density of thermocouple material, kg/m^3, c_w = specific heat, J/kg.K, V = volume of junction, m^3, h = heat transfer coefficient, W/m^2.K, A = surface area of junction, m^2, T_w = junction temperature, K, T_g = gas temperature, K and t is time, s.

Rearranging,

$$\tau \frac{dT_w}{dt} + T_w = T_g \tag{A.2}$$

Where

$$\tau = \frac{\rho c_w V}{Ah} \tag{A.3}$$

is the time constant of thermocouple.

Nusselt number for flow across sphere is given by

$$\mathrm{Nu} = \frac{hd}{k_g} = 2 + 0.35\mathrm{Re}^{0.5} \tag{A.4}$$

Where Reynolds number Re = Gd/μ, G is the mass flux through the fuel port, kg/m^{2}s and d is the junction diameter, m. For Pt — Pt13% Rh thermocouple material, the properties are: ρ = 21450 kg/m^3 and c_w = 127 J/kg.K. For chromel–alumel thermocouple material, ρ = 8700 kg/m^3 and c_w = 450 J/kg.K.

Substituting for h in equation A.3

$$\tau = \frac{\rho c_w d^2}{6 k_g \mathrm{Nu}} \tag{A.5}$$

Typical mass flux through the fuel port is 0.32 kg/m^{2}s. Properties of gas through fuel port are, assuming it to be that of air at 1000 K, $\mu = 4.152 \times 10^{-5}$ Pa.s and k = 0.06752 W/m.K. This gives τ = 12 ms for a 120μm R type junction.

A.2 Compensation for radiation error

From steady heat balance of thermocouple junction,

> Convective heat transfer from gas to junction = Heat lost by junction through radiation.

$$h_g A_s (T_g - T_s) = \epsilon_s \sigma A_s T_s^4 - \epsilon_w \epsilon_s \sigma A_s T_w^4 \tag{A.6}$$

Where h_g is g-phase heat transfer coefficient, A_s is the surface area of sphere for heat transfer, T_g is the g-phase temperature, T_s is the surface temperature, T_w is the wall temperature, ϵ_s is the surface emissivity and σ is the Stefan–Boltzmann constant, 5.67×10^{-8} W/m^2.K^4. ϵ_w is assumed unity.

Nusselt number is obtained from equation A.4

Gas temperature T_g is calculated as

$$T_g = T_s + \frac{\epsilon \sigma d}{k_g \mathrm{Nu}} (T_s^4 - T_w^4) \tag{A.7}$$

For ϵ_s = 0.17 and gas properties mentioned in section A.1, the radiation correction for a 250μm junction is given by

$$T_g - T_s = 1.67 \times 10^{-11} (T_s^4 - T_w^4) \tag{A.8}$$

and for a 120μm junction, it is

$$T_g - T_s = 0.835 \times 10^{-11} (T_s^4 - T_w^4) \tag{A.9}$$

These corrections are shown in Fig. A.1 as a function of T_s with T_w assumed 800 K.

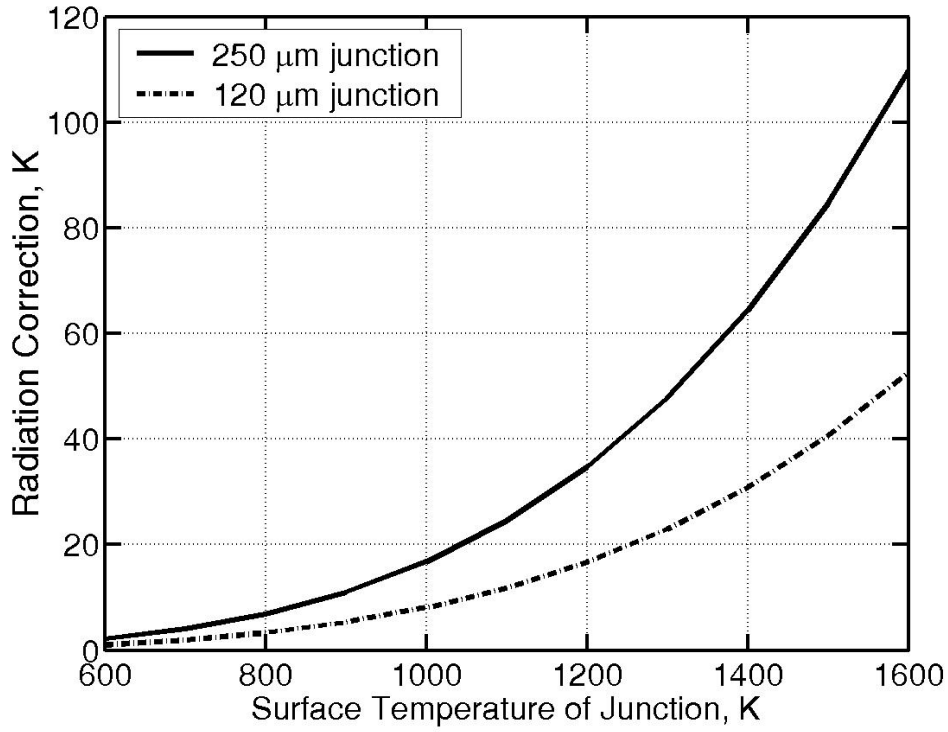

Figure A.1: Radiation correction as a function of indicated temperature.

A.3 Data Format for RS232 Acquisition

Data formatting for Weighing balance was done after examining the sample data string from the machine given below.

`00149.5<CR> 00000.0<CR><LF>`

This data string represents a gross weight of 149.5 g and a tare weight of 0 g. Format used extract this information is given in Table A.1. Prefix of x represents number of characters to be skipped while prefix of a represents number of subsequent alphanumeric characters to be read into the channel. The character n represents end of a line of data.

The sample output data string from MAIHAK analyser had the form shown below.

`#MS 21.02.02 12:51:50 0.247 Vol% CO 1.001 Vol% CO2 -0.32 Vol% CH4 17.663 Vol% O2 -0.281 Vol% H2`

Data contained in this string are status of machine, date of acquisition, time of acquisition followed by measured volumetric compositions of constituent gases with chemical symbols. Data format used to extract only the

Table A.1: Data format for mass measurement

channel	Format	Measured quantity
0	2x 7a	Gross weight
1	7a \n	Tare weight

Table A.2: Data Format for Composition measurement

channel no	Format	Measured quantity
0	21x 7a	CO
1	9x 7a	CO_2
2	9x 7a	CH_4
3	9x 7a	O_2
4	9x 7a\n	H_2

required elements in the data string (ie, the composition values) is given in Table A.2

Appendix B

Emission Calculations

Consider combustion of biomass CH_kO_m shown in reaction B.1.

$$\mathrm{CH_kO_m + p(O_2 + 3.76N_2) = aCO_2 + bCO + cH_2O + dO_2 + 3.76pN_2} \quad \text{(B.1)}$$

Let CO_2, CO, and O_2 be composition of products on dry volumetric basis. CO and O_2 are measured. If combustion is assumed to take place according to the above reaction, then, CO_2 can be calculated. If $t = a + b + d + 3.76p$, then CO_2 = a/t, CO = b/t and O_2 = d/t.

C: $a + b = 1$

H: $c = k/2$

O: $2a + b + c + 2d = m + 2p$

Using elemental balance equations p can be evaluated as

$$p = \frac{(\mathrm{m} - (\mathrm{k}/2) - 2)(1 - \mathrm{O_2}) - (2\mathrm{O_2} - \mathrm{CO})}{3.76(2\mathrm{O_2} - \mathrm{CO}) - 2(1 - \mathrm{O_2})} \quad \text{(B.2)}$$

from which d, moles of O_2, can be obtained as

$$d = \frac{\mathrm{O_2}(1 + 3.76\mathrm{p})}{1 - \mathrm{O_2}} \quad \text{(B.3)}$$

This gives b, moles of CO as

$$b = \frac{\mathrm{CO}(1 + \mathrm{d} + 3.76\mathrm{p})}{1 - \mathrm{O_2}} \quad \text{(B.4)}$$

From which dry volumetric fraction of CO_2 can be evaluated as

$$\mathrm{CO_2} = \frac{1 - \mathrm{b}}{1 + \mathrm{d} + 3.76\mathrm{p}} \quad \text{(B.5)}$$

Emission factor of CO is mass of CO formed per kg fuel. One kg biomass will contain about 500 g carbon or 41.6 moles of carbon. If the carbon bearing species generated are CO and CO_2 only, then these 41.6 moles will be distributed between CO and CO_2 only. Moles of CO formed is equal to moles of C going to CO. Moles of CO_2 formed is equal to moles of C going to CO_2 therefore

$$\epsilon_{\mathrm{CO}} = 41.6 \times 28 \frac{\mathrm{CO}}{\mathrm{CO} + \mathrm{CO_2}} \tag{B.6}$$

$$\epsilon_{\mathrm{CO_2}} = 41.6 \times 44 \frac{\mathrm{CO_2}}{\mathrm{CO} + \mathrm{CO_2}} \tag{B.7}$$

Similarly emission of NO can be determined as follows. Total moles of dry flue gases generated by combustion of one mole of fuel is $t = a+b+d+3.76p$. One kg biomass will thus generate $flue = t/(12 + k + 16m)$ moles of dry products. From this, emission factor of NO can be calculated as

$$\epsilon_{\mathrm{NO}} = 30 \frac{\mathrm{NO}}{\mathrm{flue}} \tag{B.8}$$

Appendix C

Standards

Table C.1: Aluminium Vessels for Thermal Efficiency Test (Clause A-3.4)

Sl No	Heat Input Rate kcal/h	Vessel Diameter mm(±5%)	Vessel Height mm(±5%)	Total Mass with Lid g(±20%)	Water Mass in Vessel kg
1	Up to 2000	180	100	356	2.0
2	2001–2800	205	110	451	2.8
3	2801–3200	220	120	519	3.7
4	3201–3800	245	130	632	4.8
5	3801–4200	260	140	750	6.1
6	4201–4800	285	155	853	7.7
7	4801–5400	295	165	920	9.4
8	5401–6000	320	175	1100	11.4
9	6001–6600	340	185	1200	12.5
10	6601–7200	350	195	1310	14.0
11	7201–7800	370	200	1420	16.0
12	7801–8400	380	210	1530	18.0

References

Abramowitz, M., and I. Stegun, *Hand book of Mathematical Functions*, Applied Mathematics series, National Bureau of Standards, 1964.

Agarwal, A. L., R. M. Dave, and K. R. Smith, *ASSET*, *18*, 1983.

Anon, http://members.lycos.co.uk/woodyplantecology/docs.

Anon, Energy data from different sources, *Wood energy news*, *11*, 6, 1996.

Anon, Biomass energy in asean countries, *Wood energy news*, *12*, 11, 1997.

Baldwin, S. F., Biomass stoves: Engineering design, development and dessemination, Ph.D. thesis, Center for Energy and Environmental Studies, Princeton University, 1986.

Ballard-Trameer, G., and H. H. Jawurek, Comparison of five rural woodburning cooking devices: Effiiencies and emissions, *Biomass and Bioenergy*, *11*, 419–430, 1996.

Bhattacharya, S. C., D. O. Albina, and K. A. M, Effects of selected parameters on performance and emission of biomass-fired cookstoves, *Biomass and Bioenergy*, *23*, 387–395, 2002a.

Bhattacharya, S. C., D. O. Albina, and A. P. Salam, Emission factors of wood and charcoal fired cookstoves, *Biomass and Bioenergy*, *23*, 453–469, 2002b.

Coffee, T. P., A. J. Kotlar, and M. S. Miller, The overall reaction concept in premixed, laminar, steady-state flames. i. stoichiometries, *Combustion and Flame*, *54*, 155–169, 1983.

Emmons, H. W., and A. Atreya, The science of wood combustion, *Proc. Indian Acad. Sci.(Engg. Sci.)*, *5*, 259–268, 1982.

Gordon, S., and B. J. McBride, *Computer Program for Calculation of Complex Chemical Equilibrium Compositions, Rocket performance, Incident and Reflected Shocks and Chapman - Jouguet Detonations*, NASA Lewis Research Center, 1971.

Holman, J. P., *Heat Trasfer*, si metric ed., McGRAW-HILL Book Company, 1989.

Kanury, A. M., and P. L. Blackshear, On the combustion of wood: Ii the influence of internal convection on the transient pyrolisis of cellulose, *Combustion Science and Technology*, *2*, 5–9, 1970.

Kapur, P. C., R. Singh, and J. Srinivasan, Tube-in-basket burner for rice husk. i: Properties of husk as a fuel and basic design considerations, *Sadhana*, *7*, 291–300, 1984.

Mukunda, H. S., *Understanding Combustion*, IIT Madras series in Science and Engineering, Macmillan India Limited, 1989.

Mukunda, H. S., P. J. Paul, U. Srinivasa, and N. K. S. Rajan, Combustion of wooden spheres – experiments and modal analysis, *Twentieth Symposium (International) on Combustion*, pp. 1619–1628, 1984.

Mukunda, H. S., U. Shrinivasa, and S. Dasappa, Portable single-pan wood stoves for high efficiency, *Sadhana*, *13*, 237–270, 1988.

Mukunda, H. S., S. Dasappa, B. Swati, and U. Shrinivasa, Studies on stove for powdery biomass, *International Journal of energy research*, *17*, 281–291, 1993.

Mukunda, H. S., S. Dasappa, P. J. Paul, N. K. S. Rajan, and U. Shrinivasa, Gasifiers and combustors for biomass - technology and field studies, *Energy for Sustainable Development*, *1*, 27–38, 1994.

Natarajan, I., Demand forecast for bio-fuels in rural households, 1993.

Perry, R. H., and C. H. Chilton, *Chemical Engineer's hand book*, 5 ed., McGraw Hill Kogakusha, 1973.

Prasad, K. K., E. Sangen, and P. Visser, Wood burning cook stoves, *Advances in Heat transfer*, *17*, 1985.

Ravi, M. R., K. Sangeeta, and A. Ray, Use of cfd simulation as a design tool for biomass stoves, *Energy for Sustainable Development*, *6*, 20–26, 2002.

Reed, T. B., and R. Larson, A wood-gas stove for developing countries, *Energy for Sustainable Development*, *3*, 34–37, 1996.

Reed, T. B., E. Anselmo, and K. Kircher, Testing and modelling the wood -gas turbo stove, in *The International Conference on Biomass-based Fuels and Cooking Systems*, edited by K. Priyadarshini, Appropriate Rural Technology Institute (ARTI), 2000.

Smith, K. R., Health energy and greenhouse-gas impacts of biomass combustion in household stoves., *Energy for Sustainable Development*, *1*, 23–29, 1994.

Smith, K. R., R. Uma, V. V. N. Kishore, K. Lata, V. Joshi, J. Zhang, R. A. Rasmussen, and M. A. K. Khalil, Greenhouse gases from small-scale combustion devices in developing countries. phase iia: Household stoves in india, Report for USEPA, 1998.

Turns, S. R., *Introduction to Combustion concepts and applications*, McGRAW-HILL international edition, 2000.

Zhang, J., et al., Greenhouse gases and other airborne pollutants from household stoves in china: a database for emission factors., *Atmospheric Environment*, *34*, 4537–4549, 2000.